SPREADING PROCESSES OVER MULTILAYER AND INTERCONNECTED NETWORKS

by

FARYAD DARABI SAHNEH

B.S., Amirkabir University (Tehran Polytechnic), Iran, 2008

M.S., Kansas State University, 2010

AN ABSTRACT OF A DISSERTATION

submitted in partial fulfillment of the
requirements for the degree

DOCTOR OF PHILOSOPHY

Department of Electrical and Computer Engineering
College of Engineering

KANSAS STATE UNIVERSITY
Manhattan, Kansas

2014

Abstract

Society increasingly depends on networks for almost every aspect of daily life. Over the past decade, network science has flourished tremendously in understanding, designing, and utilizing networks. Particularly, network science has shed light on the role of the underlying network topology on the dynamic behavior of complex systems, including cascading failure in power-grids, financial contagions in trade market, synchronization, spread of social opinion and trends, product adoption and market penetration, infectious disease pandemics, outbreaks of computer worms, and gene mutations in biological networks. In the last decade, most studies on complex networks have been confined to a single, often homogeneous network. An extremely challenging aspect of studying these complex systems is that the underlying networks are often heterogeneous, composite, and interdependent with other networks. This challenging aspect has very recently introduced a new class of networks in network science, which we refer to as *multilayer* and *interconnected networks*.

Multilayer networks are an abstract representation of interconnection among nodes representing individuals or agents, where the interconnection has a multiple nature. For example, while a disease can propagate among individuals through a physical contact network, information can propagate among the same individuals through an online information-dissemination network. Another example is viral information dissemination among users of online social networks; one might disseminate information received from a Facebook contact to his or her followers on Twitter. *Interconnected networks* are abstract representations where two or more simple networks, possibly with different dynamics over them, are interconnected to each other. For example, in zoonotic diseases, a virus can move from the network of animals, with some transmission dynamics, to a human network, with possibly very different dynamics. As communication systems are evolving more and more toward

integration with computing, sensing, and control systems, the theory of multilayer and interconnected networks seems to be crucial to successful communication systems development in cyber-physical infrastructures.

Among the most relevant dynamics over networks is *epidemic spreading*. Epidemic spreading dynamics over simple networks exhibit a clear example where interaction between non-complex dynamics at node level and the topology leads to a complex emergent behavior. A substantial line of research during the past decade has been devoted to capturing the role of the network on spreading dynamics, and mathematical tools such as spectral graph theory have been greatly useful for this goal. For example, when the network is a simple graph, the dominant eigenvalue and eigenvector of the adjacency matrix have been proven to be key elements determining spreading dynamics features, including epidemic threshold, centrality of nodes, localization of spreading sites, and behavior of the epidemic model close to the threshold. More generally, for many other dynamics over a single network, dependency of dynamics on spectral properties of the adjacency matrix, Laplacian matrix, or some other graph-related matrix, is well-studied and rigorously established, and practical applications have been successfully derived. In contrast, limited established results exist for dynamics on multilayer and interconnected networks. Yet, an understanding of spreading processes over these networks is very important to several realistic phenomena in modern integrated and composite systems, including cascading failure in power grids, financial contagions in trade market, synchronization, spread of social opinion and trends, product adoption and market penetration, infectious disease pandemics, and outbreak in computer worms.

This dissertation focuses on spreading processes on multilayer and interconnected networks, organized in three parts. The first part develops a general framework for modeling epidemic spreading in interconnected and multilayer networks. The second part solves two fundamental problems: introducing the concept of an epidemic threshold curve in interconnected networks, and coexistence phenomena in competitive spreading over multilayer networks. The third part of this dissertation develops an epidemic model incorporating

human behavior, where multi-layer network formulation enables modeling and analysis of important features of human social networks, such as an information-dissemination network, as well as contact adaptation. Finally, I conclude with some open research directions in the topic of spreading processes over multilayer and interconnected networks, based on the resulting developments of this dissertation.

SPREADING PROCESSES OVER MULTILAYER AND INTERCONNECTED NETWORKS

by

FARYAD DARABI SAHNEH

B.S., Amirkabir University (Tehran Polytechnic), Iran, 2008

M.S., Kansas State University, 2010

A DISSERTATION

submitted in partial fulfillment of the
requirements for the degree

DOCTOR OF PHILOSOPHY

Department of Electrical and Computer Engineering
College of Engineering

KANSAS STATE UNIVERSITY
Manhattan, Kansas

2014

Approved by:

Major Professor
Caterina Scoglio

Copyright

Abstract

Society increasingly depends on networks for almost every aspect of daily life. Over the past decade, network science has flourished tremendously in understanding, designing, and utilizing networks. Particularly, network science has shed light on the role of the underlying network topology on the dynamic behavior of complex systems, including cascading failure in power-grids, financial contagions in trade market, synchronization, spread of social opinion and trends, product adoption and market penetration, infectious disease pandemics, outbreaks of computer worms, and gene mutations in biological networks. In the last decade, most studies on complex networks have been confined to a single, often homogeneous network. An extremely challenging aspect of studying these complex systems is that the underlying networks are often heterogeneous, composite, and interdependent with other networks. This challenging aspect has very recently introduced a new class of networks in network science, which we refer to as *multilayer* and *interconnected networks*.

Multilayer networks are an abstract representation of interconnection among nodes representing individuals or agents, where the interconnection has a multiple nature. For example, while a disease can propagate among individuals through a physical contact network, information can propagate among the same individuals through an online information-dissemination network. Another example is viral information dissemination among users of online social networks; one might disseminate information received from a Facebook contact to his or her followers on Twitter. *Interconnected networks* are abstract representations where two or more simple networks, possibly with different dynamics over them, are interconnected to each other. For example, in zoonotic diseases, a virus can move from the network of animals, with some transmission dynamics, to a human network, with possibly very different dynamics. As communication systems are evolving more and more toward

integration with computing, sensing, and control systems, the theory of multilayer and interconnected networks seems to be crucial to successful communication systems development in cyber-physical infrastructures.

Among the most relevant dynamics over networks is *epidemic spreading*. Epidemic spreading dynamics over simple networks exhibit a clear example where interaction between non-complex dynamics at node level and the topology leads to a complex emergent behavior. A substantial line of research during the past decade has been devoted to capturing the role of the network on spreading dynamics, and mathematical tools such as spectral graph theory have been greatly useful for this goal. For example, when the network is a simple graph, the dominant eigenvalue and eigenvector of the adjacency matrix have been proven to be key elements determining spreading dynamics features, including epidemic threshold, centrality of nodes, localization of spreading sites, and behavior of the epidemic model close to the threshold. More generally, for many other dynamics over a single network, dependency of dynamics on spectral properties of the adjacency matrix, Laplacian matrix, or some other graph-related matrix, is well-studied and rigorously established, and practical applications have been successfully derived. In contrast, limited established results exist for dynamics on multilayer and interconnected networks. Yet, an understanding of spreading processes over these networks is very important to several realistic phenomena in modern integrated and composite systems, including cascading failure in power grids, financial contagions in trade market, synchronization, spread of social opinion and trends, product adoption and market penetration, infectious disease pandemics, and outbreak in computer worms.

This dissertation focuses on spreading processes on multilayer and interconnected networks, organized in three parts. The first part develops a general framework for modeling epidemic spreading in interconnected and multilayer networks. The second part solves two fundamental problems: introducing the concept of an epidemic threshold curve in interconnected networks, and coexistence phenomena in competitive spreading over multilayer networks. The third part of this dissertation develops an epidemic model incorporating

human behavior, where multi-layer network formulation enables modeling and analysis of important features of human social networks, such as an information-dissemination network, as well as contact adaptation. Finally, I conclude with some open research directions in the topic of spreading processes over multilayer and interconnected networks, based on the resulting developments of this dissertation.

Table of Contents

List of Figures

Acknowledgments

Many things are much more fun than writing a dissertation. I can finally be done after putting a check mark sign next to the 'write acknowledgment section' item at the end of my to-do list. Seems easy, right? Not quite, though. When I look back, I cannot believe how much I have been blessed by all the wonderful people around me during the past few years. Words are not capable of describing my gratitude and acknowledgment.

First and foremost, I would like to thank my advisor, Caterina Scoglio, for her continuous encouragement and support, her trust, and her enormous endeavor to help me grow academically. I honestly feel honored and lucky to have had an advisor like her. She always had time to listen to my smallest problems along the way and tried her best to guide me through overcoming them. She let me make mistakes and made sure that I learned from them. Last, but not least, I have greatly benefited from her technical and editorial advice to complete this dissertation.

I would like to especially thank Sameer Madanshetty for always being there throughout my graduate studies at K-State. I feel highly privileged to have met him. I would like to thank my beloved wife, Ala Fard, for her endless love, patience, and support. I cannot imagine being able to finish my work without her unconditional and unending support.

One of the greatest pleasures of my Ph.D. study has been collaborating with Fahmida Chowdhury, who is also on my committee. I have greatly benefited from her guidance to outreach my research to social and public health communities. I have learned great lifetime lessons from her expertise and cross-disciplinary experience.

It has been a pleasure for me to have collaborated with Piet Van Mieghem. Indeed, most of the research work in this dissertation has been motivated by his seminal work on epidemic spreading over graphs. He has been a constant source of inspiration and encouragement.

It has been my privilege to collaborate with Pietro Poggi-Corradini and Victor Preciado during my Ph.D. study. I have learned many great things from them. I also wish to thank Don Gruenbacher, head of the electrical and computer engineering department at K-State, for all his support.

I wish to express my gratitude to my committee members Fahmida Chowdhury, Stephen Dyer, and Byron Jones for their time and effort reviewing my dissertation manuscript, and providing me with their constructive comments and suggestions to improve this work.

I would like to thank Jim Riviere and Nancy Monteiro-Riviere, and their fellow members of the Institute of Comparative Computational Medicine at K-State for their support.

In particular, I would like to thank Fabio Schiattarella and Shawn Nouri for all their support and friendship.

My deep appreciation is due to my fellow office mates at Sunflower Networking Group: Phillip Schumm, Mina Youssef, Sakshi Pahwa, Ling Xue, Heman Shakeri,and Behnaz Moradi, for their friendship, collaboration, and all the fun we had. I wish to thank my colleagues, friends, and other faculty members at K-State for sharing happy moments and being with me through hard times.

Finally, there are not enough words to thank my parents for their unconditional love.

Dedication

To Sameer Madanshetty

Preface

This dissertation is submitted for partial fulfillment of the requirements for the degree Doctor of Philosophy at Kansas State University. The thesis work was conducted from January 2010 to August 2014 under the supervision of Professor Caterina Scoglio in Department of Electrical and Computer Engineering, Kansas State University.

This work is to the best of my knowledge, original, except where acknowledgments and references are made to previous work. Part of this work has been presented in the following publications.

Journal articles:

[1] F.D. Sahneh, C. Scoglio, P. Van Mieghem, "Generalized Epidemic Mean-Field Model for Spreading Processes over Multi-Layer Complex networks," *Networking, IEEE/ACM Transactions on*, vol. 21, no.5, pp. 1609–1620, 2013.

[2] F.D. Sahneh, C. Scoglio, "Competitive Epidemic Spreading over Arbitrary Multi-Layer Networks," *Physical Review E*, vol. 89, no. 6, p. 062817, 2014.

[3] F.D. Sahneh, F. Chowdhury, C. Scoglio, "On the Existence of a Threshold for Preventive Behavioral Responses to Suppress Epidemic Spreading," *Nature Scientific Reports*, vol 2:632, 2012.

[4] F.D. Sahneh, F. Chowdhury, G. Brase, and C. Scoglio "Individual-based Information Dissemination in Multilayer Epidemic Modeling," *Mathematical Modelling of Natural Phenomena*, vol. 9, no. 5, pp. 136-152, 2014.

Refereed conference proceedings:

[5] F.D. Sahneh, C. Scoglio, "Epidemic Spread in Human Networks," in *Proceedings of 50th IEEE Conference on Decision and Control and European Control Conference (CDC-ECC)*, pp. 3008–3013, 2011.

[6] F.D. Sahneh, C. Scoglio, "Optimal Information Dissemination in Epidemic Networks," in *Proceedings of IEEE 51st Annual Conference on Decision and Control (CDC)*, pp. 1657-1662, 2012.

[7] F.D. Sahneh, C. Scoglio, and F. Chowdhury, "Effect of Coupling on the Epidemic Threshold in Interconnected Complex Networks: A Spectral Analysis," in *Proceedings of American Control Conference*, pp. 2307- 2312, 2013.

This dissertation should be of interest to broad communities of engineers, mathematicians, and physicists with interest in network science, controls theory, mathematical epidemiology, and public health.

The conducted researched has been partially supported by National Science Foundation under Award No. DMS-1201427, National Agricultural Biosecurity Center at Kansas State University, and Kansas Bioscience Authority (KBA) funds to the Institute of Computational Comparative Medicine at Kansas State University. Any opinions, findings, or conclusions, or recommendations expressed in this dissertation do not necessarily reflect the views of these funding agencies.

Chapter 1

Introduction

1.1 Background

A network representation describes pair-wise relationships/interconnections among components of a system or members of a population of interest. Numerous biological, social, economical, physical, and technological systems possess pair-wise dependencies among their subsystems. Network science–in general–aims at studying such systems described as networks. Conventionally, network science has greatly benefited from graph theory as a rigorous mathematical tool to address several problems regarding networks. In graph theory, each member of a system is assigned to a node and links between node pairs denote relationship. For example, a friendship network denotes each individual by a node, and connects a pair of nodes if the corresponding individuals are friends. Another example is a telecom network, where nodes are routers and links are lines capable of transmitting numerous bytes per second.

1.1.1 Epidemic Spreading Process

One of the most relevant dynamics over networks is *epidemic spreading*. An epidemic model describes how infections spread throughout a network. Epidemic spreading dynamics over

simple networks is a clear example where interaction between non-complex dynamics at the node level and the topology leads to a complex emergent behavior. Epidemics are critical phenomena, not only from a biological viewpoint as caused by transmittable pathogens, but also from a technological viewpoint as caused by malware propagation. Epidemic modeling has a long history in biological systems, and recently such modeling has attracted substantial attention in modeling propagation phenomena in networks [8–10]. Epidemic models have been successful in providing insight and deep understanding of the epidemic process leading to successful conclusions about prediction and prevention of epidemics. Epidemic models have been used to study propagation of malware in the Internet [11–15] and to design delay tolerant networks for routing purposes.

In most epidemic models, the population is divided into several different groups referred to as *compartments*. Among the compartmental epidemic models, the susceptible- infected-susceptible (SIS) and susceptible-infected-removed (SIR) models have been widely used. In the SIS model, a susceptible node becomes infected with a given infection rate and an infected node becomes susceptible with a given curing rate. Therefore, in the SIS model, a node can become infected and susceptible several times. In the SIR model, a susceptible node becomes infected with a given infection rate and an infected node is removed at a given removing/recovery rate. Hence, in the SIR model, a node can only become infected once and then is removed from the population. SIS and SIR models are the basis of most other more complicated disease models. Aside from compartmental disease dynamics, contact patterns among members of the population are also important.

Early compartmental epidemic models studied epidemic spreading in a well-mixed homogenous population [16] and predicted a threshold behavior, which was in agreement with recorded epidemic data. In order to account for heterogeneity of contact patterns among individuals within a population, Moreno et al. [17] considered a network with independent heterogeneous node degree distribution, and Pastor-Satorras and Vespignani [18] studied epidemic spreading over scale-free networks. The main observation is that the contact net-

work plays a major role in the behavior of epidemic spreading. In the search for capturing the role of a contact network in greater detail, individual-based epidemic models were proposed, where the contact network is represented by a generic graph [19–22]. As a consequence, graph theory obtained a central role in analysis of networked epidemic processes, attracting broad attention from different communities of physics, computer science, engineering, controls, and network science.

1.1.2 Multilayer and Interconnected Networks

In many realistic systems, interconnections are so complicated that conventional simple networks cannot properly model the interconnections. Notions of *multilayer* and *interconnected* networks are among emerging topics in network science which go beyond conventional network representations [23, 24].

Multilayer networks (Figure 1.1) are an abstract representation of interconnection among nodes representing individuals or agents, where the interconnection has a multiple nature. For example, while a disease can propagate among individuals through a physical contact network, information can propagate among the same individuals through an on-line information dissemination network. Another example is viral information dissemination among users of online social networks; one might disseminate information received from a Facebook contact to followers in Twitter.

In several large-scale systems, it is not possible to isolate a network completely: there are often many interconnections with one or more networks. *Interconnected networks* (Figure 1.2) are abstract representations where two or more simple networks, possibly with different and separate dynamics upon them, are interconnected to each other. For example, in zoonotic diseases, a virus can move from an animals network, with some transmission dynamics, to a human network, with possibly very different dynamics.

Studying multilayer and interconnected networks is an emerging topic in network science, with numerous potential applications to realistic social, biological, and technological

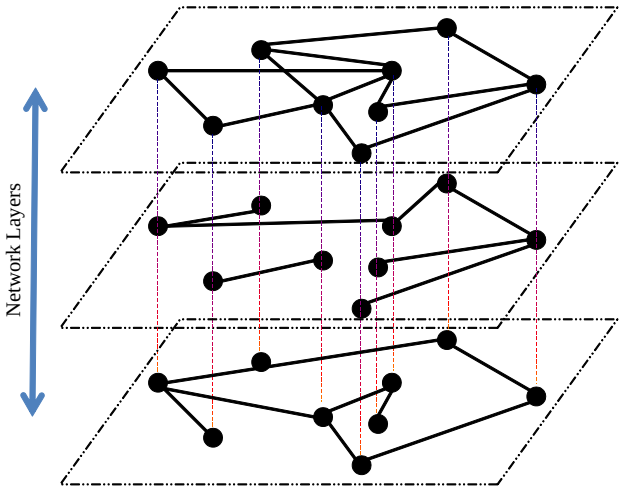

Figure 1.1: *Schematics of a multilayer network.*

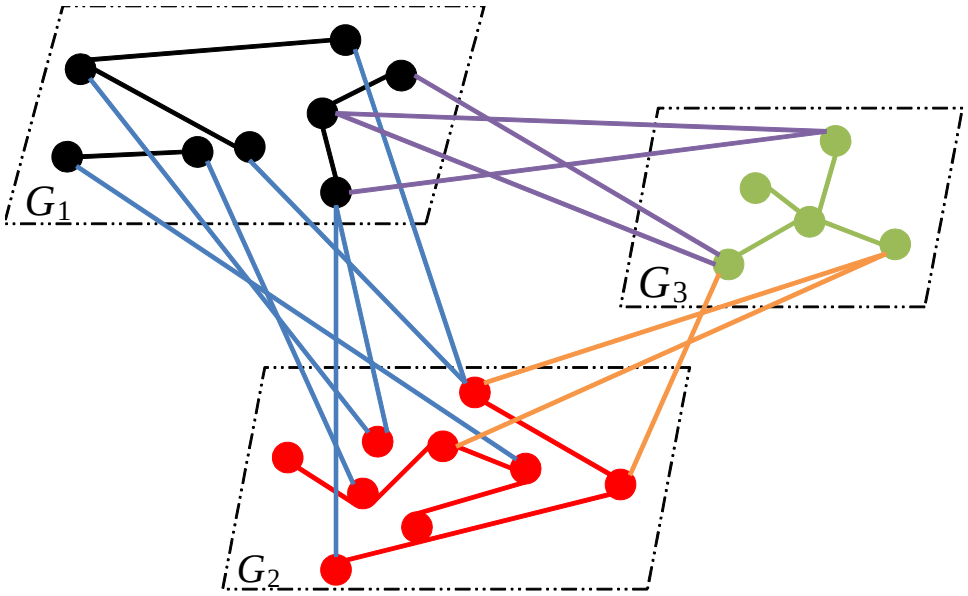

Figure 1.2: *Schematics of an interconnected network.*

networked systems. In particular, as communication systems are evolving more and more toward integration with computing, sensing, and control systems, the theory of multilayer and interconnected networks seems to be crucial to successful design of cyber-physical systems.

Dynamical processes on these networks have become popular in recent years with diverse applications to cascading failure [25–28], diffusion [29, 30], synchronization [31], and evolutionary games [32, 33]. In particular, the study of the spreading of epidemics in interconnected networks is a major challenge of complex networks, which has recently attracted substantial attention [6, 34–40].

1.2 Motivation

A substantial line of research during the past decade has been devoted to capturing the role of the network on spreading dynamics. Mathematical tools, such as spectral graph theory, have been highly useful for this goal. For example, for an SIS epidemic process on a simple graph, the dominant eigenvalue and eigenvector of the adjacency matrix prove to be key elements to determine the spreading dynamics features, including epidemic threshold [19, 21, 22], centrality of nodes, localization of spreading sites [41], and behavior of the epidemic model close to the threshold [42]. In contrast, limited established results exist for dynamics on multilayer and interconnected networks.

Several open problems on these types of networks are due to their inherent complexity. Dynamics on a simple graph usually depend on the spectral properties of its adjacency matrix, the Laplacian matrix, or some other graph-related matrices, which have been well-studied and rigorously established, enabling successful applications in practice. Analyzing dynamics on interconnected and multilayer networks is much more challenging. Researchers have formulated some problems in multilayer and interconnected networks which can be effectively analyzed through spectral properties of a "bigger matrix," hence, making use of rigorous mathematical tools of graph spectra. In the topic of multilayer and interconnected

networks, however, numerous problems cannot be transformed to studying these "bigger matrices." Instead, very often, we can characterize solutions through spectral properties of each layer/component separately, in addition to some function that represents the interrelation/interconnection.

The rationale for this dissertation is that epidemic-spreading dynamics over multilayer and interconnected networks are very relevant in practice and exhibit behaviors that cannot be attributed to single-networks characteristics. Our results are peculiar and different from some results in the literature for the following three reasons: 1) our work focuses on interconnected or multi-layer networks with arbitrary, generic structure, while most existing results in the literature assume fully mixed population models or degree-distribution random network models, which both have strong assumptions on the underlying network with limited application to engineered networked systems; 2) our proposed problems on interconnected or multilayer networks cannot be related to a larger, single-network problem, in contrast with several results where the problems are in fact studying a single network in terms of properties of its graph partitions; and 3) we focus on understanding the role of the topology of the multilayer/interconnected networks, identifying key quantitative characteristics, advancing current state of the art where analytical results are limited, or expressive topological interpretations are absent, due to technical challenges of analyzing these networks.

Understanding spreading processes over interconnected and multilayer networks is very important to several realistic phenomena in modern integrated and composite systems, including cascading failure in power-grids, financial contagions in the trade market, synchronization, spread of social opinion and trends, product adoption and market penetration, infectious disease pandemics, and outbreak of computer worms.

1.3 Thesis Overview

This dissertation is divided into three main parts. Part I is devoted to epidemic modeling on networks. Part II addresses fundamental SIS-type spreading problems in interconnected and multilayer networks. Finally, in Part III, we study the application of multilayer networks when incorporating human behavior into epidemic models.

Chapter 2 introduces networked epidemic models and formally defines multilayer and interconnected networks. In this chapter we review the networked SIS epidemic model and show how mean-field deterministic epidemic models have been successful in uncovering several important dynamic properties of stochastic epidemic spreading processes over complex networks. In particular, we study the impact of the network topology on spreading dynamics.

The existing epidemic models are generalized to develop a class of models with multiple compartments and multiple network layers in Chapter 3. We provide a detailed description of the stochastic process at the agent-level, where the agents interact through different layers. The set of differential equations that describes the time evolution of the state occupancy probabilities has an exponentially-growing state-space size in terms of the number of agents. Based on a mean-field type approximation, we develop a set of nonlinear differential equations that has linearly-growing state-space size. We find that the latter system, referred to as the *generalized epidemic mean-field* (GEMF) model, has a simple structure characterized by the elements of the adjacency matrices of the network layers and the Laplacian matrices of the transition rate graphs. Finally, we present several examples of epidemic models, including spreading of viruses and information on computer networks and spreading of multiple pathogens in a host population.

Chapter 4 studies the spreading process of an SIS epidemic model in an interconnected network of two generic graphs with generic interconnection and different epidemic-related parameters. For a single arbitrary graph representing the contact network of the population under consideration, the epidemic threshold turns out to be equal to the inverse of the

spectral radius of the contact graph. Multiple degrees of freedom in this interconnected network extend the concept of epidemic threshold value to that of threshold curve. To this end, using bifurcation theory and spectral graph theory, we find the epidemic threshold of one network as a function of the effective infection rate of the other coupled network and adjacency matrices of each graph and their interconnection, and provide a quantitative measure to distinguish between weak and strong interconnection topology.

Chapter 5 extends the SIS epidemic model for single-virus propagation over an arbitrary graph to an SI_1SI_2S epidemic model of two exclusive, competitive viruses over a two-layer network with generic structure, where network layers represent distinct transmission routes of the viruses. We find analytical expressions determining extinction, coexistence, and absolute dominance of the viruses after we introduce the concepts of *survival threshold* and *absolute-dominance threshold*. The main outcome of our analysis is discovery and proof of a region for long-term coexistence of competitive viruses in nontrivial multilayer networks. We show coexistence is impossible if network layers are identical, yet possible if network layers are distinct. Not only do we rigorously prove a region of coexistence, but we can quantify it via interrelation of central nodes across the network layers. Little to no overlapping of the layers' central nodes is the key determinant of coexistence. For example, we show both analytically and numerically that positive correlation of network layers makes it difficult for a virus to survive, while in a network with negatively correlated layers, survival is easier, but total removal of the other virus is more difficult.

In Chapter 6, we add a new compartment to the classic SIS model to account for human response to epidemic spread. In our model, each individual can be infected, susceptible, or alert. Susceptible individuals can become alert with an alerting rate if infected individuals exist among their neighbors. Due to a newly adopted cautious behavior, an individual in the alert state is less probable to become infected. The problem is modeled as a continuous-time Markov process on a generic graph and then formulated as a set of ordinary differential equations. The model is then studied using results from spectral graph theory and center

manifold theorem. We analytically show that our model exhibits two distinct thresholds in the dynamics of epidemic spread. For effective infection rates below the first threshold, infection dies out exponentially. For values larger than the second threshold, infection persists in the steady state. Between the two thresholds, infection spreads at the first stage but then dies out asymptotically as a result of increased alertness in the network. Finally, simulations are provided to support our findings.

Built upon the SAIS model, Chapter 7 investigates how information dissemination can help boost the resilience of the population against disease spread. The information dissemination is realized through an additional network among individuals, which has the same nodes but different links with respect to the contact network. Each link in the information dissemination network is directed, which provides the health status of the source agent to the end agent. We introduce an information dissemination metric, which is a quadratic form of the adjacency matrix of the information dissemination network and the dominant eigenvector of the adjacency matrix of the contact graph. By tools of perturbation theory, we analytically show the effect of the information dissemination is explicitly related to the information dissemination metric. It is proven that the spectral centrality of the nodes and edges determines the optimal information dissemination network. Our results suggest that monitoring the health status of a small subgroup of the agents and circulating the information can greatly enhance the resilience of the network, with multiple potential areas of application, from infectious disease mitigations to malware impact reduction.

Chapter 8 studies the propagation of infectious diseases in a population where individuals change their physical contact neighborhood as a preventive response to sensing infection (e.g., avoiding crowded locations like movie theater, etc.). In our modeling, each agent i normally has a contact neighborhood set $\mathcal{N}_i^A$. However, once she becomes alert, she switches her contacts to a new set $\mathcal{N}_i^B$. As a result, overall contact topology switches among 2^N possible configurations. We show this state-dependent, locally switching network can be formulated as a two-layer network. Bifurcation analysis of equilibrium infection probabilities

finds the epidemic threshold determining the conditions for occurrence of epidemic outbreak. We show the epidemic threshold of our adaptive contact network is the solution of a nonlinear Perron-Frobenius (NPF) problem. This result is substantially different from the case of independently time-varying contact networks, where the epidemic threshold corresponds to the joint spectral radius of contact adjacency matrices. We develop a numerical method to solve the NPF problem. Additionally, we develop explicit analytical results characterizing the epidemic threshold in terms of spectral properties of the two contact layers and their interrelation. Our results are both technically and practically important for studying viral spreading over adaptive social networks. Particularly, we discover scenarios where preventive contact change counter-intuitively worsens the virus spreading.

Finally, Chapter 9 summarizes and concludes this dissertation, providing open research issues in the field of spreading processes on multilayer and interconnected networks.

1.4 Contributions

Below is summary of main contributions of this dissertation:

- Developed a generalized epidemic model GEMF (Chapter 3) capable of systematically modeling a broad class of epidemic models on multilayer networks.
- Conceptualized the notion of epidemic threshold curve for interconnected networks (Chapter 4) and proposed a structural index to quantify interconnection strength.
- Studied the competitive spreading process of two viruses on multilayer networks (Chapter 5), finding conditions for coexistence and absolute dominance of viruses.
- Implemented a new component to the networked SIS epidemic model to incorporate human response to epidemics, identifying the importance of alert behavior to control and mitigate epidemics (Chapter 6).

- Captured the potential role of an information dissemination network to promote healthy behavior in social networks, with emphasis on its optimal design (Chapter 7).

- Showed the effect of contact network adaptation on progression of infectious disease in social networks, characterizing possible scenarios where alertness counter-intuitively amplifies the epidemics (Chapter 8).

Part I

Networked Epidemic Modeling

Chapter 2

Networked SIS Spreading Model

2.1 Introduction

Epidemic spreading, like many other processes (see, e.g., [43–45]) on complex networks, can be modeled as a network of coupled stochastic agents. A common approach of existing individual-based models is to consider Markovian interacting agents (i.e., dynamics of the agents satisfy the Markov property [46,47]) while the interaction is represented by a generic graph. This approach avoids random network models (e.g., Erdös-Réyni [48], Barábasi-Albert [49], etc.), which may fail to properly represent many systems including engineered networks [50]. The study of the dynamic behavior of epidemic spreading processes on graphs is very challenging, even for simple scenarios, due to the stochastic nature of this behavior. For example, the system governing state occupancy probabilities has an exponentially growing space size in terms of the number of agents. Therefore, the problem soon becomes intractable as the number of agents increases.

Through a mean-field closure approximation approach, size of the governing equations reduces dramatically although at the expense of exactness. Mean-field epidemic models have been used successfully in finding several interesting results for individual-based epidemic spreading processes. For example, researchers have shown that the epidemic threshold in

the SIS model is actually the inverse of the spectral radius of the adjacency matrix of the contact graph [19, 21]. In particular, individual-based SIS epidemic models on arbitrary networks predict the epidemic threshold is equal to (lower-bounded by) the inverse of the spectral radius of the contact graph [19, 21, 22]. Moreover, The N-intertwined mean-field approximated (NIMFA) model, also called microscopic Markov process approximation, first proposed by Van Mieghem [21], has triggered a pervasive amount of research on epidemic spreading on general networks, in different scenarios, and with different compartments [5, 6, 41, 51]. The key aspect of this class of models relies on use of the rigorous spectral graph theory to determine the evolution of the epidemic.

2.2 Graph Theory

Graph theory (see [52,53]) is widely used for representing the contact topology in an epidemic network, where each agent is a vertex and edges denote contact among agents. Let $G = \{V, E\}$ be a *directed* graph with a set of vertices $V = \{1, ..., N\}$ and the set of edges $E \subset V \times V$. An edge is an ordered pair $(i, j) \in E$, if agent i can potentially be directly infected by agent j. Graph G is *undirected* if for any edge $(i, j) \in E$, edge $(j, i) \in E$. We assume there is no self loop in the graph, i.e., $(i, i) \notin E$, and the contact graph is undirected. A *path* is referred by the sequence of its vertices. A path $\mathcal{P}$ of length $k = |\mathcal{P}|$ between i, j is the ordered sequence $(v_0 = i, v_1, ..., v_{k-1}, v_k = j)$ where $(v_{p-1}, v_p) \in E$ for $p = 1, ..., k$. Such a path can be interpreted as a walk from i to j consisting of *steps* (v_{p-1}, v_p). Graph G is connected if any two vertices are connected with a path in G. $A = [a_{ij}] \in \mathbb{R}^{N \times N}$ denotes the adjacency matrix of G, where $a_{ij} = 1$ if and only if $(i, j) \in E$, otherwise $a_{ij} = 0$. We define $\boldsymbol{d} = [d_1, d_2, \ldots, d_N]^T$ as the node-degree vector, i.e., $d_i = \sum_{j=1}^{N} a_{ij}$ is the degree of node i. A graph is connected iff its associated adjacency matrix is irreducible, i.e., it cannot be transformed into block upper-triangular form by permutations. The largest eigenvalue of the adjacency matrix A is called *spectral radius* of A and is denoted by $\lambda_1(A)$. The

dominant eigenvector of A is the eigenvector corresponding to $\lambda_1(A)$, denoted by $v_1(A)$. If graph G is connected, A is a non-negative irreducible matrix. Therefore, according to the Perron-Frobenius (PF) theorem, $\lambda_1(A)$ is real, positive, and single. Furthermore, dominant eigenvector $v_1(A)$ is the only eigenvector with all strictly positive entries.

2.3 Networked SIS Model

Consider a network of N agents where the contact is determined by the adjacency matrix A. Agent j is a neighbor of i, denoted by $j \in \mathcal{N}_i$, if it can transmit the infection to agent i. If j is a neighbor of i, then $a_{ij} = 1$; otherwise, $a_{ij} = 0$. In the SIS model, the state $x_i(t)$ of an agent i at time t is a Bernoulli random variable, where $x_i(t) = 0$ if agent i is susceptible and $x_i(t) = 1$ if it is infected. The *curing process* for infected agent i has an exponential time distribution with average duration $1/\delta$, where $\delta \in \mathbb{R}^+$ is called the curing rate. Similarly, *infection process* for susceptible agent i in contact with infected agent $j \neq i$ has an exponential time distribution with average duration $1/\beta$, where $\beta \in \mathbb{R}^+$ is called the infection rate. Therefore, a susceptible agent effectively becomes infected at rate $\beta Y_i(t)$, where $Y_i(t) \triangleq \sum_{j=1}^{N} a_{ij} x_j(t)$ is the number of infected neighbors of agent i at time t. The node-level description of the Markov process describing SIS model is

$$\Pr(x_i(t + \Delta t) = 1 | x_i(t) = 0, X(t)) = \beta Y_i(t) \Delta t + o(\Delta t) \tag{2.1}$$

$$\Pr(x_i(t + \Delta t) = 0 | x_i(t) = 1, X(t)) = \delta \Delta t + o(\Delta t) \tag{2.2}$$

where

$$Y_i(t) \triangleq \sum a_{ij} x_j(t) \tag{2.3}$$

is the number of infected neighbors, $X(t)$ is the total network state, and Δt is time step. The ratio of the infection rate β over the curing δ is the *effective infection rate* $\tau \triangleq \frac{\beta}{\delta}$. A schematic of an SIS epidemic-spreading model over a graph is shown in Fig. 2.1.

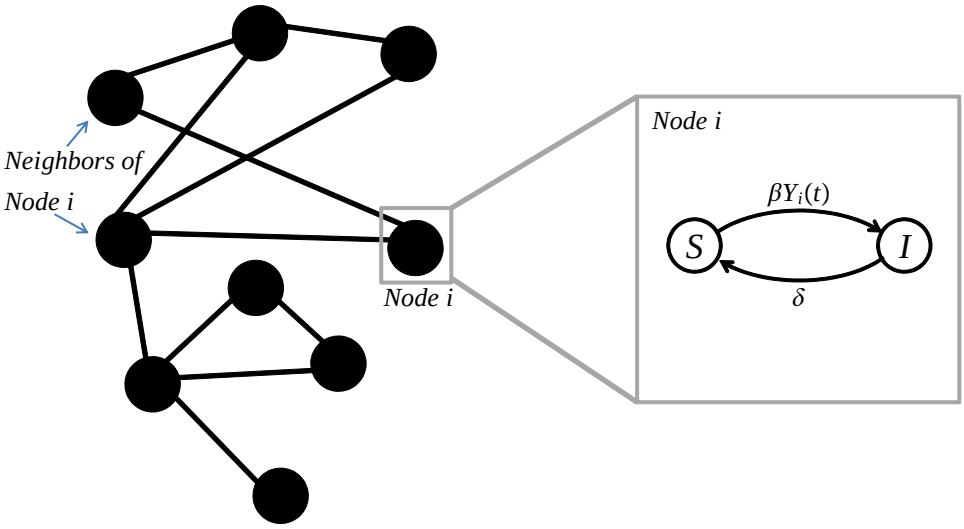

Figure 2.1: *Schematics of a contact network, along with the agent-level stochastic transition diagram for agent i according to the SIS epidemic-spreading model. Parameters β and δ denote the infection rate and curing rate, respectively. $Y_i(t)$ is the number of the neighbors of agent i that are infected at time t.*

According to the node-level description of the SIS process, expected value $E[x_i]$ evolves according to

$$\frac{d}{dt}E[x_i] = \beta \sum a_{ij} E[(1 - x_i)x_j] - \delta E[x_i] \tag{2.4}$$

$$= \beta \sum a_{ij} E[x_j] - \beta \sum a_{ij} E[x_i x_j] - \delta E[x_i], \tag{2.5}$$

for $i \in \{1, ..., N\}$. Unfortunately, this set of equations is not closed as evolution of marginal probabilities $E[x_i]$ depends on the joint probability of pairs. Similarly, evolution of pair probabilities $E[x_i x_j]$ depend on joint probabilities of triplets of the form $E[x_i x_j x_k]$, and so on. Therefore, the exact Markov equations describing the time evolution of probabilities have state-space size 2^N exponentially growing with N, which is both analytically and numerically intractable.

A first-order closure approximation assumes x_i and x_j are uncorrelated, and therefore $E[x_i x_j] = E[x_i]E[x_j]$. By this approximation, a set of nonlinear differential equations are

obtained that approximate the time evolution of infection probabilities as

$$\dot{p}_i = \beta(1 - p_i) \sum a_{ij} p_j - \delta p_i, \tag{2.6}$$

for $i \in \{1, ..., N\}$, where $p_i \triangleq E[x_i]$. Van Mieghem et al. [21] showed the response of this system always upperbounds the actual probability of infection.

Bifurcation theory of the NIMFA model [21] concludes that the epidemic threshold τ_c is the inverse of the spectral radius of adjacency matrix $A = [a_{ij}]$. Since this the derivation of this result is fundamental to future derivations in this dissertation, we detail the procedure here.

The disease-free state, i.e., $p_i^* = 0$ for $i \in \{1, ..., N\}$, is always an equilibrium point of (2.6). Using bifurcation theory, a second equilibrium point emerges for effective infection rate $\tau > 1/\lambda_1$. The idea is that exactly at τ_c, $p_i^* = 0$ for $i \in \{1, ..., N\}$; however, we should have $p_i^* > 0$ for $\tau > \tau_c$. The equilibrium points of (2.6) satisfy

$$\frac{p_i^*}{1 - p_i^*} = \tau \sum a_{ij} p_j^*. \tag{2.7}$$

Taking the (right) derivative with respect to τ, we have

$$\frac{1}{(1 - p_i^*)^2} \frac{dp_i^*}{d\tau} = \sum a_{ij} p_j^* + \tau \sum a_{ij} \frac{dp_j^*}{d\tau}. \tag{2.8}$$

Replacing for $\tau = \tau_c$ and $p_i^* = 0$, yields

$$\frac{dp_i^*}{d\tau}|_{\tau=\tau_c} = \tau_c \sum a_{ij} \frac{dp_j^*}{d\tau}|_{\tau=\tau_c}, \tag{2.9}$$

which in the collective form is

$$\frac{dP^*}{d\tau}|_{\tau=\tau_c} = \tau_c A \frac{dP^*}{d\tau}|_{\tau=\tau_c}, \tag{2.10}$$

where $P^* \triangleq [p_1^*, ..., p_N^*]^T$.

According to (2.10), $\frac{dP^*}{d\tau}|_{\tau=\tau_c}$ must be an eigenvector of the adjacency matrix of the contact graph. Since only the dominant eigenvector has all positive entries, according to the Perron-Frobenius theorem for irreducible matrices, $\frac{dP^*}{d\tau}|_{\tau=\tau_c}$ must be of the form

$$\frac{dP^*}{d\tau}|_{\tau=\tau_c} = cv_1, \tag{2.11}$$

where c is some constant to be determined and v_1 is the normalized dominant eigenvector of A corresponding to the largest eigenvalue λ_1, i.e., $Av_1 = \lambda_1 v_1$ and $\|v_1\|_2 = v_1^T v_1 = 1$. According to (2.10), $\tau_c \lambda_1 = 1$, hence $\tau_c = 1/\lambda_1$.

Additionally, we can explicitly derive the value of c. Taking the derivative another time from both sides of (2.8), we have

$$\frac{2}{(1-p_i^*)^3}(\frac{dp_i^*}{d\tau})^2 + \frac{1}{(1-p_i^*)^2}\frac{d^2p_i^*}{d\tau^2} = 2\sum a_{ij}\frac{dp_j^*}{d\tau} + \tau\sum a_{ij}\frac{d^2p_j^*}{d\tau^2}. \tag{2.12}$$

At $\tau = \tau_c$, $P^* = 0$ and $\frac{dP^*}{d\tau}|_{\tau=\tau_c} = cx_1$ according to (2.11). Therefore, after replacing for τ, p_i^*, and $\frac{dp_i^*}{d\tau}$ we get

$$(I - \tau_c A)\frac{d^2P^*}{d\tau^2}|_{\tau=\tau_c} + 2c^2 v_1^{(2)} - 2c\lambda_1 v_1 = 0, \tag{2.13}$$

where $v_1^{(2)} \triangleq [v_{1,1}^2, ..., v_{1,N}^2]$ is the entry-wise square of eigenvector v_1. Multiplying (2.13) by v_1^T from the right, the first terms becomes zero and we get

$$2c^2 v_1^T v_1^{(2)} - 2c\lambda_1 v_1^T v_1 = 0. \tag{2.14}$$

Therefore, since v_1 is normalized, we get

$$c = \frac{\lambda_1}{\sum v_{1,j}^3}. \tag{2.15}$$

This expression for c has been reported in [42], and later used to address localization phenomena in SIS spreading on graphs in [41].

2.4 Multilayer and Interconnected Networks Representation

We define interconnected network $\boldsymbol{G} = ([V_s]_{s=1}^{S}, [E_{ss'}]_{s,s'=1}^{S})$ as the interconnection of S coupled graphs $G_s = (V_s, E_{ss})$, $s \in \{1, \ldots, S\}$, where $E_{ss'} \subset V_s \times V_{s'}$ denotes the coupling between graphs G_s and $G_{s'}$. Furthermore, we define $\mathcal{G} = (V, [E_l]_{l=1}^{L})$ as a multilayer network of L graph layers $G_l = (V, E_l)$, $l \in \{1, \ldots, L\}$. A simple graph G can be represented by an adjacency matrix $A = [a_{ij}] \in \mathbb{R}_{\geq 0}^{N \times N}$, where a_{ij} represents the connection from node i to node j. The definition of an adjacency matrix for an interconnected network $\boldsymbol{G}$ is fairly straightforward. For S groups of networks of sizes $N_1, N_2, ..., N_S$, we can label the nodes of the first graph G_1 from 1 to N_1, the nodes of the second graph G_2 from $N_1 + 1$ to $N_1 + N_2$, and so on. The collective adjacency matrix $\boldsymbol{A}$ can be defined as

$$\boldsymbol{A} \triangleq \begin{bmatrix} A_{11} & \cdots & A_{1S} \\ \vdots & \ddots & \vdots \\ A_{S1} & \cdots & A_{SS} \end{bmatrix} \in \mathbb{R}_{\geq 0}^{\Sigma N_s \times \Sigma N_s}, \tag{2.16}$$

representing the connection between all of the nodes, where $A_{ss'} = A_{s's}^{T}$ for $s, s' \in \{1, ..., L\}$.

A proper definition of an adjacency for multilayer networks is challenging. The most promising definition so far is proposed by De Domenico et al. [54], adopting a three-dimensional tensor as the adjacency tensor. Following this representation, we can denote the adjacency tensor by

$$\mathcal{A} \triangleq [A_1; A_2; \cdots; A_L] \in \mathbb{R}_{\geq 0}^{N \times N \times L}. \tag{2.17}$$

The tonsorial approach to multilayer networks is convenient for representation purposes.

However, rich tools of matrix theory are not directly applicable. De Domenico et al. [54] have reformulated several concepts of matrix theory–relevant to network science–for tensors. However, many times the difficulty of multilayer networks analysis is not due to an extra dimension of the network data; rather, it is due to nonlinear, implicit interactions of the network layers. The complexity of layer interactions makes the analysis of dynamics over multilayer networks fundamentally much more challenging than that of single networks.

Another approach is to transform the problem under study into a problem on a "bigger matrix," allowing the use of matrix theory tools for interconnected and multilayer networks. For interconnected networks, this "bigger matrix" is the collective adjacency matrix $\boldsymbol{A}$ defined in (2.16). A multilayer network is more problematic. Some researchers have defined a "supra-adjacency" matrix [55] as

$$\boldsymbol{A}^{\sharp} \triangleq \begin{bmatrix} A_1 & I & & \mathbf{0} \\ I & A_2 & \ddots & \\ & \ddots & \ddots & I \\ \mathbf{0} & & I & A_L \end{bmatrix} \in \mathbb{R}_{\geq 0}^{LN \times LN}. \tag{2.18}$$

Unfortunately, this formulation is not suitable for multilayer networks according to our definitions. The supra-adjacency matrix is the adjacency matrix of the multilayer network in Figure 1.1, assuming the dotted lines are actual edges. Therefore, it indeed represents a specifically structured interconnected network.

In this dissertation, we analyze spreading processes over multilayer networks in terms of graph properties of individual network layers, in addition to layers' interrelation characteristics.

Chapter 3

Generalized Epidemic Mean-Field Model for Spreading Processes over Multi-Layer Complex Networks

3.1 Introduction

In most existing individual-based epidemic models, the interaction is driven by a single graph. However, studying epidemics in communication networks and cyber-physical systems requires a more elaborate description of the interaction. Several researchers from computer science, communication, networking, and control communities are working on describing this complex interaction by using multiple interconnected networks [27, 28, 56]. Ultimately, the study of the spreading of epidemics in interconnected networks is a major challenge of complex networks [34–37, 57].

In this chapter, we provide a novel and generalized formulation of the epidemic spreading problem and a modeling solution. We consider a spreading process among a group of agents that can be in M different compartments and where the agents interact through a multi-layer network, which is explained in detail in Section 3.4. We follow a rigorous method-

ology to develop a general epidemic spreading model. The modeling starts with a simple agent-level description of the underlying stochastic process. The exact Markov equations, which describe the time evolution of the state occupancy probabilities, are linear differential equations, however, with exponentially growing state space size in terms of the number of agents. Through a mean-field type approximation, the state space dramatically reduces. The approximate system is a set of nonlinear ordinary differential equations that we call the generalized epidemic mean-field (GEMF) model. We apply GEMF to interesting problems, such as (a) the spread of infection in a population where the infection spreads through a contact network while agents respond to the spreading by learning about the existence of the infection through information dissemination networks, and (b) the bi-spreading of two types of interacting viruses in a host population demanding different transmission routes for the infection propagation.

The contribution of this study is two-fold. First, we propose a general epidemic-like spreading Markov model with multi-compartment agent dynamics and a multi-layer interaction network. Second, we propose GEMF as a generalized epidemic mean-field model suitable for a large class of individual-based spreading scenarios. GEMF is rigorously derived from an agent-level description of the spreading process and is elegantly expressed (see equation (3.26)) in terms of the adjacency matrix of each network layer and of the Laplacian of the transition rate diagrams. In GEMF, there is no approximation of the network topology; the only approximation is a mean-field type approximation of the dynamics of the agents. The impact of this approximation is a function of the network topologies and epidemic parameters. For complete development, we have also explicitly derived the exact Markov equations in the Appendix.

3.2 Motivating Examples

In this section, first we review some of the existing individual-based epidemic models, and at the end, we discuss what generalizations are important to develop a general class of epidemic models.

3.2.1 SIS Individual-based Model

In the Susceptible-Infected-Susceptible (SIS) model (cf., [20–22]), each agent can be either '*susceptible*' or '*infected.*' Hence, the number of compartments, denoted by M, in the SIS model is $M = 2$. A susceptible agent can become infected if it is surrounded by infected agents. The infection process of an agent with one infected neighbor is a Poisson process with transition rate β. The infection processes are stochastically independent of each other. Therefore, for a susceptible agent with more than one infected agent in its neighborhood, the transition rate is the infection rate β times the number of the infected agents. The neighborhood of each agent is determined by a graph G_c, which represents the *contact network*. In addition to the infection process, there exists also a curing process. An infected agent becomes susceptible with a curing rate δ. A schematic for the SIS model is shown in Fig. 3.1.

3.2.2 SAIS Spreading Model

The Susceptible-Alert-Infected-Susceptible (SAIS) model was developed in [5] to incorporate agent reactions to the spread of the virus. In the SAIS spreading model, each agent can be either '*susceptible,*' '*infected,*' or '*alert.*' Hence, the number of compartments in the SAIS model is $M = 3$. The curing process in SAIS is the same as the curing process in the SIS model, and is characterized by curing rate δ. The infection process of a susceptible agent is also similar to that of the SIS model, which is determined by infection rate β and contact graph G_c. However, in the SAIS model, a susceptible agent can become alert if it senses

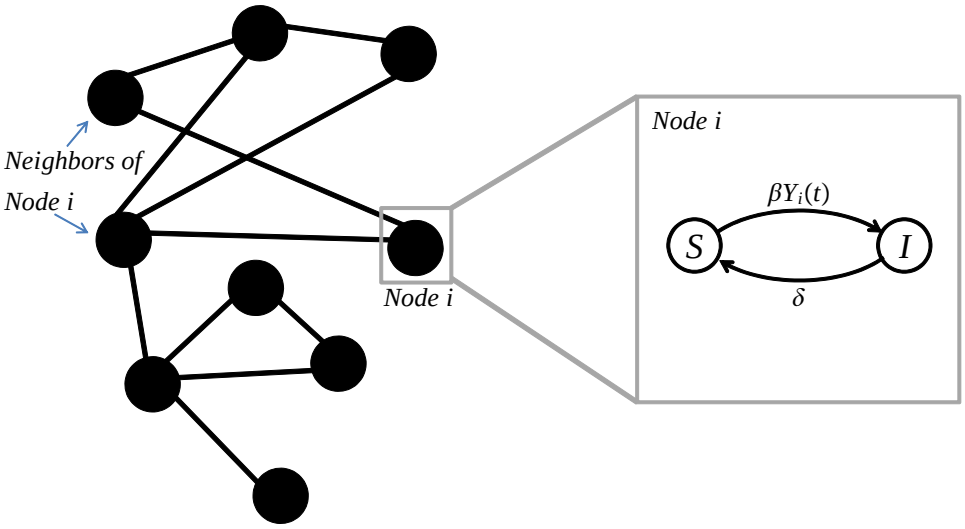

Figure 3.1: *Schematic of a contact network along with the agent-level stochastic transition diagram for agent i according to the SIS epidemic spreading model (explained in Section 3.2.1). The parameters β and δ denote the infection rate and curing rate, respectively. $Y_i(t)$ is number of the neighbors of agent i that are infected at time t.*

infected agents in its neighborhood. In the SAIS model, the alerting transition rate is κ times the number of infected agents. An alert agent can also become infected by the process similar to the infection process of a susceptible agent. However, the infection rate for alert agents is lower due to increased security for computer networks or better hygiene in the human population. The alert infection rate is denoted by $\beta_a < \beta$. Fig. 3.2 is a schematic for the SAIS spreading model.

3.2.3 Generalization of Epidemic Models

The SIS and SAIS models are good examples of how a simple compartmental model at the node level along with a network topology can lead to very rich and complex dynamics. While following the structure and underlying assumptions of these existing epidemic models, we propose to develop a generalized individual-based spreading model where (a) the node model has multiple compartments, and (b) the network topology has multiple layers. Both generalizations are important. For example, many epidemic models can be created by adding

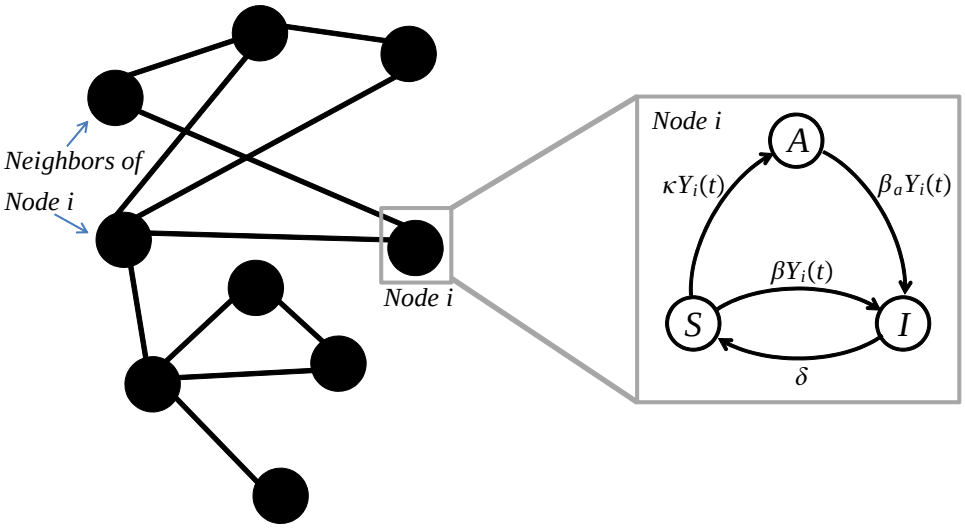

Figure 3.2: *As in Fig. 3.1, the SAIS epidemic is sketched (see 3.2.2) on a contact network G_c. In addition to the infection rate β and the curing rate δ, parameters β_a and κ denote the alerted infection rate and the alerting rate, respectively. $Y_i(t)$ is the number of neighbors of agent i that are infected at time t.*

new compartments to the basic SIS or SIR epidemic models. Also, for applications in cyber-social and cyber-physical systems, more network layers need to be taken into account (see Fig 3.3). For example, in the SAIS model, the agents can observe the infection status of their neighbors in the contact network. However, a more realistic scenario is that agents learn about the infection status of other agents through an *infection information dissemination network*, represented by G_{iIDN}, which can be very different from the contact network. We can also take into account an *alert information dissemination network* among the agents, represented by G_{aIDN}. Through this network, agents can become alert if some of their neighbors (determined by G_{aIDN}) are alert. In this case, the network topology has three layers. In Section 3.6.3, we develop an SAIS model with information dissemination.

Multi-layer epidemic modeling can also have applications in biological networks. Consider the scenario where two pathogens are spreading through the host population. Infection by one pathogen can effectively influence the infection process by the other pathogen. Since the infection transmission routes may be different, the contact networks for each virus can potentially be separate from each other. In Section 3.6.4, we develop an individual-based

SIS bi-spreading model with separate contact networks for each pathogen.

The GEMF class of models developed in this study allows not only an arbitrary number of compartments, but also accounts for multiple network layers.

3.3 Definitions

The network consists of N interacting agents, each of which can be in one of M states (compartments). The stochastic transitions of an agent not only depend on its own state but also on the states of the other agents. The group of agents is assumed to be *jointly Markovian*, i.e., the collective system is a Markov process. The state of the collective system, which we refer to as the network state, is actually the joint state of all the agents' states. Assuming that all the agents can take values among M compartments, the size of the network state space is M^N. In the following section, the agent state and network state are precisely defined.

3.3.1 Agent State and Network Markov State

One of the generalizations of GEMF concerns the compartment set, where each agent can be in one compartment in the set $\mathcal{S} = \{s_1, s_2, ..., s_m, ..., s_M\}$. For example, in the SIS model for epidemic spread, $M = 2$ and $\mathcal{S} = \{$'*Susceptible*','*Infected*'$\}$. From now on, without loss of generality, each compartment is labeled with a number from 1 to M. The *agent state* $x_i(t)$ of agent i at time t is $x_i(t) = e_m$ if the agent i is in compartment m at time t. Here, e_m is the $m-$th standard unit vector in the $\mathbb{R}^M$ Euclidean space, i.e., all entries of e_m are zero except for the $m-$th entry, which is equal to one.

$$e_m \triangleq [0...0 \underbrace{1}_{m-th \text{ entry}} 0...0]^T \in \mathbb{R}^M. \tag{3.1}$$

The definition $x_i(t) = e_m$ illustrates that each entry of $x_i(t)$ is a Bernoulli random vari-

able. Therefore, the expected value of $x_i(t)$ is in fact the *compartment occupancy probability vector*, i.e.,

$$E[x_i] = [\Pr[x_i = e_1], ..., \Pr[x_i = e_M]]^T. \tag{3.2}$$

The above property is very important in future developments, particularly in (3.14), (3.17), and (3.24-3.26).

There are other possibilities for defining the node state $x_i(t)$. For example, one might define $x_i = m - 1$ if node i is in compartment m. By this definition, x_i takes values from 0 to $M-1$. This definition is particularly useful if $M = 2$. In this case, x_i is a binary random variable. Van Mieghem et al. [21] used this definition for the SIS N-Intertwined model.

As stated, the dynamics of an individual agent depend on the states of the other agents. Therefore, the state of a single agent is not enough to describe the evolution of the agent state. Instead, the joint state of all the agents follows a Markov process. Therefore, the *network state* at time t, denoted by $X(t)$, is the joint state of all the agents defined as [58]

$$X(t) = \bigotimes_{i=1}^{N} x_i(t) = x_1(t) \otimes x_2(t) \otimes \cdots \otimes x_N(t), \tag{3.3}$$

where $\otimes$ is the Kronecker product.

By (3.3), $X(t)$ is an $M^N \times 1$ random vector with exactly one element equal to one and the rest equal to zero. Therefore, the expected value of $X(t)$ is the joint probability distribution function of the network state. For example, for the SIS model, the first element of the expectation of $X(t)$ is the probability that all the agents are simultaneously susceptible.

One could define the network state as a $MN \times 1$ vector $X \triangleq [x_1^T, x_2^T, \cdots, x_N^T]^T$. However, in this case, the expectation of $X(t)$ will only provide the marginal probability distribution of the node states. As Section 3.5.1 shows, the information about marginal probabilities at a given time is not enough to describe the evolution of the marginal probabilities, and the joint probability distribution is required. Hence, we adopt definition (3.3) for the network state.

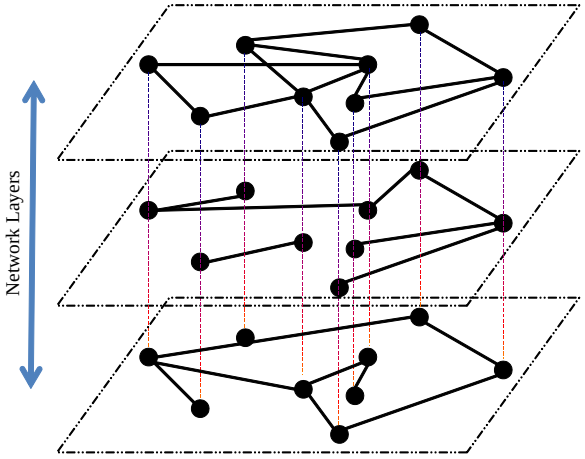

Figure 3.3: *Network layers describe the different types of interactions among agents in GEMF. The vertical dotted lines emphasize that all graphs have the same nodes, but the edges are different.*

3.3.2 Multi-Layer Network Topology

The other generalization in GEMF concerns the topology. In most epidemic models, the interaction among the agents is represented by the contact network. However, as discussed in Section 3.2.3, the types of interaction can be different in a complex network. For our modeling purpose, we represent the topology by a multilayer network $\mathcal{G} = (V, [E_l]_{l=1}^{L})$ consisting of L layers of graphs $G_l = (V, E_l)$, where V is the set of nodes denoting the agents, and E_l is the set of edges that represent the interaction between each pair of individuals in the l-th layer. These graphs have the same nodes, but the edges can be different. The adjacency matrix corresponding to graph G_l is denoted by $A_l = [a_{l,ij}]_{N\times N}$. If agent j can *influence* agent i in the layer l, $a_{l,ij} = 1$ otherwise $a_{l,ij} = 0$. In Section 3.4.1, we define precisely what 'influence' implies in our model. A representation of the network layering structure is depicted in Fig. 3.3.

3.4 Agent-Level Description of the Markov Spreading Process

The network state $X(t)$ follows a continuous-time Markov process. Knowing that the network is in state $X(t)$ at time t, what is the network state $X(t+\Delta t)$ at time $t+\Delta t$? In a network of interacting agents, this question can be very complicated. Instead, a more direct approach is to describe the agent state $x_i(t+\Delta t)$ given the network state $X(t)$ at time t. The spreading process is fully described if the probability to record a transition from compartment m to compartment n for agent i, conditioned on the network state $X(t)$, is known for all possible values of m, n, and i. Therefore, in this section, we focus on deducing an expression for $\Pr[x_i(t+\Delta t) = e_n | x_i(t) = e_m, X(t)]$, which will be used later to develop the GEMF model. The challenge in deducing an expression for $\Pr[x_i(t+\Delta t) = e_n | x_i(t) = e_m, X(t)]$ is that too many possibilities exist for the dependence of the transition $m \to n$ of the individual agent i on the network state. Here are a few examples: the transition $m \to n$ happens completely independently from the states of other agents; the transition $m \to n$ happens if the number of other agents in compartment m are more than the number of agents in compartment n; the transition $m \to n$ happens if agents 1 and 2 are both in compartment m and the rate of the transition is the logarithm of the number of agents in compartment m. All of these examples are legitimate so far. However, we need to specify the transition possibilities properly to develop a coherent and consistent epidemic spreading model.

3.4.1 Epidemic Spreading Process Modeling

The SIS model (see 3.2.1) gives very good insights into how to properly define the transition possibilities to describe an epidemic spreading process. In the SIS model, there are two transitions. The curing process, which is basically the transition from '*infected*' state to '*susceptible,*' occurs independently of the states of other agents. Instead, the infection process, which refers to transition from '*susceptible*' state to '*infected*' state, happens through

a different mechanism. A susceptible agent is in contact with some other agents, and during the time interval $(t, t+\Delta t]$, the susceptible agent receives the infection from its infected neighbor with some probability. The process of receiving the infection from one infected neighbor is independent of the process of receiving the infection from another neighbor. Indeed, all the infected neighbors compete to infect the susceptible agent. The susceptible agent becomes infected when one of the neighbors succeeds transmitting the infection. Next, since the transitions in the SIS epidemic model are very similar to the transitions in most existing epidemic models, we impose a similar structure of independent competing processes to the generalized spreading model.

Assumption 1. *A transition $m \to n$ for agent i is the result of several stochastically independent competing processes: the process $m \to n$ for agent i that happens independently of the states of other agents, and the process $m \to n$ for agent i because of interaction with agent $j \neq i$, for each $j \in \{1, ..., N\} \backslash \{i\}$.*

According to Assumption (1), the interaction of agent i with agent $j \neq i$ is stochastically independent of its interaction with agent $k \notin \{i, j\}$. Next, define the auxiliary counting process $T_{(i,j)}^{m \to n}(t)$ corresponding to the interaction of agent i with agent j. For convenience of notations, let $T_{(i,i)}^{m \to n}(t)$ correspond to the transition for agent i occurring independently of the states of other agents. According to Assumption 1, conditioned on the network state, these counting processes are stochastically independent. The transition $m \to n$ occurs in the time interval $(t, t+\Delta t]$ if any of these counting processes records an event. Therefore, $\Pr[x_i(t+\Delta t) = e_n | x_i(t) = e_m, X(t)]$ can be written as

$$\Pr[x_i(t+\Delta t) = e_n | x_i(t) = e_m, X(t)] = \\ \Pr[\exists j \in \{1, ..., N\} \text{ s.t. } T_{(i,j)}^{m \to n}(t+\Delta t) - T_{(i,j)}^{m \to n}(t) \neq 0 | X(t)]. \quad (3.4)$$

Each of the counting processes $T_{(i,j)}^{m \to n}(t)$ is a Poisson process with the rate $\lambda_{(i,j)}^{m \to n}(t)$, to

be determined. Therefore,

$$\Pr[T_{(i,j)}^{m\to n}(t+\Delta t) - T_{(i,j)}^{m\to n}(t) \neq 0 | X(t)] = \lambda_{(i,j)}^{m\to n}(t)\Delta t + o(\Delta t). \tag{3.5}$$

The sum of independent Poisson processes is also a Poisson process with aggregate rate equal to the sum of the individual rates (see Th. 7.3.4 in [47]). Therefore,

$$\Pr[x_i(t+\Delta t) = e_n | x_i(t) = e_m, X(t)] = \Delta t \sum_{j=1}^{N} \lambda_{(i,j)}^{m\to n}(t) + o(\Delta t). \tag{3.6}$$

The remaining part of this section is to determine $\lambda_{(i,j)}^{m\to n}(t)$ properly. For this end, we define notions of nodal and edge-based transitions.

Nodal Transition

As discussed earlier in 3.2.1, the curing process in SIS model happens with rate δ regardless of the infection status of other agents. Correspondingly, we call a process that occurs independently of the states of other agents a *nodal transition*. In general, for the nodal transition $m \to n$, we can consider a rate[1] $\delta_{mn} \geq 0$, which is actually the rate for the counting process $T_{(i,i)}^{m\to n}(t)$, i.e.,

$$\lambda_{(i,i)}^{m\to n}(t) = \delta_{mn}. \tag{3.7}$$

Edge-Based Transition

In the SIS model, a susceptible agent i becomes infected with rate β if it is in contact with infected agent j. Correspondingly, we call a process that occurs as the result of interaction between a pair of agents an *edge-based transition*. Edge-based transitions are different from nodal transitions because they depend on the states of other agents. For example, in the SIS model, the infection process is an edge-based transition, where, the contact network

[1]Here, δ_{mn} is a non-negative scalar that represents nodal transitions. It should not be confused with the Kronecker delta symbol.

graph determines the contact among agents. However, as described in Section 3.3.2, we extend the concept of contact network to multi-layer networks. In our formulation, the interactions among agents consist of L graph layers. Corresponding to each layer l, there is one *influencer compartment* q_l, i.e., transition $m \to n$ can occur for agent i as the result that a neighbor j in layer l, i.e., $a_{l,ij} = 1$, is in q_l. For example, in the SIS model, '*infected*' is the influencer compartment for the contact network, i.e., $q_1 = 2$. In general, the transition from compartment m to n is characterized by the transition rate $\beta_{l,mn} \geq 0$ for layer l. Therefore, the edge-based transition from m to $n \neq m$ through interaction of agent i with agent j is described by the rate

$$\lambda_{(i,j)}^{m \to n}(t) = \sum_{l=1}^{L} \beta_{l,mn} a_{l,ij} 1_{\{x_j(t) = e_{q_l}\}}, \tag{3.8}$$

where $1_{\{.\}}$ is the indicator function.

It is possible that the influencer compartment of two distinct layers is the same. For example, recall the extended SAIS model with three network layers proposed in Section 3.2.3. For the contact network and the infection information dissemination network, '*infected*' is the influencer compartment. However, for the alert information dissemination network, '*alert*' is the influencer compartment.

Assigning only one influencer compartment to a graph layer allows the elegant development of the subsequent analysis. However, a more general possibility is that a transition $m \to n$ occurs if a neighbor j, i.e., $a_{l,ij} = 1$, is in a subset of the compartments, say $q_{l,1}$ or $q_{l,2}$. This case can be treated within the same structure of GEMF, and if so, we can count the network layer twice, i.e., we assume that the first time, the graph has the influencer compartment $q_{l,1}$ and the second time, the graph has the influencer compartment $q_{l,2}$. An example of this case is in Section 3.6.4.

3.4.2 Transition Rate Graphs

To make the subsequent developments systematic, we propose to use transition rate graphs defined as follows. A *nodal transition rate graph* is graph with M nodes where each node represents a compartment. A directed link (m, n) from m to n represents the nodal transition $m \to n$ weighted by the positive transition rate $\delta_{mn} > 0$. Corresponding to the nodal transition rate graph, the adjacency matrices of the nodal transition rates A_δ is

$$A_\delta \triangleq [\delta_{mn}]_{M\times M}. \tag{3.9}$$

An *edge-based transition rate graph*, corresponding to the network layer l, is a graph with M nodes where each node represents a compartment. A directed link (m, n) from m to n represents the edge-based transition $m \to n$ weighted by the positive transition rate $\beta_{l,mn} > 0$ in network layer l with influencer compartment q_l. Corresponding to the edge-based transition rate graph, the adjacency matrices of the edge-based transition rates A_{β_l} are

$$A_{\beta_l} \triangleq [\beta_{l,mn}]_{M\times M}. \tag{3.10}$$

For example, in both the SIS and SAIS model described in Section 3.2.1 and Section 3.2.2, only the curing process is a nodal transition. The nodal transition rate graphs for the SIS and SAIS models are shown in Fig. 3.4 and Fig. 3.5, respectively. The schematic of the nodal transition rate graph in general is drawn in the left hand side of Fig. 3.6. In both the SIS and SAIS models, the contact network is the only network layer. Therefore, they have one edge-based transition rate graph. The edge-based transition rate graphs for the SIS and SAIS models are shown in Fig. 3.4 and Fig. 3.5, respectively. The schematic of the transition rate graphs in general is drawn in the right hand side of Fig. 3.6.

In Section 3.5 (see (3.26), below), the Laplacian matrices (see, [53]) associated to the transition rate graphs appears in the expression of GEMS.

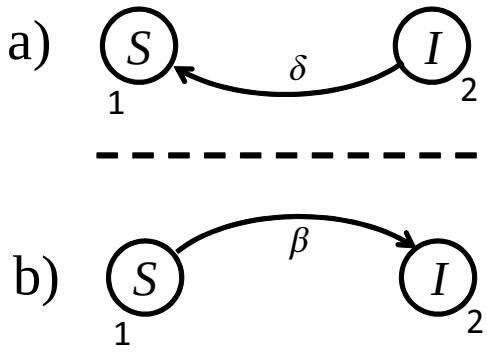

Figure 3.4: *Transition rate graphs in the SIS model: a) nodal transition rate graph; nodes represent the two compartments* 'susceptible' *and* 'infected'*, directed link from I to S represents curing process (a nodal transition) weighted by the curing rate $\delta > 0$, and b) edge-based transition graph of the contact network layer G_c; directed link from S to I represents the infection process (edge-based transition) weighted by the infection rate $\beta > 0$. For the contact network, the influencer compartment is $q_1 = 2$, i.e.,* 'infected'*.*

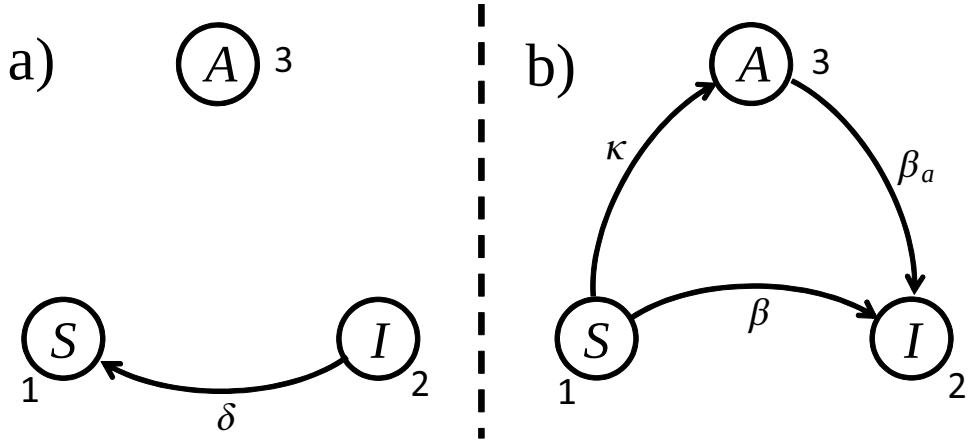

Figure 3.5: *Transition rate graphs in the SAIS model: a) nodal transition rate graph; nodes represent the three compartments* 'susceptible'*,* 'infected'*, and* 'alert'*, directed link from I to S represents curing process (a nodal transition) weighted by the curing rate $\delta > 0$, and b) edge-based transition graph of the contact network layer G_c; directed link from S to I represents the infection process (edge-based transition) weighted by the infection rate $\beta > 0$, directed link from S to A represents the alerting process (edge-based transition) weighted by the alerting rate $\kappa > 0$, directed link from A to I represents the alerted infection process (edge-based transition) weighted by the alerted infection rate $\beta_a > 0$. For the contact network, the influencer compartment is $q_1 = 2$, i.e.,* 'infected'*.*

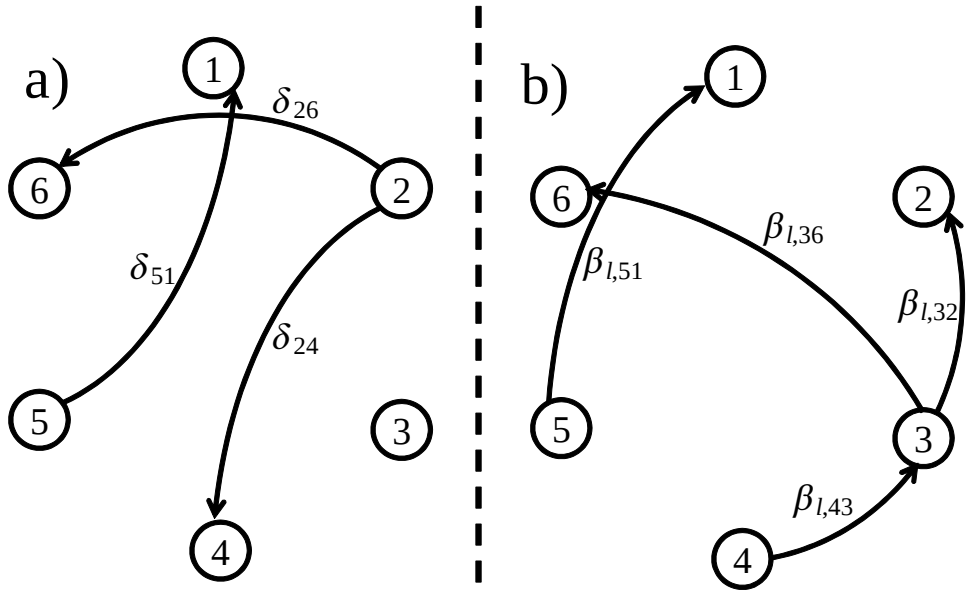

Figure 3.6: *Transition rate graphs in GEMF: a) nodal transition rate graph; nodes represent compartments, directed link* (m, n) *represent nodal transition* $m \to n$ *weighted by the transition rate* $\delta_{mn} > 0$*, and b) edge-based transition graph of network layer* G_l*; directed link* (m, n) *represent the edge-based transition* $m \to n$ *weighted by the transition rate* $\beta_{l,mn} > 0$ *in network layer* l*. The inducer compartment of layer* l *is* q_l*.*

3.4.3 Agent-Level Markov Description of the Spreading Process

In Section 3.4.1, we developed the expressions for the nodal transition and edge-based transitions. Substituting (3.7) and (3.8) into (3.6) yields

$$\Pr[x_i(t+\Delta t) = e_n | x_i(t) = e_m, X(t)] = \delta_{mn}\Delta t + \Delta t \sum_{l=1}^{L} \beta_{l,mn} y_{l,i}(t) + o(\Delta t), \tag{3.11}$$

for $i = \{1, ..., N\}$ and $m \neq n$, where

$$y_{l,i}(t) \triangleq \sum_{j=1}^{N} a_{l,ij} 1_{\{x_j(t) = e_{q_l}\}} \tag{3.12}$$

is the number of neighbors of agent i in G_l that are in the corresponding influencer compartment q_l.

Equation (3.11) provides an agent-level description of the Markov process. It can be

used directly for Monte Carlo numerical simulation of the spreading process.

3.5 GEMF: Generalized Epidemic Mean-Field Model

The objective of this section is to derive the time evolution of the state occupancy probabilities.

3.5.1 Exact Markov Differential Equation

In the previous section, the spreading model was described, and the corresponding Markov process was derived in (3.11). The evolution of the state occupancy probabilities associated with a Markov process follows a set of differential equations known as the Kolmogorov differential equations. The derivation of the Kolmogorov differential equation of a Markov process is fairly standard (see, [47, 59]) when the transition rates between the states of the Markov process are known. However, the challenge here is that the network states are the actual Markov states, and instead of the transition rates between the network states, we have the agent-level description of the transitions in (3.11). Thus in this section, we derive the differential equations directly from (3.11).

According to (3.11), the probability of remaining in the previous state is

$$\Pr[x_i(t+\Delta t) = e_m | x_i(t) = e_m, X(t)] = 1 - \sum_{n \neq m} \Pr[x_i(t+\Delta t) = e_n | x_i(t) = e_m, X(t)]. \quad (3.13)$$

Combining (3.2), (3.11), and (3.13) leads to

$$E[x_i(t+\Delta t)|x_i(t)=e_m, X(t)] = \begin{bmatrix} \delta_{m1}+\sum_{l=1}^{L}\beta_{l,m1}y_{l,i}(t) \\ \vdots \\ \delta_{m(m-1)}+\sum_{l=1}^{L}\beta_{l,m(m-1)}y_{l,i}(t) \\ -\tilde{\delta}_{mm}-\sum_{l=1}^{L}\tilde{\beta}_{l,mm}y_{l,i}(t) \\ \delta_{m(m+1)}+\sum_{l=1}^{L}\beta_{l,m(m+1)}y_{l,i}(t) \\ \vdots \\ \delta_{mM}+\sum_{l=1}^{L}\beta_{l,mM}y_{l,i}(t) \end{bmatrix} \Delta t + e_m + \epsilon(\Delta t), \quad (3.14)$$

where $\tilde{\delta}_{mm} \triangleq \sum_{n\neq m}\delta_{mn}$, $\tilde{\beta}_{l,mm} \triangleq \sum_{n\neq m}\beta_{l,mn}$, and $\epsilon(\Delta t)$ is a function of higher order terms of Δt satisfying the condition

$$u^T\epsilon(\Delta t) = 0, \quad (3.15)$$

where u is the all ones vector with appropriate dimensions.

Next we define the generalized transition matrices $Q_\delta \in \mathbb{R}^{M\times M}$ and $Q_{\beta_l} \in \mathbb{R}^{M\times M}$ with the elements

$$\begin{aligned} (Q_\delta)_{mn} &\triangleq -\delta_{mn},\ (Q_{\beta_l})_{mn} \triangleq -\beta_{l,mn},\ m\neq n \\ (Q_\delta)_{mm} &\triangleq \sum_{n\neq m}\delta_{mn},\ (Q_{\beta_l})_{mn} \triangleq \sum_{n\neq m}\beta_{l,mn}. \end{aligned} \quad (3.16)$$

According to definitions (3.16), the matrices Q_δ and Q_{β_l} are actually the Laplacian matrices of transition rate graphs defined in Section 3.4.2.

Using (3.14) and the definition (3.16), $E[x_i(t+\Delta t)|X(t)]$ is

$$\begin{aligned} E[x_i(t+\Delta t)|X(t)] = &-Q_\delta^T x_i(t)\Delta t \\ &- \sum_{l=1}^{L} y_{l,i}(t) Q_{\beta_l}^T x_i(t)\Delta t \\ &+ x_i(t) + \epsilon(\Delta t), \end{aligned} \tag{3.17}$$

where $y_{l,i}(t)$ is defined in (3.12). Computing the expected value of each side of (3.17), we get

$$\begin{aligned} E[x_i(t+\Delta t)] = &-Q_\delta^T E[x_i(t)]\Delta t \\ &- \sum_{l=1}^{L} Q_{\beta_l}^T E\left[y_{l,i}(t)x_i(t)\right]\Delta t \\ &+ E[x_i(t)] + \bar{\epsilon}(\Delta t), \end{aligned} \tag{3.18}$$

where $\bar{\epsilon}(\Delta t) = E[\epsilon(\Delta t)]$ and we have used the formula for iterative expectation (see [60]) rule $E[E[X|Y]] = E[X]$ to find $E[x_i(t+\Delta t)]$. Moving the $E[x_i(t)]$ term in (3.18) to the left side and dividing both sides by Δt yields

$$\frac{E[x_i(t+\Delta t)] - E[x_i(t)]}{\Delta t} = -Q_\delta^T E[x_i(t)] - \sum_{l=1}^{L} Q_{\beta_l}^T E\left[y_{l,i}(t)x_i(t)\right] + \frac{1}{\Delta t}\bar{\epsilon}(\Delta t), \tag{3.19}$$

Letting $\Delta t \to 0$ in (3.19), we obtain

$$\frac{d}{dt}E[x_i(t)] = -Q_\delta^T E[x_i(t)] - \sum_{l=1}^{L} Q_{\beta_l}^T E\left[y_{l,i}(t)x_i(t)\right]. \tag{3.20}$$

Furthermore, according to (3.12), the term $E\left[y_{l,i}(t)x_i(t)\right]$ in (3.20) can be written as

$$E\left[y_{l,i}(t)x_i(t)\right] = \sum_{j=1}^{N} a_{l,ij} E\left[(x_j)_{q_l} x_i(t)\right]. \tag{3.21}$$

The term $E\left[(x_j)_{q_l} x_i(t)\right]$ in 3.21 is actually embedded in $E[x_i(t) \otimes x_j(t)]$. Therefore, the evolution of $E[x_i(t)]$ depends on the $E[x_i(t) \otimes x_j(t)]$ term, which is the joint state of pairs of nodes. This means that the marginal information about the compartmental occupancy probabilities is not enough to fully describe the time evolutions of the marginal probabilities. If we continue to derive the evolution law for $E[x_i(t) \otimes x_j(t)]$, it turns out that the time derivative of $E[x_i(t) \otimes x_j(t)]$ depends on terms of the form $E[x_i(t) \otimes x_j(t) \otimes x_k(t)]$, which are the joint states of triplets. This dependency of the evolution of expectation of K-node groups upon expectation of $(K+1)$-node groups continues until K reaches $K = N$. As a result, any system describing the evolution of the expected value of the joint state of any group of $K < N$ nodes is not a closed system. When $K = N$, the expectation of the joint state of all nodes $E[x_1(t) \otimes \cdots \otimes x_N(t)]$, which according to definition (3.3) is actually the expectation of the network state, satisfies a differential equation of the form

$$\frac{d}{dt} E[X] = -\mathbf{Q}^T E[X], \tag{3.22}$$

where $\mathbf{Q} \in \mathbb{R}^{M^N \times M^N}$ is the infinitesimal generator (see [47, 59]) of the underlying Markov process. The Kolmogorov differential equation (3.22), which we refer to as the exact Markov model, is derived explicitly in the Appendix.

The exact Markov equation (3.22) fully describes the system. However, the above differential equation has M^N states. Therefore for large values of N, it is neither analytically nor computationally tractable. The following section shows that through a *mean-field type approximation*, a differential equation with MN states can be derived.

3.5.2 GEMF: Generalized Epidemic Mean-Field Model

One way to reduce the M^N state space size is to use closure approximation techniques. As explained in the previous section, expectations of order K depend on expectation of order $K+1$. The goal of closure techniques is to *approximate* the expectations of order $K+1$, and express them in terms of expectations of order less than or equal to K. In this way, a new set of differential equations is obtained that is closed and has the state space size $M^K\binom{N}{K}$, which is polynomially growing by N. The simplest approximation is the mean-field type approximation [61]. In first order mean-field models [21], the states of nodes are assumed to be independent random variables. It is also possible to consider higher order mean-field approximations. Cator and Van Mieghem [62] used a second order mean-field approximation and found more accurate performance of the model. Another approach is called the *moment closure* technique, where the joint states of triplets are assumed to have a specific distribution (usually normal or lognormal) [20,61]. In this way, the joint expectation of triplets is expressed in terms of expectations of pairs. Taylor et al. [61] have compared the performances of different approximations.

In this study, we use a first order mean-field type approximation. Using this approximation, the joint expected values are approximated in terms of marginal expected values. Specifically, the term $E\left[(x_j)_{q_l}x_i(t)\right]$ in (3.21) is approximated by

$$E\left[(x_j)_{q_l}x_i(t)\right] \simeq \left(E\left[(x_j)_{q_l}\right]\right)E[x_i(t)]\,. \tag{3.23}$$

This approximation assumes independence among the random variables. Using the approximation (3.23), we can describe the time evolution of the expected values through a set of ordinary differential equations with MN states.

We can denote by $v_i(t)$, the expected value of x_i at time t, i.e.,

$$v_i(t) \triangleq E[x_i(t)]. \tag{3.24}$$

Substituting $E\left[y_{l,i}(t)x_i(t)\right] = \sum_{j=1}^{N} a_{l,ij}(v_j(t))_{q_l} v_i(t)$ in (3.20), from (3.21), (3.23), and (3.24), yields

$$\frac{d}{dt}v_i(t) = -Q_\delta^T v_i(t) - \sum_{l=1}^{L} Q_{\beta_l}^T \sum_{j=1}^{N} a_{l,ij}(v_j(t))_{q_l} v_i(t). \tag{3.25}$$

Arranging the terms in (3.25) specifies our generalized epidemic mean-field model GEMF:

$$\frac{dv_i}{dt} = -Q_\delta^T v_i - \sum_{l=1}^{L}(\sum_{j=1}^{N} a_{l,ij} v_{j,q_l}) Q_{\beta_l}^T v_i, \qquad i = \{1, ..., N\}. \tag{3.26}$$

Having initially $u^T v_i(t_0) = 1$, the sum of the probabilities is guaranteed to be 1 at any time. The reason is that from (3.26) $u^T v_i$ does not change over time because

$$\begin{aligned}
\frac{d}{dt}u^T v_i &= -u^T Q_\delta^T v_i - \sum_{l=1}^{L}(\sum_{j=1}^{N} a_{l,ij} v_{j,q_l}) u^T Q_{\beta_l}^T v_i \\
&= -(Q_\delta u)^T v_i - \sum_{l=1}^{L}(\sum_{j=1}^{N} a_{l,ij} v_{j,q_l})(Q_{\beta_l} u)^T v_i \\
&= \mathbf{0}.
\end{aligned} \tag{3.27}$$

The last conclusion is for the fact that $Q_\delta u = 0$ and $Q_{\beta_l} u = 0$, since indeed Q_δ and Q_{β_l} are the graph Laplacians for which u is the eigenvector corresponding to a zero eigenvalue.

GEMF has a systematic procedure to develop different spreading mean-field models. For any specific scenario, the compartment set, the network layers, and their corresponding influencer compartments should be identified, and the transition rate graphs should be drawn. Next, the individual-based mean-field model of the spreading scenario is found by plugging the matrices Q_δ and Q_{β_l}, obtained from the transition rate graphs, into GEMF (3.26).

3.5.3 Capabilities and Limitations of GEMF

GEMF can be used to describe a wide range of spreading scenarios in a systematic way. In part, this is because in GEMF, there is no approximation of the underlying networks. The only approximation belongs to the mean-field-type approximation (3.23) and how much this results in deviation from exactness is outside the scope of this dissertation. However, the available studies for the mean-field SIS model (see, [63, 64]) can shed some light on this problem. Concerning the SIS model, extensive numerical simulations have shown that for sparser graphs, the mean-field model is less accurate, while for graphs with more mixing, the mean-field model is closer to the exact process. For a homogeneous mixing contact network, it has been proved that the mean-field model is asymptotically exact, i.e., as $N \to \infty$. Furthermore, the accuracy of the mean-field model very much depends on the range of the epidemic parameters. For example, in the SIS spreading process, the mean-field model is accurate for large values of the infection rate for any graph, while for infection rates close to the epidemic threshold, there is considerable difference between the response of the mean-field model and the exact model. Additionally, studies have shown that mean-field SIS models fail to explain the existence of a stable, disease-free, absorbing state [65].

If the initial states are seeded according to an uncorrected distribution, i.e., at the initial time equation (3.23) is actually exact, then the mean-field model performs fairly accurately during the early stages of system response. The reason for this is that nodes are poorly correlated at the early stage but become more and more correlated as time goes on. Consequently, accuracy of the transient response of mean-field models has been reported in [66] for the SIS spreading process. The steady-state solution of the mean-field models is also important. For example, the steady-state solution of SIS model belongs to the metastable state in the SIS epidemic process [21]. If accuracy is of greater concern, then higher order closure techniques can be used. However, this will result in a much larger state space size. Alternatively, GEMF has the smallest state space size to describe the spreading process of the type considered in this chapter. Any further reduction of the state space

essentially implies adopting approximation of the network structure.

One of the great benefits of the GEMF model is its analytical tractability. The SIS mean-field model suggests that the epidemic threshold is the inverse of the spectral radius of the contact network [21]. Finding relationships between spectral properties of underlying network layers and the spreading process is a problem of great interest. In particular, optimal design of some network layers given other network layers is very important from a technological view point. For example, Sahneh and Scoglio [6] used a mean-field SAIS model to find optimal topology of the information dissemination network given a contact network to reduce the impact of an epidemic.

3.6 Case Studies

In this section, we show that GEMF can reproduce the N-Intertwined SIS model [21] and the SIR model [51]. Furthermore, the section develops an SAIS model with information dissemination and a model for a scenario where two pathogens are spreading in a host population.

3.6.1 SIS N-Intertwined Model

The SIS model, explained in Section 3.2.1, has $M = 2$ number of compartments. The epidemic parameters are the infection rate β and the curing rate δ. In this model, the interaction is only through the contact graph, where '*infected*' is the influencer compartment. Hence, $L = 1$ and $q_1 = 2$. The transition rate graphs for the SIS model are shown in Fig. 3.4. The adjacency matrices corresponding to the nodal and edge-based transition rate graphs follow from Fig. 3.4,

$$A_\delta = \begin{bmatrix} 0 & 0 \\ \delta & 0 \end{bmatrix}, \; A_\beta = \begin{bmatrix} 0 & \beta \\ 0 & 0 \end{bmatrix}. \tag{3.28}$$

Therefore, GEMF (3.26) suggests the following set of differential equations

$$\frac{dv_i}{dt} = -Q_\delta^T v_i - \sum_{j=1}^{N} a_{ij} v_{j,2} Q_\beta^T v_i, \tag{3.29}$$

for the evolution of the compartment probability vectors, where the Q_δ and Q_β matrices, corresponding to A_δ and A_β respectively, are

$$Q_\delta = \begin{bmatrix} 0 & 0 \\ -\delta & \delta \end{bmatrix}, Q_\beta = \begin{bmatrix} \beta & -\beta \\ 0 & 0 \end{bmatrix}. \tag{3.30}$$

We can denote the probabilities of being susceptible by S_i and being infected by I_i, i.e., $v_i = [S_i, I_i]^T$. Therefore, the evolution of these probabilities according to GEMF is described as

$$\begin{aligned} \begin{bmatrix} \dot{S}_i \\ \dot{I}_i \end{bmatrix} &= - \begin{bmatrix} 0 & 0 \\ -\delta & \delta \end{bmatrix}^T \begin{bmatrix} S_i \\ I_j \end{bmatrix} - (\sum_{j=1}^{N} a_{ij} I_j) \begin{bmatrix} \beta & -\beta \\ 0 & 0 \end{bmatrix}^T \begin{bmatrix} S_i \\ I_j \end{bmatrix} \\ &= \begin{bmatrix} \delta I_i - \beta S_i (\sum_{j=1}^{N} a_{ij} I_j) \\ -\delta I_i + \beta S_i (\sum_{j=1}^{N} a_{ij} I_j) \end{bmatrix}. \end{aligned} \tag{3.31}$$

Since $S_i + I_i = 1$, the differential equation

$$\frac{dI_i}{dt} = -\delta I_i + \beta (1 - I_i)(\sum_{j=1}^{N} a_{ij} I_j) \tag{3.32}$$

is obtained for I_i and $i \in \{1, ..., N\}$, which is exactly the SIS N-Intertwined model in [21].

3.6.2 SIR N-Intertwined Model

Youssef and Scoglio [51] developed the SIR N-Intertwined model where each agent can be either '*susceptible,*' '*infected,*' or '*recovered*'. Therefore, the number of compartments in this model is $M = 3$. In this model, a susceptible agent can become infected if it is

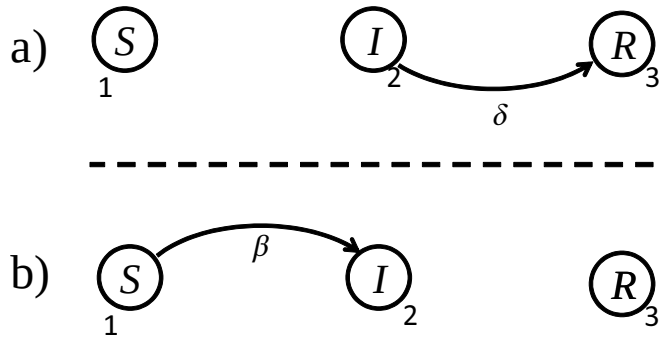

Figure 3.7: *Transition rate graphs in the SIR model: a) nodal transition rate graph; nodes represent the two compartments* 'susceptible', 'infected', *and* 'recovered', *directed link from I to R represents curing process (a nodal transition) weighted by the curing rate $\delta > 0$, and b) edge-based transition graph of the contact network layer G_c; directed link from S to I represents the infection process (edge-based transition) weighted by the infection rate $\beta > 0$. For the contact network, the influencer compartment is $q_1 = 2$, i.e.,* 'infected'.

surrounded by infected agents, and the infection process is characterized by the infection rate β. Furthermore, an '*infected*' agent becomes '*recovered*' with rate δ. Unlike the SIS model, a recovered agent does not become infected again in the SIR model. Similar to SIS, there is only $L = 1$ graph layer and $q_1 = 2$. The transition rate graphs, shown in Fig. 3.7, illustrate that

$$A_\delta = \begin{bmatrix} 0 & 0 & 0 \\ 0 & 0 & \delta \\ 0 & 0 & 0 \end{bmatrix}, \; A_\beta = \begin{bmatrix} 0 & \beta & 0 \\ 0 & 0 & 0 \\ 0 & 0 & 0 \end{bmatrix}. \tag{3.33}$$

Therefore, GEMF (3.26) suggests the following set of differential equations

$$\frac{dv_i}{dt} = -Q_\delta^T v_i - \sum\nolimits_{j=1}^{N} a_{ij} v_{j,2} Q_\beta^T v_i \tag{3.34}$$

for the evolution of the compartment probability vectors, where the Q matrices are

$$Q_\delta = \begin{bmatrix} 0 & 0 & 0 \\ 0 & \delta & -\delta \\ 0 & 0 & 0 \end{bmatrix}, Q_\beta = \begin{bmatrix} \beta & -\beta & 0 \\ 0 & 0 & 0 \\ 0 & 0 & 0 \end{bmatrix}, \tag{3.35}$$

based on (3.33).

We can denote the probabilities of being susceptible, infected, and recovered by S_i, I_i, and R_i, respectively; i.e., $v_i = [S_i, I_i, R_i]^T$. The evolution of these probabilities are then described as

$$\begin{aligned}
\begin{bmatrix} \dot{S}_i \\ \dot{I}_i \\ \dot{R}_i \end{bmatrix} &= - \begin{bmatrix} 0 & 0 & 0 \\ 0 & \delta & -\delta \\ 0 & 0 & 0 \end{bmatrix}^T \begin{bmatrix} S_i \\ I_i \\ R_i \end{bmatrix} \\
&\quad - (\sum_{j=1}^{N} a_{ij} I_j) \begin{bmatrix} \beta & -\beta & 0 \\ 0 & 0 & 0 \\ 0 & 0 & 0 \end{bmatrix}^T \begin{bmatrix} S_i \\ I_i \\ R_i \end{bmatrix} \\
&= \begin{bmatrix} \beta S_i (\sum_{j=1}^{N} a_{ij} I_j) \\ -\beta S_i (\sum_{j=1}^{N} a_{ij} I_j) - \delta I_i \\ \delta I_i \end{bmatrix}
\end{aligned} \tag{3.36}$$

Since, $S_i + I_i + R_i = 1$, the differential equation

$$\begin{aligned}
\frac{dI_i}{dt} &= -\delta I_i + \beta(1 - I_i - R_i)(\sum_{j=1}^{N} a_{ij} I_j) \\
\frac{dR_i}{dt} &= \delta I_i
\end{aligned} \tag{3.37}$$

is obtained for I_i and R_i, which is exactly the SIR N-Intertwined model in [51].

3.6.3 SAIS Model with Information Dissemination

Consider the SAIS model in Section 3.2.3, and assume that a susceptible agent becomes alert not only if there are infected individuals in its neighborhood, but also if there are alert individuals in the neighborhood. Also, assume that the latter happens with rate α. Moreover, assume that alert agents can go back to susceptible state with an un-alerting rate γ. The

interaction is through the contact network G_1, infection information dissemination network G_2, and the alert information dissemination network G_3. For both the contact network and the infection information dissemination network, '*alert*' is the influencer compartment. For the alert information dissemination network, '*alert*' is the influencer compartment. Hence, $L = 3$ and $q_1 = 2$, $q_2 = 2$, $q_3 = 3$.

From Fig. 3.8,

$$A_\delta = \begin{bmatrix} 0 & 0 & 0 \\ \delta & 0 & 0 \\ \gamma & 0 & 0 \end{bmatrix}, A_{\beta_1} = \begin{bmatrix} 0 & \beta_0 & 0 \\ 0 & 0 & 0 \\ 0 & \beta_a & 0 \end{bmatrix},$$
$$A_{\beta_2} = \begin{bmatrix} 0 & 0 & \kappa \\ 0 & 0 & 0 \\ 0 & 0 & 0 \end{bmatrix}, A_{\beta_3} = \begin{bmatrix} 0 & 0 & \alpha \\ 0 & 0 & 0 \\ 0 & 0 & 0 \end{bmatrix}. \tag{3.38}$$

Therefore, GEMF (3.26) suggests the following set of differential equations

$$\begin{aligned} \frac{dv_i}{dt} &= -Q_\delta^T v_i - \sum_{j=1}^{N} a_{1,ij} v_{j,2} Q_{\beta_1}^T v_i \\ &\quad - \sum_{j=1}^{N} a_{2,ij} v_{j,2} Q_{\beta_2}^T v_i - \sum_{j=1}^{N} a_{2,ij} v_{j,3} Q_{\beta_3}^T v_i \end{aligned} \tag{3.39}$$

for the evolution of the compartment probability vectors, where the Q matrices are

$$Q_\delta = \begin{bmatrix} 0 & 0 & 0 \\ -\delta & \delta & 0 \\ -\gamma & 0 & \gamma \end{bmatrix}, Q_{\beta_2} = \begin{bmatrix} \beta_0 & -\beta_0 & 0 \\ 0 & 0 & 0 \\ 0 & -\beta_a & \beta_a \end{bmatrix},$$
$$Q_{\beta_2} = \begin{bmatrix} \kappa & 0 & -\kappa \\ 0 & 0 & 0 \\ 0 & 0 & 0 \end{bmatrix}, Q_{\beta_3} = \begin{bmatrix} \alpha & 0 & -\alpha \\ 0 & 0 & 0 \\ 0 & 0 & 0 \end{bmatrix}, \tag{3.40}$$

according to (3.38).

Sahneh and Scoglio [6] used a model very similar to (3.39), where there are only two layers of graphs, namely, the contact network and the infection information dissemination network, to assess the effectiveness of the information networks in reducing the impact of an epidemic. A novel information dissemination metric is introduced that measures the impact of information network on improving the resilience of the system against epidemic spreading. The developed information dissemination metric leads to an analytical solution for the optimal topology of the information network to minimize the impact of an epidemic.

3.6.4 Multiple Interacting Pathogen Spreading

The problem of multiple pathogen spreading has recently attracted substantial attention (see e.g. [67–70]). Most models consider a full-cross immunity between pathogens, i.e., a node infected by one type of pathogen cannot be infected with any other type of pathogen at the same time. Beutel et al. [69] considered the case where the pathogens also have an interacting effect on each other and spread on the same contact network. In the model introduced by Marceau et al. [70], pathogens do not interact but each pathogen has a separate contact network. In the following, we apply GEMF to develop an individual-based bi-spreading SIS model for epidemic spreading of multiple interacting pathogens, very similar to [69], where

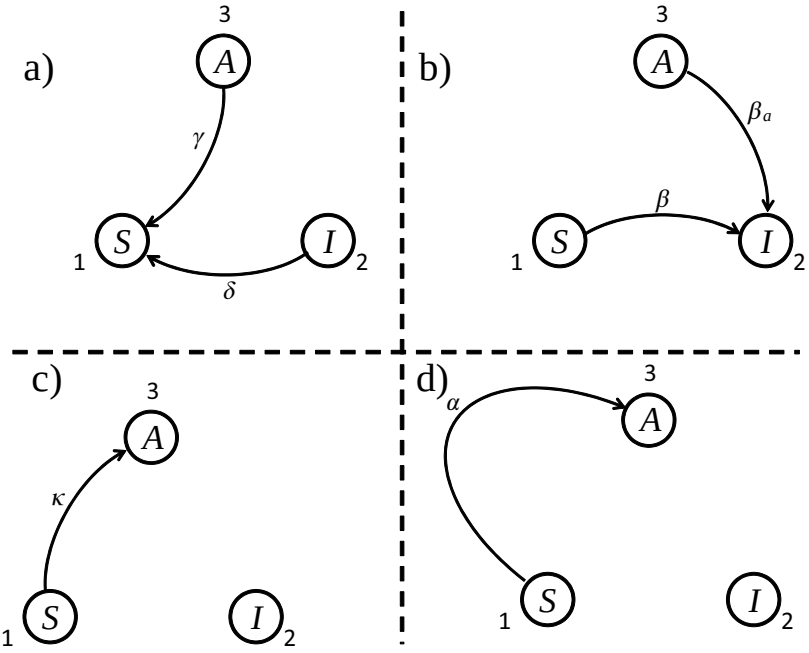

Figure 3.8: *Transition rate graphs in the SAIS model: a) nodal transition rate graph; nodes represent the three compartments* 'susceptible', 'infected', *and* 'alert', *directed link from I to S represents curing process weighted by the curing rate $\delta > 0$, directed link from A to S represents the un-alerting process weighted by the un-alerting rate $\gamma > 0$, and b) edge-based transition graph of the contact network layer G_c; directed link from S to I represents the infection process (edge-based transition) weighted by the infection rate $\beta > 0$, directed link from A to I represents the alerted infection process (edge-based transition) weighted by the alerted infection rate $\beta_a > 0$. For the contact network, the influencer compartment is $q_1 = 2$, i.e.,* 'infected'. *c) edge-based transition graph of the infection information dissemination network layer G_{iIDN}; directed link from S to A represents the alerting process weighted by the alerting rate $\kappa > 0$, For the infection information dissemination network, the influencer compartment is $q_1 = 2$, i.e.,* 'infected'. *d) edge-based transition graph of the alert information dissemination network layer G_{aIDN}; directed link from S to A represents the alerting process weighted by the alerting rate $\alpha > 0$, For the alert information dissemination network, the influencer compartment is $q_1 = 3$, i.e.,* 'alert'.

each pathogen, as in [70], has a different contact network.

Consider a spreading scenario where two pathogens A and B are spreading among a host population. The contact network for virus A is G_A, while B spreads through G_B. The transition rates for the pathogens depend on each other. For example, the infection process of a susceptible agent by pathogen A has different infection rate if it is already infected by B versus being susceptible to B. In general, we assume the transition rates are $\delta_{A0}, \delta_{A1}, \beta_{A0}, \beta_{A1}$, and $\delta_{B0}, \delta_{B1}, \beta_{B0}, \beta_{B1}$. For example, if an agent is infected by A but is not infected by B, then it recovers by rate δ_{A0}. Where as, if it is also infected by B, disease A gets cured by rate δ_{A1}. Similar arguments apply for other rate terms.

For this spreading scenario, $M = 4$ compartments can be defined to model the problem. Agent i is in compartment 1 if it is susceptible to both A and B. It is 2 if it is susceptible to A but infected by B. It is 3 if infected by A and susceptible to B. And finally, it is 4 if it is infected by both A and B. The nodal and edge-based transitions are shown in Fig. 3.9.

It follows from Fig. 3.9,

$$A_\delta = \begin{bmatrix} 0 & 0 & 0 & 0 \\ \delta_{B0} & 0 & 0 & 0 \\ \delta_{A0} & 0 & 0 & 0 \\ 0 & \delta_{A1} & \delta_{B1} & 0 \end{bmatrix}, \; A_{\beta_A} = \begin{bmatrix} 0 & 0 & \beta_{A0} & 0 \\ 0 & 0 & 0 & \beta_{A1} \\ 0 & 0 & 0 & 0 \\ 0 & 0 & 0 & 0 \end{bmatrix},$$

$$A_{\beta_B} = \begin{bmatrix} 0 & \beta_{B0} & 0 & 0 \\ 0 & 0 & 0 & 0 \\ 0 & 0 & 0 & \beta_{B1} \\ 0 & 0 & 0 & 0 \end{bmatrix}. \tag{3.41}$$

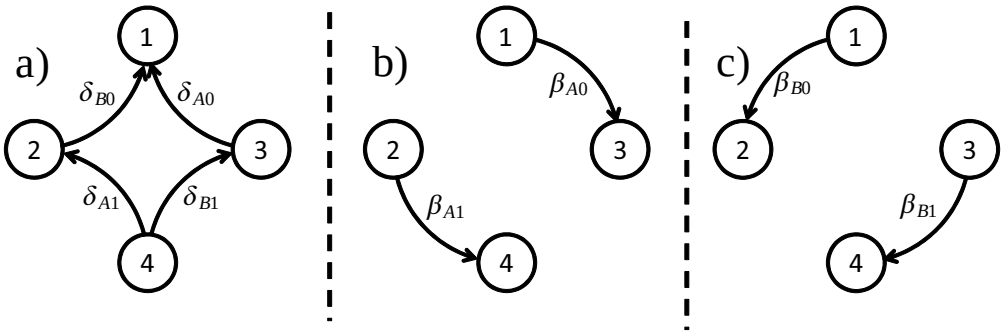

Figure 3.9: *Transition rate graphs in the SIS-type interacting disease propagation: a) nodal transition rate graph; nodes represent the four compartments '*$\mathrm{S}_A\mathrm{S}_B$*', '*$\mathrm{S}_A\mathrm{I}_B$*', , '*$\mathrm{I}_A\mathrm{S}_B$*', and '*$\mathrm{I}_A\mathrm{I}_B$*', directed links from* $\mathrm{I}_A\mathrm{S}_B$ *to* $\mathrm{S}_A\mathrm{S}_B$ *and from* $\mathrm{I}_A\mathrm{I}_B$ *to* $\mathrm{S}_A\mathrm{I}_B$ *represents curing process for virus A weighed with curing rates* δ_{A0} *and* δ_{A1}*, respectively, and the directed links from* $\mathrm{S}_A\mathrm{I}_B$ *to* $\mathrm{S}_A\mathrm{S}_B$ *and from* $\mathrm{I}_A\mathrm{I}_B$ *to* $\mathrm{I}_A\mathrm{S}_B$ *represents curing process for virus B weighted by the curing rates* δ_{B0} *and* δ_{B1}*, respectively, and b) edge-based transition graph of the contact network layer* G_A *for virus A; directed link from* $\mathrm{S}_A\mathrm{S}_B$ *to* $\mathrm{I}_A\mathrm{S}_B$ *and from* $\mathrm{S}_A\mathrm{I}_B$ *to* $\mathrm{I}_A\mathrm{I}_B$ *represents infection process for virus A weighed with infection rates* β_{A0} *and* β_{A1}*, respectively. For the contact network* G_A*, the influencer compartment is* $q_A = 3, 4$*, i.e.,* $\mathrm{I}_A\mathrm{S}_B$ *and* $\mathrm{I}_A\mathrm{I}_B$*. c) edge-based transition graph of the contact network layer* G_B *for virus B; directed link from* $\mathrm{S}_A\mathrm{S}_B$ *to* $\mathrm{S}_A\mathrm{I}_B$ *and from* $\mathrm{I}_A\mathrm{S}_B$ *to* $\mathrm{I}_A\mathrm{I}_B$ *represents infection process for virus B weighed with infection rates* β_{B0} *and* β_{B1}*, respectively. For the contact network* G_B*, the influencer compartment is* $q_B = 2, 4$*, i.e.,* $\mathrm{S}_A\mathrm{I}_B$ *and* $\mathrm{I}_A\mathrm{I}_B$*.*

Therefore, GEMF (3.26) suggests the following set of differential equations

$$\dot{v}_i = -Q_\delta^T v_i - \sum_{j=1}^{N} a_{A,ij}(v_{j,3} + v_{j,4}) Q_{\beta_A}^T v_i - \sum_{j=1}^{N} a_{B,ij}(v_{j,2} + v_{j,4}) Q_{\beta_B}^T v_i \tag{3.42}$$

for the evolution of the compartment probability vectors

$$Q_\delta = \begin{bmatrix} 0 & 0 & 0 & 0 \\ -\delta_{B0} & \delta_{B0} & 0 & 0 \\ -\delta_{A0} & 0 & \delta_{A0} & 0 \\ 0 & -\delta_{A1} & -\delta_{B1} & \delta_{A1} + \delta_{B1} \end{bmatrix},$$

$$Q_{\beta_A} = \begin{bmatrix} \beta_{A0} & 0 & -\beta_{A0} & 0 \\ 0 & \beta_{A1} & 0 & -\beta_{A1} \\ 0 & 0 & 0 & 0 \\ 0 & 0 & 0 & 0 \end{bmatrix},$$

$$Q_{\beta_B} = \begin{bmatrix} \beta_{B0} & -\beta_{B0} & 0 & 0 \\ 0 & 0 & 0 & 0 \\ 0 & 0 & \beta_{B1} & -\beta_{B1} \\ 0 & 0 & 0 & 0 \end{bmatrix}. \tag{3.43}$$

3.7 Conclusion

Inspired by existing individual-based epidemic models, we propose the generalized epidemic mean-field (GEMF) model. While using the same common assumptions of most of the existing individual-based epidemic models, GEMF is capable of modeling more complex

scenarios with multiple compartment and multiple network layers. The set of differential equations that fully describes the time evolution of the compartment occupancy probabilities has M^N equations. Even though the system is linear, it is both computationally and analytically intractable, managed through a mean-field type approximation by a set of MN nonlinear differential equations. The latter system, referred to as GEMF, has a simple structure. It is characterized by the Laplacian of the transition rate graphs and the elements of the adjacency matrices of the network layers. A systematic procedure for developing the model is proposed that culminates in the GEMF governing equations (3.26). The GEMF model is rigorous, allows analytical tractability, and is simple to apply to many specific spreading processes, as shown in the several examples presented in this study. We believe that the GEMF framework has the potential to allow the development of many different and novel individual-based epidemic models considering new compartments and multiple complex interaction structures.

3.8 Appendix: Derivation of Exact Markov Equation

In this section, we explicitly derive the expression for $\mathbf{Q}$ in (3.22). The idea is to derive the expression for $E[X(t+\Delta t)]$ as a function of $E[X(t)]$. For this, first we find the expression for the conditional expectation $E[X(t+\Delta t)|X(t)]$. Then, the expression for $E[X(t+\Delta t)]$ is found by averaging out the conditional. For small values of Δt, we can assume that only one transition happens at each time step, i.e., starting at network state at time t, the network state can only go to a new state at time $t+\Delta t$ for which only the state of a single node has been changed. Given the network state $X(t) = e_Z$, state $x_i(t) = e_{z_i}$ of each agent i can be determined and we have

$$e_Z = e_{z_1} \otimes \cdots \otimes e_{z_N}. \tag{3.44}$$

Since only at most one single node can make a transition, the conditional expected value of the network state at time $t + \Delta t$ is

$$E[X(t+\Delta t)|X(t) = e_Z] = \sum\nolimits_{i=1}^{N} e_{z_1} \otimes \cdots \otimes E[x_i(t+\Delta t)|X(t) = e_Z] \otimes \cdots \otimes e_{z_N}, \quad (3.45)$$

where from (3.17), the expression for $E[x_i(t+\Delta t)|X(t) = e_Z]$ is

$$\begin{aligned} E[x_i(t+\Delta t)|X(t) = e_Z] = & -Q_\delta^T e_{z_i} \Delta t \\ & - \sum_{l=1}^{L} \sum_{j=1}^{N} a_{l,ij} 1_{\{z_j = q_l\}} Q_{\beta_l}^T e_{z_i} \Delta t \\ & + e_{z_i}(t) + \epsilon(\Delta t). \end{aligned} \quad (3.46)$$

Averaging all of the possible network states yields the expected value of the network state at time $t + \Delta t$

$$\begin{aligned} E[X(t+\Delta t)] &= \sum_{Z=1}^{M^N} E[X(t+\Delta t)|X(t) = e_Z] \Pr[X(t) = e_Z] \\ &= \sum_{Z=1}^{M^N} (\sum\nolimits_{i=1}^{N} e_{z_1} \otimes \cdots \otimes E[x_i(t+\Delta t)|X(t) = e_Z] \otimes \cdots \otimes e_{z_N}) \Pr[X(t) = e_Z]. \end{aligned} \quad (3.47)$$

Substituting for $E[x_i(t+\Delta t)|X(t) = e_Z]$ from (3.46), $E[X(t+\Delta t)]$ is deduced to be

$$E[X(t+\Delta t)] = -\mathbf{Q}_\delta^T E[X(t)] \Delta t - \sum_{l=1}^{L} \mathbf{Q}_{\beta_l}^T E[X(t)] \Delta t + E[X(t)] + o(\Delta t), \quad (3.48)$$

where

$$\mathbf{Q}_\delta = \sum\nolimits_{i=1}^{N} I_{M \times M} \otimes \cdots \otimes Q_\delta \otimes \cdots \otimes I_{M \times M},$$

and $\mathbf{Q}_{\beta_l}$ is such that its $Z-$th column is

$$\text{col}(\mathbf{Q}_{\beta_l}, Z) = \sum\nolimits_{i=1}^{N} e_{z_1} \otimes \cdots \otimes (\sum_{j=1}^{N} a_{l,ij} 1_{\{z_j = q_l\}} Q_{\beta_l} e_{z_i}) \otimes \cdots \otimes e_{z_N}. \tag{3.49}$$

By letting $\Delta t \to 0$ in (3.48), the time evolution of $E[X]$ can be fully described by

$$\frac{d}{dt} E[X] = -\mathbf{Q}^T E[X], \tag{3.50}$$

where $\mathbf{Q}$ is defined as

$$\mathbf{Q} = \mathbf{Q}_\delta + \sum_{l=1}^{L} \mathbf{Q}_{\beta_l}. \tag{3.51}$$

The differential equation (3.50) is the exact Markov equation.

Part II

Problems in Interconnected Multilayer Networks

Chapter 4

Effect of Coupling on the Epidemic Threshold in Interconnected Complex Networks

4.1 Introduction

Understanding spreading processes in interconnected networks is a major challenge of complex networks, which has recently attracted substantial attention [34–37]. A problem of special interest is how interconnection of network influences robustness measures like epidemic threshold. Dickison et al. [35] studied two interconnected networks following the standard configuration model and interconnected with their own intranetwork, and identified and quantitated strongly-coupled networks and weakly coupled networks. In strongly-coupled epidemics, either the epidemic invades both networks or not spread at all. In contrast, in weakly-coupled network systems, an intermediate scenario can happen where an epidemic spreads in one network but does not invade the coupled network. Saumell-Mendiola et al. [36] proposed heterogeneous mean-field approach to study epidemics on two interconnected networks, and showed cases where small number of interconnection among two net-

works exhibited endemic state. Results for epidemic threshold in interconnected networks are limited to homogeneous mixing populations and degree distribution arguments, and analysis of epidemics on interconnected network with no approximation on the underlying network is missing in the literature.

The objective of this chapter is to study the epidemic threshold in interconnected networks, with arbitrary topology. In particular, we study the spreading process of a susceptible-infected-susceptible (SIS) type epidemic model in an interconnected network of two generic graphs with a generic interconnection. In our model, the epidemic-related parameters, i.e., infection rates and recovery rates, are different and independent from one network to the other. This is crucial to our interconnected network problem formulation, since a generalization of epidemic threshold to interconnected systems must be considerate of multiple possible degrees of freedom (DOF) inherent in such networks. For example, in for a zoonotic disease one may look for critical infection rate in human population, which necessarily will be a function of infection rate in the animal population and interactions between the two populations.

For two coupled networks, our idea is that the concept of epidemic threshold value extends to *epidemic threshold curve*. Taking into account multiple DOFs for interconnected networks is critical for a more realistic and practical threshold concept, as numerous infrastructures function in a distributed manner. As a classic example, autonomous systems forming the Internet are under the control of different administrative entities.

The main contribution of this study is introduction of epidemic threshold curve. Using bifurcation theory and spectral graph theory, we find the epidemic threshold of one network as a function of the effective infection rate of the other coupled network and adjacency matrices of each graph and their interconnection, and provide a quantitative measure to distinguish weak and strong interconnection topologies. Importantly, we make use of spectral analysis to analyze epidemic spreading in interconnected networks with generic arbitrary topology.

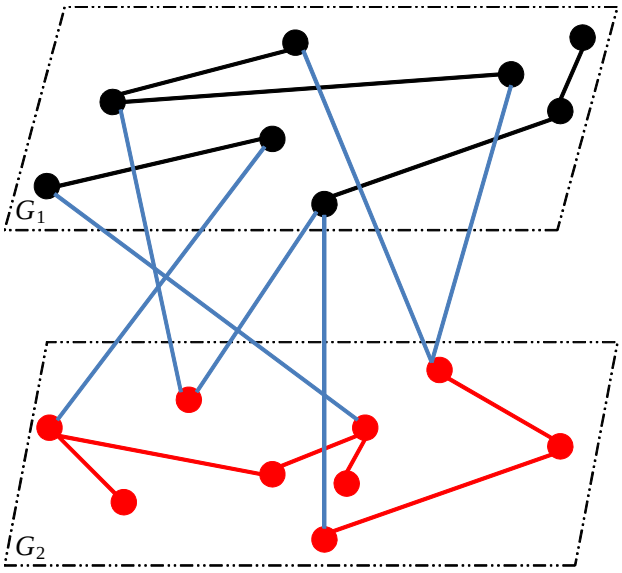

Figure 4.1: *Schematics of the coupling between graphs G_1 (in black) and G_2 (in red) contact networks. The blue links represent the coupling between the nodes of the two graphs. G_1 and G_2 are not necessarily connected. However, the whole interconnected network is connected.*

4.2 Modeling SIS Spreading in Interconnected Networks

Consider two groups of agents of sizes N_1 and N_2. In order to facilitate the subsequent developments, we label the agents of the first graph G_1 from 1 to N_1, and the agents of the second graph G_2 from $N_1 + 1$ to $N_1 + N_2$. The collective adjacency matrix $\boldsymbol{A}$, defined as

$$\boldsymbol{A} \triangleq \begin{bmatrix} A_{11} & A_{12} \\ A_{21} & A_{22} \end{bmatrix} \in \mathbb{R}^{(N_1+N_2)\times(N_1+N_2)}, \tag{4.1}$$

represents the contact between all of the agents. Since the contact topology in this study is undirected, A_{11} and A_{22} are symmetric matrices and $A_{21} = A_{12}^T$. According to definition (4.1), agent i is connected to agent j iff $(\boldsymbol{A})_{ij} = 1$. A schematic of the interconnected contact network of the agents is represented in Fig. 4.1.

The SIS spreading model over a single graph described in Chapter 2 can be generalized

in the following way. The curing rate for agents of graphs G_1 and G_2 are $\delta_1 \in \mathbb{R}^+$ and $\delta_2 \in \mathbb{R}^+$, respectively. The infection rates $\beta_{11}, \beta_{12}, \beta_{21}, \beta_{22} \in \mathbb{R}^+$ are such that a susceptible agent of graph G_s receives the infection from an infected agent in $G_{s'}$ with the infection rate $\beta_{ss'}$, for $s, s' \in \{1, 2\}$. Similar to the networked SIS model (2.6), the infection probabilities of the agents evolve according to the following set of differential equations:

$$\dot{p}_i = (1 - p_i)\{\beta_{11} \sum_{j=1}^{N_1} a_{ij} p_j + \beta_{12} \sum_{j=N_1+1}^{N_1+N_2} a_{ij} p_j\} - \delta_1 p_i, \tag{4.2}$$

for $i \in \{1, ..., N_1\}$, and

$$\dot{p}_i = (1 - p_i)\{\beta_{21} \sum_{j=1}^{N_1} a_{ij} p_j + \beta_{22} \sum_{j=N_1+1}^{N_1+N_2} a_{ij} p_j\} - \delta_2 p_j, \tag{4.3}$$

for $i \in \{N_1 + 1, ..., N_1 + N_2\}$.

Since infection process is the result of interaction between a pair of agents, it is reasonable to assume that $\beta_{11}, \beta_{12}, \beta_{21}, \beta_{22}$ are not completely independent of each other. In this study, we make the following assumption:

Assumption 2. *The following constraint exists among the infection rates*

$$\beta_{11}\beta_{22} = \alpha^2 \beta_{12}\beta_{21}, \tag{4.4}$$

where $\alpha \in \mathbb{R}^+$ is a positive scalar accounting for heterogeneity of contacts within a single network and across the two networks.

The motivation for the above assumption is that the infection rate in the SIS model (2.6) can be considered as $\beta = \mu\pi$ where $\mu \in \mathbb{R}^+$ is the rate that an infected agents transmits the infection and $\pi \in [0, 1]$ is the probability that a susceptible agent receives a transmitted infection. Similarly, for β_{11}, β_{12}, β_{21}, β_{22} in (4.2) and (4.3) we can consider $\beta_{11} = \mu_1\pi_1$ and $\beta_{22} = \mu_2\pi_2$ within each network, and $\beta_{12} = \alpha\mu_1\pi_2, \beta_{21} = \alpha\mu_2\pi_1$ across the two networks. Hence, (4.4) is justified. Furthermore, in order to facilitate the subsequent analysis, we

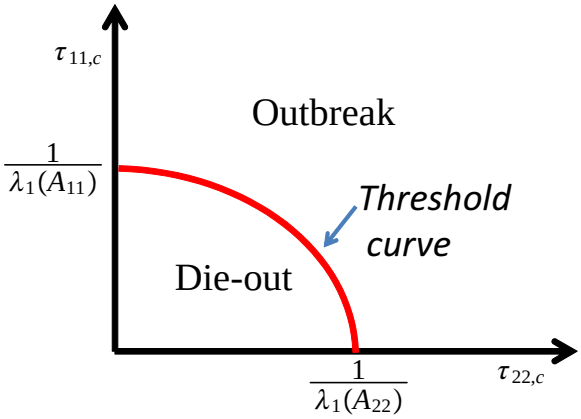

Figure 4.2: *Schematics of epidemic threshold curve.*

define

$$\tau_{11} \triangleq \frac{\beta_{11}}{\delta_1}, \tau_{12} \triangleq \frac{\beta_{12}}{\delta_1}, \tau_{21} \triangleq \frac{\beta_{21}}{\delta_2}, \tau_{22} \triangleq \frac{\beta_{22}}{\delta_2}. \tag{4.5}$$

4.3 Main Results

4.3.1 Problem Statement

Suppose that agents of graph G_1 are connected to agents of graph G_2, and the overall contact among the agents is determined by $\boldsymbol{A}$ defined in (4.1). For given values (τ_{11}, τ_{22}), either all nodes eventually become healthy, or there is an endemic state where all nodes have positive infection probabilities due to connectivity of the interconnected network $\boldsymbol{G}$. We are interested in finding the epidemic threshold curve $(\tau_{11,c}, \tau_{22,c})$ which separates these two regions. Comparing (2.6) and (4.2), it can be concluded that interconnection increases the probability of infection. This conclusion is actually intuitive: when interconnected with other agents, there is more possibility to receive the infection. Therefore, $\tau_{11,c} < 1/\lambda_1(A_{11})$, $\tau_{22,c} < 1/\lambda_1(A_{22})$. Figure 4.2 shows an illustration of the epidemic threshold curve.

Our approach to find the epidemic threshold curve is to hold τ_{22} constant and then to find a threshold value $\tau_{11,c}$ such that for effective infection rate $\tau_{11} > \tau_{11,c}$ the steady-state infection probabilities take positive values. Therefore, $\tau_{11,c}$ becomes a function of

τ_{22}. In order for existence of such a threshold value, τ_{22} must be such that if there is no interconnection, infection cannot survive in G_2, i.e.,

$$\tau_{22} < \frac{1}{\lambda_1(A_{22})}. \tag{4.6}$$

4.3.2 Equation for Epidemic Threshold

We use bifurcation theory to find the epidemic threshold. From (4.2) and (4.3), the equilibrium points of the infection probabilities satisfy the following set of algebraic equations

$$\frac{p_i^*}{1-p_i^*} = \tau_{11} \sum_{j=1}^{N_1} a_{ij} p_j^* + \tau_{12} \sum_{j=N_1+1}^{N_1+N_2} a_{ij} p_j^*, \tag{4.7}$$

for $i \in \{1, ..., N_1\}$, and

$$\frac{p_i^*}{1-p_i^*} = \tau_{21} \sum_{j=1}^{N_1} a_{ij} p_j^* + \tau_{22} \sum_{j=N_1+1}^{N_1+N_2} a_{ij} p_j^*, \tag{4.8}$$

for $i \in \{N_1+1, ..., N_1+N_2\}$.

Lemma 1. *If the overall contact network is connected, the steady-state values of the infection probabilities are either zero for all of the agents or absolutely positive for each agent.*

Proof. The steady-state values for the infection satisfies (4.7) and (4.8). Therefore, $p_i^* = 0$ for $\forall i \in \{1, ..., N_1+N_2\}$ is a solution for the steady-state infection probabilities. Suppose there exists a node j such that $p_j^* > 0$. According to (4.7) and (4.8), for any node i that is a neighbor of node j, i.e., $a_{ij} \neq 0$, the steady-state infection probability is

$$p_i^* = \frac{\tau_{11} \sum_{j=1}^{N_1} a_{ij} p_j^* + \tau_{12} \sum_{j=N_1+1}^{N_1+N_2} a_{ij} p_j^*}{1 + \tau_{11} \sum_{j=1}^{N_1} a_{ij} p_j^* + \tau_{12} \sum_{j=N_1+1}^{N_1+N_2} a_{ij} p_j^*}, \tag{4.9}$$

if $i \in \{1, ..., N_1\}$ and

$$p_i^* = \frac{\tau_{21} \sum_{j=1}^{N_1} a_{ij} p_j^* + \tau_{22} \sum_{j=N_1+1}^{N_1+N_2} a_{ij} p_j^*}{1 + \tau_{21} \sum_{j=1}^{N_1} a_{ij} p_j^* + \tau_{22} \sum_{j=N_1+1}^{N_1+N_2} a_{ij} p_j^*},$$

if $i \in \{N_1 + 1, ..., N_1 + N_2\}$, which is positive because $\sum_{j=1}^{N_1} a_{ij} p_j^* > 0$ or $\sum_{j=N_1+1}^{N_1+N_2} a_{ij} p_j^* > 0$. Same procedure applies to the neighbors of node i, and so on. Hence, if the overall contact network is connected and at least one of the agents have nonzero infection probability, then $p_i^* > 0$ for all $i \in \{1, ..., N_1 + N_2\}$. □

Before the epidemic threshold, origin is the only solution to (4.7) and (4.8). Epidemic threshold is the critical value $\tau_{11,c}$ such that a second equilibrium point starts leaving the origin. A corollary of Lemma 1 is that the epidemic threshold $\tau_{11,c}$ is such that $p_i^* = 0$ and $\frac{\partial p_i^*}{\partial \tau_{11}} > 0$ for every $i \in \{1, ..., N_1 + N_2\}$. Taking the right derivative of (4.7) and (4.8) with respect to τ_{11} at $\tau_{11} = \tau_{11,c}$ and $p_i^* = 0$ yields

$$\frac{\partial p_i^*}{\partial \tau_{11}} = \tau_{11,c} \sum_{j=1}^{N_1} a_{ij} \frac{\partial p_j^*}{\partial \tau_{11}} + \tau_{12} \sum_{j=N_1+1}^{N_1+N_2} a_{ij} \frac{\partial p_j^*}{\partial \tau_{11}}, i \in \{1, ..., N_1\}, \tag{4.10}$$

$$\frac{\partial p_i^*}{\partial \tau_{11}} = \tau_{21} \sum_{j=1}^{N_1} a_{ij} \frac{\partial p_j^*}{\partial \tau_{11}} + \tau_{22} \sum_{j=N_1+1}^{N_1+N_2} a_{ij} \frac{\partial p_j^*}{\partial \tau_{11}}, i \in \{N_1 + 1, ..., N_1 + N_2\}. \tag{4.11}$$

Defining $V_1 \triangleq [\frac{\partial p_1^*}{\partial \tau_{11}}, ..., \frac{\partial p_{N_1}^*}{\partial \tau_{11}}]^T$ and $V_2 \triangleq [\frac{\partial p_{N_1+1}^*}{\partial \tau_{11}}, ..., \frac{\partial p_{N_1+N_2}^*}{\partial \tau_{11}}]^T$, the equations (4.10) and (4.11) can be equivalently expressed in the collective form as

$$\begin{bmatrix} \tau_{11,c} A_{11} & \tau_{12} A_{12} \\ \tau_{21} A_{12}^T & \tau_{22} A_{22} \end{bmatrix} \begin{bmatrix} V_1 \\ V_2 \end{bmatrix} = \begin{bmatrix} V_1 \\ V_2 \end{bmatrix}. \tag{4.12}$$

The critical value of the effective infection rates are those for which the above equation has a positive solution.

According to Assumption 4.6, if V_1 is positive then $V_2 = \tau_{21}(I - \tau_{22} A_{22})^{-1} A_{12}^T V_1$ exists

and is non-negative. Therefore, (4.12) is equivalently expressed as

$$HV_1 = V_1 \tag{4.13}$$

where H is defined as

$$H \triangleq \tau_{11,c} A_{11} + \tau_{21}\tau_{12} A_{12}(I - \tau_{22}A_{22})^{-1} A_{12}^T. \tag{4.14}$$

4.3.3 Effect of Coupling on Epidemic Threshold

The rest of the analysis is to find the threshold value $\tau_{11,c}$ such that (4.13) has a positive solution for V_1. The following results facilitate the proof of Theorem 2, which is the main result in this work.

Definition 1. *A path from node $i \in G_1$ to node j is of class $(l_1, ..., l_s)$, with non-negative integers $l_1, ..., l_s$, if it first take l_1 steps in G_1 then goes to G_2 and take l_2 steps in G_2 then goes back to G_1 and takes l_3 steps in G_1 and so on until it takes the last l_s steps to reach j.*

It can be inferred from the above definition that a path of class $(l_1, ..., l_s)$, has length $L = (s-1) + l_1 + \cdots + l_s$.

Lemma 2. *The number of paths of length L from node $i \in G_1$ to node j corresponding to the class $(l_1, ..., l_s)$ is:*

- *the (i,j)-th entry of $A_{11}^{l_1} A_{12} A_{12}^{l_2} A_{21} \cdots A_{21} A_1^{l_s}$, if $j \in \{1, ..., N_1\}$,*
- *the $(i, j-N_1)$-th entry of $A_{11}^{l_1} A_{12} A_{12}^{l_2} A_{21} \cdots A_{12} A_2^{l_s}$, if $j \in \{N_1+1, ..., N_1+N_2\}$,*

where $A_{11}^0 = I_{N_1 \times N_1}$ and $A_{22}^0 = I_{N_2 \times N_2}$, by convention.

Proof. We use induction for the proof. For $L = 1$, the number of paths from node i to j is equal to 1 if i is connected to j, and is zero otherwise. If $j \in \{1, ..., N_1\}$, path of length

$L = 1$ corresponds to the class (1). Therefore, the number of paths from node i to j is equal to the (i, j)-th entry of A_{11}. If $j \in \{N_1 + 1, ..., N_1 + N_2\}$, then a path of length $L = 1$ corresponds to the class $(0, 0)$. In this case, the number of paths from node i to j is equal to the $(i, j - N_1)$-th entry of $A_{12} = A_1^0 A_{12} A_2^0$. Therefore for $L = 1$, the Lemma is correct. Assume that for $L = L_0$ the lemma statement is correct. Consider the first case where $j \in \{1, ..., N_1\}$. A path of length $L = L_0 + 1$ from i to j is either of the class $(l_1, ..., l_s + 1)$ or $(l_1, ..., l_s, 0)$. Such a path can be constructed from paths of length L_0 from i to k of the class $(l_1, ..., l_s)$ then connected to node j from node k. If the path from i to j is of class $(l_1, ..., l_s + 1)$, then the number of such paths is

$$\sum_{k=1}^{N_1} (A_{11}^{l_1} A_{12} A_{12}^{l_2} A_{21} \cdots A_{21} A_1^{l_s})_{ik} (A_1)_{kj} = A_{11}^{l_1} A_{12} A_{12}^{l_2} A_{21} \cdots A_{21} A_1^{l_s+1}.$$

If the path from i to j is of class $(l_1, ..., l_s, 0)$, then the number of such paths is

$$\sum_{k=N_1+1}^{N_1+N_2} (A_{11}^{l_1} A_{12} A_{12}^{l_2} A_{21} \cdots A_{21} A_1^{l_s})_{i(k-N_1)} (A_{12})_{(k-N_1)j}$$
$$= A_{11}^{l_1} A_{12} A_{12}^{l_2} A_{21} \cdots A_{21} A_1^{l_s} A_{12} = A_{11}^{l_1} A_{12} A_{12}^{l_2} A_{21} \cdots A_{21} A_1^{l_s} A_{12} A_2^0.$$

Hence, the theorem statement is correct for $L = L_0 + 1$ and $j \in \{1, ..., N_1\}$. Similar procedure can be followed to conclude the same result for $j \in \{N_1 + 1, ..., N_1 + N_2\}$. □

Theorem 1. *The matrix H_T defined as*

$$H_T \triangleq A_{11} + \alpha^2 \tau_{22} A_{12} (I - \tau_{22} A_{22})^{-1} A_{12}^T. \tag{4.15}$$

is irreducible if the overall coupled network is connected.

Proof. We show that

$$\bar{H}_T \triangleq A_{11} + A_{12} A_{12}^T + \sum_{k=1}^{N_2-1} A_{12} A_{22}^k A_{12}^T \tag{4.16}$$

is irreducible. If $\bar{H}_T$ is shown to be irreducible, then $A_{11}+\alpha^2\tau_{22}A_{12}A_{12}^T+\alpha^2\tau_{22}\sum_{k=1}^{N_2-1}\tau_{22}^k A_{12}A_2^kA_{12}^T$ is irreducible. And hence, $H_T = A_{11} + \alpha^2\tau_{22}A_{12}A_{12}^T + \alpha^2\tau_{22}\sum_{k=1}^{\infty}\tau_{22}^k A_{12}A_2^kA_{12}^T = A_{11} + \alpha^2\tau_{22}A_{12}(I-\tau_{22}A_{22})^{-1}A_{12}^T$ is irreducible and the proof is completed. If G_1 is a connected graph, then A_{11} and as consequence $\bar{H}_T$ is irreducible. Assume that A_{11} does not represent a connected graph. Therefore, there exists a pair i, j such that there is no path between them in G_1. However, since the whole interconnected network is connected, there exists a path from i to j. Suppose, the path is of class $(l_{1,1}, l_{2,1}, l_{1,2}, l_{2,2}, ..., l_{2,s}, l_{1,s+1})$, i.e., it takes $l_{1,1}$ steps in G_1 to reach vertex k_1^{out}, then it leaves G_1 and enters G_2 and takes $l_{2,1}$ steps in G_2, then enters G_1 at vertex k_1^{in}. This process goes on until it takes $l_{1,s+1}$ steps in G_1 from k_s^{in} to reach vertex j. Matrix $\bar{H}_T$ is proved to be irreducible if we show that entry (k_u^{out}, k_u^{in}) of $\bar{H}_T$ is positive for $u = 1, ..., s$. Since, there is path from k_u^{out} to k_u^{in} which is of the class $(0, l_{2,u}, 0)$, the (k_u^{out}, k_u^{in})-th entry of $A_{12}A_{22}^{l_{2,u}}A_{12}^T \geq 1$,because it is the number of such paths according to Lemma 2. As a consequence, (k_u^{out}, k_u^{in})-th entry of $\bar{H}_T$ is positive and therefore $\bar{H}_T$ is irreducible. Hence, the proof is completed. □

Theorem 2. *The epidemic threshold $\tau_{11,c}$, for which the equation (4.12) has positive solution for V_1 and V_2, is the inverse of the spectral radius of H_T defined in (4.15), i.e.,*

$$\tau_{11,c} = \frac{1}{\lambda_1(H_T)}, \tag{4.17}$$

Proof. According to (4.4) and the definitions (4.5), we have

$$\tau_{21}\tau_{12} = \alpha^2\tau_{11,c}\tau_{22}. \tag{4.18}$$

Substituting for $\tau_{21}\tau_{12}$ in (4.14), equation (4.13) gets the form

$$\tau_{11,c}H_TV_1 = V_1, \tag{4.19}$$

where H_T is defined in (4.15). In order for (4.19) to have solutions, $\tau_{11,c}$ must be the inverse

of one of the eigenvalues of H_T. However, the corresponding eigenvector V_1 must have all positive entries. Since, according to Theorem 1, H_T is an irreducible matrix, Perron–Frobenius Theorem guarantees that such V_1 exists and is equal to the dominant eigenvector of H_T. Therefore, $\tau_{11,c}$ is equal to $1/\lambda_1(H_T)$. □

4.3.4 Quantitating the Interconnection Topology

Theorem 1 derives the value of the epidemic threshold $\tau_{11,c}$ of G_1 as a function of the effective infection rate τ_{22} of G_2 and adjacency matrices of each graph and their interconnection. If $\tau_{22} = 0$, then $\tau_{11,c} = 1/\lambda_1(A_{11})$, which is the known result in [21] for a single contact network. Furthermore, for $\tau_{22} \to \lambda_1(A_{22})$, we claim that $\tau_{11,c} \to 0$. The reason is, in this case, an arbitrarily small value of τ_{11} will make the the probability of infection in G_2 non-zero, and therefore according to Lemma 1, the probability of infection in G_1 also becomes positive. Despite the extreme cases of $\tau_{22} = 0$ and $\tau_{22} \to \lambda_1(A_{22})$, the value of $\tau_{11,c}$ as function of τ_{22} can be qualitatively different depending on the interconnection topology.

The numerical simulations in Section 4.4 illustrates three possible curves of $\tau_{11,c}$ as a function of τ_{22}, as shown in Fig. 4.3. Here, the blue curve belongs to the case of *weak interconnection* between the two graphs. As can be seen, the decrease in the epidemic threshold $\tau_{11,c}$ is very slow for small values of τ_{22}, while there is a quite sharp drop in the values of $\tau_{11,c}$ as $\tau_{22} \to \lambda_1(A_{22})$. In this case, the infection in G_1 starts to grow mainly as the result of receiving the infection from G_2. For *strong interconnection* topology, shown by the green curve, the value of $\tau_{11,c}$ decreases quickly even for very small values of τ_{22}. In this case, the infection in G_1 starts to grow most dominantly because of the increased effective contact among nodes of G_1. The red curve is an intermediate between the two spreading modes.

Theorem 3. *The derivative* $\frac{d\tau_{11,c}}{d\tau_{22}}$ *at* $\tau_{22}=0$ *is*

$$\left.\frac{d\tau_{11,c}}{d\tau_{22}}\right|_{\tau_{22}=0}=\frac{\alpha^2\left\|A_{12}^T x_1\right\|_2^2}{\lambda_1^2(A_{11})}, \tag{4.20}$$

where x_1 *is the eigenvector of* A_{11} *belonging to* $\lambda_1(A_{11})$.

Proof. The matrix H_T from (4.15) can be written as

$$H_T \triangleq A_{11}+\alpha^2\tau_{22}A_{12}A_{12}^T+o(\tau_{22}).$$

Therefore, taking the derivative of (4.19) with respect to τ_{22} at $\tau_{22}=0$ yields

$$\frac{d\tau_{11,c}}{d\tau_{22}}A_{11}x_1+\frac{1}{\lambda_1(A_{11})}(\alpha^2A_{12}A_{12}^T)x_1+(\frac{1}{\lambda_1(A_{11})}A_{11}-I)\frac{dV_1}{d\tau_{22}}=0. \tag{4.21}$$

Multiplying (4.21) by x_1^T from left, and considering that $x_1^TA_{11}x_1=\lambda_1(A_{11})$ and $x_1^T(\frac{1}{\lambda_1(A_{11})}A_{11}-I)=0$ for A_{11} is symmetric and $x_1$is the normalized eigenvector of A_{11}, (4.21) becomes

$$\lambda_1(A_{11})\frac{d\tau_{11,c}}{d\tau_{22}}+\frac{\alpha^2}{\lambda_1(A_{11})}(A_{12}^Tx_1)^T(A_{12}^Tx_1)=0. \tag{4.22}$$

Hence, $\frac{d\tau_{11,c}}{d\tau_{22}}$ is found to be (4.20). □

Remark 1. *According to (4.20) and the proceeding arguments, we can define interconnection topology measure*

$$\Omega\left(G_1,G_2\right)\triangleq\frac{\alpha^2\left\|A_{12}^Tx_1\right\|_2^2}{\lambda_1(A_{11})\lambda_1(A_{22})}. \tag{4.23}$$

to distinguish weak and strong coupling. When $\Omega\left(G_1,G_2\right)$ *is small, the positive infection probability in* G_1 *is mostly due to external infections from* G_2 *for* τ_{11} *right above the threshold* $\tau_{11,c}$. *Moreover, when* $\Omega\left(G_1,G_2\right)$ *is large, the positive infection probability in* G_1 *is mostly due to the increased effective level of contact among agents of* G_1 *for* τ_{11} *right above the threshold* $\tau_{11,c}$.

4.4 Numerical Simulation Results

We have generated two graphs according to the small world random network model [71]. The first network G_1 has $N_1 = 500$ vertices with Watts and Strogatz parameters for mean degree $K_1 = 10$ and the rewiring probability $\beta_1 = 0.2$, and the second network G_2 has $N_2 = 100$ vertices with the mean degree $K = 2$ and the rewiring probability $\beta_2 = 0.1$. All the potential edges between G_1 and G_2 are active with some probability ω, to be chosen. Therefore, increasing ω implies increasing the interconnection strength.

Fig. 4.3 shows $\bar{\tau}_{c1} = \lambda_1(A_{11})\tau_{11,c}$ as a function of $\bar{\tau}_2 = \lambda_1(A_{22})\tau_{22}$, for three different values of $\omega = 0.01, 0.042, 0.2$. As argued in Section , the blue curve with $\omega = 0.01$ indicates a weak interconnection between G_1 and G_2, while the green curve with $\omega = 0.2$ determines a strong coupling. The red curve in Fig. 4.3 belongs to an intermediate interconnection strength, here $\omega = 0.042$, which separates the strong coupling region from the weak coupling region.

According to Fig. 4.3,a %50 reduction of the epidemic threshold is observed in $G_1$for (a) $\omega = 0.01$ and $\bar{\tau}_2 = 0.925$, (b) $\omega = 0.042$ and $\bar{\tau}_2 = 0.5$, (c) $\omega = 0.2$ and $\bar{\tau}_2 = 0.05$. We have plotted the curves of $\bar{p}_1^* = \frac{1}{N_1}\sum_{i=1}^{N_1} p_i^*$ as a function of $\tau_{11}\lambda_1(A_{11})$. We have found the equilibrium values of p_i^* by solving the algebraic equations (4.7) and (4.8).

4.5 Conclusion

In this chapter, we study SIS epidemic spreading among two interconnected networks with different size and epidemic-specific parameters. The main contribution of this work is developing the concept of epidemic threshold curve for interconnected networks. Importantly, we employed spectral analysis to study epidemics over interconnected networks. In particular, we found the value of the epidemic threshold $\tau_{11,c}$ of first graph G_1 as a function of the effective infection rate τ_{22} of G_2 and adjacency matrices of each graph and their interconnection in Theorem 1. Furthermore, we proposed an interconnection measure $\Omega(G_1, G_2)$ to

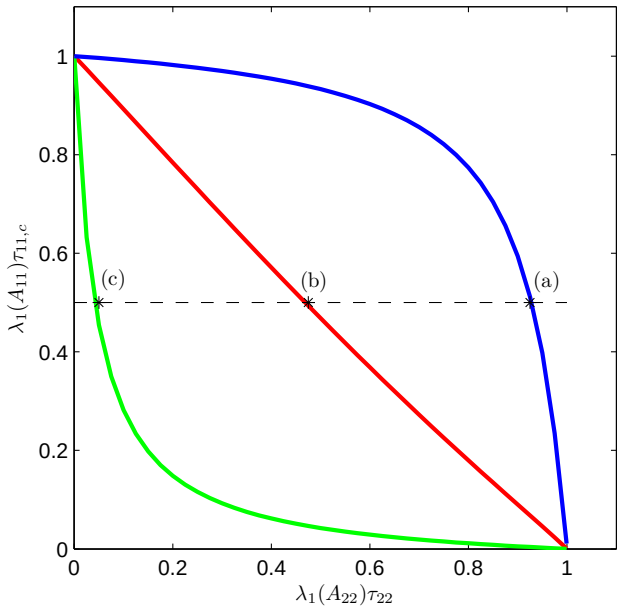

Figure 4.3: *Normalized epidemic threshold* $\bar{\tau}_{c1} = \lambda_1(A_{11})\tau_{11,c}$ *of graph* G_1 *as a function of the normalized effective infection rate* $\bar{\tau}_2 = \lambda_1(A_{22})\tau_{22}$ *of graph* G_2*. The interconnection in (a)* $\omega = 0.01$*, the blue curve, (b)* $\omega = 0.042$*, red curve, and (c)* $\omega = 0.2$*, green curve. A %50 reduction of the epideemic threshold is observed for the normalized effective infection rates (a)* $\bar{\tau}_2 = 0.925$*, (b)* $\bar{\tau}_2 = 0.5$*, (c)* $\bar{\tau}_2 = 0.05$*.*

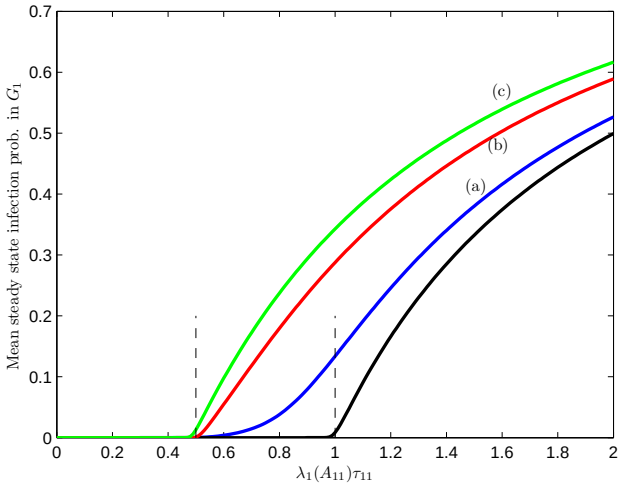

Figure 4.4: *The mean steady-state infection probability in* G_1 *as a function of the normalized effective infection rate of* $\lambda_1(A_{11})\tau_{11}$ *for graph* G_1*. Black curve corresponds to the case where there is no interconnection. In this case, the epidemic threshold is* $\tau_{11,c} = 1/\lambda_1(A_{11})$*. All the other curves correspond to the case where* $\tau_{11,c} = \frac{1}{2} \times 1/\lambda_1(A_{11})$*. For (a) the blue curve* $\omega = 0.01$ *and* $\bar{\tau}_2 = 0.925$*, (b) the red curve* $\omega = 0.042$ *and* $\bar{\tau}_2 = 0.5$*, (c) the green curve* $\omega = 0.2$ *and* $\bar{\tau}_2 = 0.05$*.*

quantitate strongly coupled and weakly coupled networks. A very interesting property of $\Omega(G_1, G_2)$ defined in (4.23) is that it is a purely topological measure and does not depend on the epidemic-specific parameters. Our results have great implication to analyze and control epidemics over interconnected networks.

Chapter 5

Competitive Epidemic Spreading over Arbitrary Multi-Layer Networks

5.1 Introduction

Multiple viral spreading within a single population involves very rich dynamics [72], attracting substantial attention [34, 39, 73]. Applications of these types of models extend beyond physiological viruses, as 'virus' may refer to products [74], memes [75,76], pathogens [77,78], etc. Multiple virus propagation is a mathematically challenging problem. One source of complexity for this problem are multiple interaction possibilities among viruses. For example, viruses may be reinforcing [79], weakening [40], exclusive [67], or asymmetric [73, 80].

In competitive spreading scenario, if infected by one virus, a node (individual) cannot be infected by the other virus. This type of models have implications in several applications like product adoption (e.g., Apple vs. Android smart phones), virus-antidode propagation, meme propagation, opposing opinions propagation, and etc. Newman [67] employed bound percolation to study the spread of two SIR viruses in a host population through a single contact network, where a virus takes over the network, then a second virus spreads through the resulting residual network. The paper proved a coexistence threshold above the classi-

cal epidemic threshold, indicating the possibility of coexistence in SIR model. Karrer and Newman [72] extended the work to the more general case where both viruses spread simultaneously. Poletto et al. [78] studied propagation of two competitive SIR pathogens within a host population, finding the impact of mobility patterns on domination of one strain versus co-domination of both pathogens. For SIS epidemic spreading, Wang et al. [81] studied competitive viruses and proved exclusive, competitive SIS viruses cannot coexist in scale-free networks. For an arbitrary network, Prakash et al. [82] proved competitive SIS virus cannot coexist. Beutel et al. [69] showed coexistence of viruses in case of the SIS viruses with partial immunity, that is a node can be infected by both viruses simultaneously.

This problem becomes particularly much more complicated if the network through which viruses propagate are distinct. Current knowledge of how hybridity of underlying topology influences fate of the pathogens is very little and limited. These systems are usually mathematically intractable, hindering conclusive results on spreading of multiple viruses on multi-layer networks. Funk and Jansen [34] extended the bond-percolation analysis of two competitive viruses to the case of a two-layer network, investigating effects of layer overlapping. Granell et al. [40] studied the interplay between disease and information co-propagation in a two-layer network consisting of one physical contact network spreading the disease and a virtual overlay network propagating information to stop the disease. They found a meta-critical point for the epidemic onset leading to disease suppression. Importantly, this critical point depends on awareness dynamics and the overlay network structure. Wei et al. [38] studied SIS spreading of two competitive viruses on an arbitrary two-layer network, deriving sufficient conditions for exponential die-out of both viruses. They introduced a statistical tool, EigenPredict, to predict viral dominance of one competitive virus over the other [39].

In this study, we address the problem of two competitive viruses propagating in a host population where each virus has distinct contact network for propagation. In particular, we study an SI_1SI_2S model as the simplest extension from SIS model for single virus

propagation to competitive spreading of two viruses on a two-layer network. From topology point of view, our study is comprehensive because our multilayer network is allowed to have any arbitrary structure.

Our study is most relevant to [38] and [39]. Wei et al. conjectured in [38] and numerically observed in [39] that "*the meme whose first eigenvalue*[1] *is larger tends to prevail eventually in the composite networks.*" We challenge this argument from two aspects: First, the definition of viral dominance in [39] is related to comparison of fractions of nodes infected by each virus. However, when comparing two viruses with two different contact networks, having a larger eigenvalue is not a direct indicator of a higher final fraction of infected nodes. In fact, it is possible to create two distinct network layers where a meme spreading in the population with smaller eigenvalue takes over a much larger fraction of the population. We find the definition of viral dominance presented in [39] cannot be corroborated with eigenvalues without severe restriction to a specific family of networks.

Second, and of paramount interest in this study, first eigenvalues are graph properties[2] of each layer in isolation, with no information about layers interrelation, and thus cannot capture the joint influence of the network layers, unless some sort of symmetry or homogeneity is assumed. In fact, the generation of one layer in their synthetic multi-layer network via the Erdős Réyni model [39] dictated a homogeneity in their multilayer networks, creating a biased platform for further observations of layer interrelations. Our work more accurately characterizes the competitive spreading problem than presented by Wei *et al.* [39], as our analytical results clearly express the effect of layers' interrelation.

Multilayer networks generate interesting results for competitive viral spreading, as it has generated interesting results in case of single virus (see [7, 83, 84], to name a few). The main outcome of our analysis is discovery and proof of long-term coexistence of viruses as an emergent phenomenon for SIS-type competitive spreading over multilayer networks,

[1] Wei et al. [39] defined first eigenvalue of a meme as $\boldsymbol{\beta}\lambda_1 - \boldsymbol{\delta}$, where $\boldsymbol{\beta}$ is infection probability, $\boldsymbol{\delta}$ is curing probability, and λ_1 is spectral radius of the underlying graph layer.

[2] A graph property is any property on a graph that is invariant under relabeling of nodes. Eigenvalues, degree moments, graph diameter, etc. are examples of graph properties.

which cannot be attributed to any single-layer contact network topology. We show when the contact graphs of each virus are the same, i.e., the contact network is single-layer, either both viruses die out or there is only one absolute winner. In other words, it is not possible that both viruses survive in the long term over a single-layer contact network. Furthermore, the winner virus is solely determined by epidemic-related parameters, irrespective of the underlying contact topology. However, when the contact graphs are distinct, i.e., the contact topology is a two-layer network, a new phenomenon emerges: it is possible that both viruses coexist long-term. Furthermore, the fate of the viruses depends on epidemic-related parameters, as well as the topology of the multilayer network. In particular, we show no or little overlapping of central nodes across the layers is a key determinant of coexistence.

Our results are not limited to any homogeneity assumption or degree-distribution and network-model arguments. We find analytical results determining extinction, coexistence, and absolute dominance of the viruses by introducing concepts of survival threshold and absolute-dominance threshold. We employ a novel multilayer network-generation framework to obtain a set of networks so that individual layers have identical graph properties while the interrelation of network layers varies. Therefore, any difference in outputs is purely the result of interrelation. This makes ours a paradigmatic contribution to shed light on topology hybridity in multilayer networks.

5.2 Competitive Spreading in Multi-Layer Networks

We study a continuous time SI_1SI_2S model of two competitive viruses propagating on a two-layer network, initially proposed in discrete time[3] [38].

[3]Wei et al. [38] referred to their model as SI_1I_2S. We prefer SI_1SI_2S as a better candidate to emphasize impossibility of direct transition between I_1 and I_2 in this model.

5.2.1 Multilayer Network Topology

Consider a population of size N among which two viruses propagate, acquiring distinct transmission routes. For example, an air-borne pathogen and a blood-borne pathogen spread within a population through different transmission routes. Represented mathematically, the network topology is a multi-layer network because two link types are present; one type allows transmission of virus 1 and the other type allows transmission of virus 2. We represent this multilayer network as $\mathcal{G}(V, E_A, E_B)$, where V is the set of vertices (nodes) and E_A and E_B are set of edges (links). By labeling vertices from 1 to N, adjacency matrices $A \triangleq [a_{ij}]_{N\times N}$ and $B \triangleq [b_{ij}]_{N\times N}$ correspond to edge sets E_A and E_B, respectively, where $a_{ij} = 1$ if node j can transmit virus 1 to node i, otherwise $a_{ij} = 0$, and similarly $b_{ij} = 1$ if node j can transmit virus 2 to node i, otherwise $b_{ij} = 0$. We assume the network layers are symmetric, i.e., $a_{ij} = a_{ji}$ and $b_{ij} = b_{ji}$. Corresponding to adjacency matrices A, we define $\boldsymbol{d}_A$ as the node degree vector, i.e., $d_{A,i} = \sum_{j=1}^{N} a_{ij}$, $\lambda_1(A)$ as the largest eigenvalue (or spectral radius) of A, and $\boldsymbol{v}_A$ as the normalized dominant eigenvector, i.e., $A\boldsymbol{v}_A = \lambda_1(A)\boldsymbol{v}_A$ and $\boldsymbol{v}_A^T\boldsymbol{v}_A = 1$. We similarly define $\boldsymbol{d}_B$, $\lambda_1(B)$, and $\boldsymbol{v}_B$ for adjacency matrix B.

Unlike simple, single-layer graphs, multilayer networks are rather new in network science. We define simple graphs $G_A(V, E_A)$ and $G_B(V, E_B)$ to refer to each isolated layer of the multilayer network $\mathcal{G}(V, E_A, E_B)$. This allows us to argue multilayer network $\mathcal{G}$ in terms of simple graphs G_A and G_B properties and their *interrelation*. FIG. 5.1 shows a schematics of the two-layer network.

5.2.2 SI_1SI_2S Model

The SI_1SI_2S model is an extension of continuous-time SIS spreading of a single virus on a simple graph [21, 22] to modeling of competitive viruses on a two-layer network. In this model, each node is either '*Susceptible*,' 'I_1-*Infected*,' or 'I_2-*Infected*' (i.e., infected by virus 1 or 2, respectively), while virus 1 spreads through E_A edges and virus 2 spreads through E_B edges.

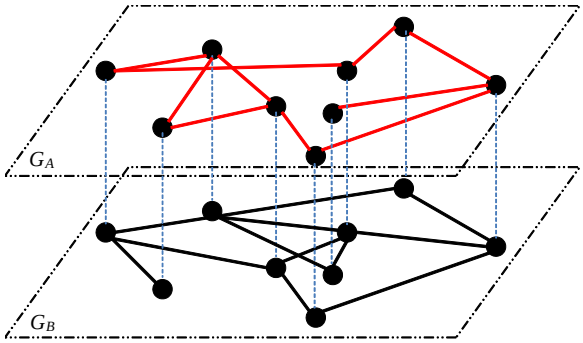

Figure 5.1: *Schematics of two-layer contact topology $\mathcal{G}(V, E_A, E_B)$, where a group of nodes share two distinct interactions. In our SI_1SI_2S model, virus 1 transmits exclusively via E_A links (red) while virus 2 transmits only through E_B links (black). Dotted vertical lines reiterate individual nodes are the same in both layers of $\mathcal{G}$.*

In this competitive scenario the two viruses are exclusive: *a node cannot be infected by virus 1 and virus 2 simultaneously.*

Consistent with SIS propagation on a single graph (cf. [21,22]), the infection and curing processes for virus 1 and 2 are characterized by (β_1, δ_1) and (β_2, δ_2), respectively. To illustrate, the curing process for I_1-infected node i is a Poisson process with curing rate $\delta_1 > 0$. The infection process for susceptible node i effectively occurs at rate $\beta_1 Y_i(t)$, where $Y_i(t)$ is the number of I_1-infected neighbors of node i at time t in layer G_A. *Effective infection rate* of a virus, defined as the ratio of the infection rate over the curing rate, measures the expected number of attempts of an infected node to infect its neighbor before recovering [85], thus quantifying contagiousness of a virus per contact. Curing and infection processes for virus 2 are similarly described. FIG. 5.2 depicts a schematic of the SI_1SI_2S competitive epidemic spreading model over a two-layer network.

The SI_1SI_2S model is essentially a coupled Markov process. For a network with arbitrary structure, this model becomes mathematically intractable due to exponential explosion of its Markov state space size [1]. To overcome this issue with coupled Markov processes, applying closure techniques results in approximate models with much smaller state-space size, however at the expense of accuracy. Specifically, a first-order mean-field type approximation [1] suggests the following differential equations for the evolution of infection probabilities of

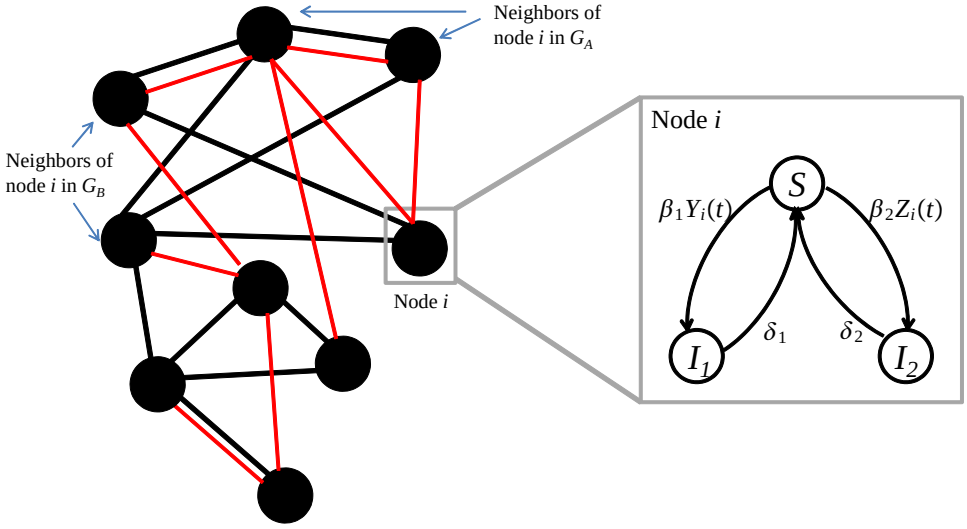

Figure 5.2: *Schematics of a contact network with the node-level stochastic transition diagram for node i, according to the SI_1SI_2S epidemic spreading model. Parameters β_1 and δ_1 denote virus 1 infection rate and curing rate, respectively, and $Y_i(t)$ is the number of node i neighbors in layer G_A infected by virus 1 at time t. Similarly, β_2 and δ_2 denote virus 2 infection rate and curing rate, respectively, and $Z_i(t)$ is the number of node i neighbors in layer G_B infected by virus 2 at time t.*

virus 1 and 2, denoted by $p_{1,i}$ and $p_{2,i}$ for node i, respectively:

$$\dot{p}_{1,i} = \beta_1(1 - p_{1,i} - p_{2,i}) \sum_{j=1}^{N} a_{ij} p_{1,j} - \delta_1 p_{1,i}, \tag{5.1}$$

$$\dot{p}_{2,i} = \beta_2(1 - p_{1,i} - p_{2,i}) \sum_{j=1}^{N} b_{ij} p_{2,j} - \delta_2 p_{2,i}, \tag{5.2}$$

for $i \in \{1, ..., N\}$, with the state-space size of $2N$. This model is an extension of NIMFA model [21] for SIS spreading on simple graphs.

Our competitive virus propagation model (5.1-5.2) exhibits rich dynamical behavior dependent on epidemic parameters and contact network multi-layer structure. Values of effective infection rates $\tau_1 \triangleq \frac{\beta_1}{\delta_1}$ and $\tau_2 \triangleq \frac{\beta_2}{\delta_2}$ of virus 1 and 2 yields several possible outcomes for SI_1SI_2S model (5.1-5.2). In particular, both viruses may extinct ultimately, or one removes the other one, or both coexist.

5.2.3 Problem Statement

Linearization of our SI_1SI_2S model (5.1-5.2) at the disease-free equilibrium (i.e., $p^*_{1,i} = p^*_{2,i} = 0, i \in \{1, ..., N\}$) demonstrates the exponential extinction condition for both viruses. When $\tau_1 < 1/\lambda_1(A)$ and $\tau_2 < 1/\lambda_1(B)$, any initial infections exponentially die out. In this chapter, we refer to such critical value as *no-spreading threshold* because a virus with a lower effective infection rate is too weak to spread in the population even in the absence of any viral competition.

Wei et al. [38] detailed the no-spreading condition as: If $\tau_1 < 1/\lambda_1(A)$, virus 1 does not spread and exponentially dies out. Importantly, exponential extinction of both viruses occurs only if $\tau_1 < 1/\lambda_1(A)$ and $\tau_2 < 1/\lambda_1(B)$ simultaneously. Dynamical interplay between the competitive viruses does not affect the no-spreading thresholds $\tau_1^0 = 1/\lambda_1(A)$ and $\tau_2^0 = 1/\lambda_1(B)$ for virus 1 and virus 2. These thresholds remain independent of viruses competition characteristics and network layers interrelation. Exponential extinction is the only analytical outcome in Wei [38]. If the effective infection rate of one of the viruses is below its no-spreading threshold, the competitive spreading problem reduces to a single virus propagation. Thus, we addresses the case where for both viruses $\tau_1 > 1/\lambda_1(A)$ and $\tau_2 > 1/\lambda_1(B)$. In this case, the disease-free equilibrium is unstable and consequently at least one of the two viruses persists.

Problem I: Assume the effective infection rates of each virus is larger than their no-spreading threshold, i.e., $\tau_1 > 1/\lambda_1(A)$ and $\tau_2 > 1/\lambda_1(B)$:

1. Will both viruses survive (coexistence) or will one virus completely remove the other (absolue dominance)?

2. Which characteristics of multi-layer network structure allow for coexistence or absolute dominance?

This problem is essentially a two-virus problem. We are interested in predicting what happens to the viruses for given values of the pair (τ_1, τ_2). Will both die out? Will one dominate the other? Will both coexist? Our approach to answer these questions is to focus

only on one virus instead of studying the two viruses at the same time. With no loss of generality, we choose virus 1. In this approach, we consider virus 2 as an external factor reducing the susceptibility of the population for virus 1. Therefore, instead of the initial two-virus problem, we study the fate of virus 1 given virus 2 has the capability to infect the population and its effective infection rate is $\tau_2 > 1/\lambda_1(B)$. We investigate whether virus 1 dies out, or it survives when competing with virus 2. In case it survives, it may coexist with virus 2 or it may be the absolute winner, removing virus 2 completely from the population. Formally, the two-virus problem boils down to studying fate of virus 1 given virus 2.

Problem II: Assume effective infection rate of virus 2 is τ_2 and it is greater than virus 2 no-spreading threshold, i.e., $\tau_2 > 1/\lambda_1(B)$:

1. For which values of τ_1, virus 1 will survive?

2. For which values of τ_1, virus 1 survives and is the absolute winner, removing virus 2 completely?

Problem I and Problem II are equivalent. We address Problem II by introducing two critical values for the effective infection rate, namely, *survival threshold* τ_{c1} and *absolute-dominance threshold* $\tau_1^\dagger$. We then argue that absolute-dominance threshold of one virus corresponds to the survival threshold of the other virus. This further simplifies the problem to finding the survival threshold of virus 1.

These questions pertain to long-term behaviors of competitive spreading dynamics. To address these questions, we perform a steady-state analysis of SI_1SI_2S model. Specifically, bifurcation techniques are used to find two critical values, survival threshold and absolute-dominance threshold, determining if a virus will survive and whether it can completely remove the other virus. Significantly, we go beyond these threshold conditions and examine interrelation of network layers. Using eigenvalue perturbation, we find interrelations of dominant eigenvectors and node-degree vectors of network layers are critical determinants in ultimate behaviors of competitive viral dynamics.

5.3 Main Results

Dynamics of the competitive spreading SI_1SI_2S model is rather complicated and its mathematical analysis might look cumbersome. We have moved all the deductions and proofs to the Appendix section and only report the final results. The mathematical tools that we use in this study are equilibrium analysis, bifurcation theory, and eigenvalue perturbation.

5.3.1 Equilibrium Analysis and Threshold Equations

The SI_1SI_2S competitive virus propagation model (5.1-5.2) yields the equilibriums equations:

$$\frac{p^*_{1,i}}{1-p^*_{1,i}-p^*_{2,i}} = \tau_1 \sum a_{ij} p^*_{1,j}, \tag{5.3}$$

$$\frac{p^*_{2,i}}{1-p^*_{1,i}-p^*_{2,i}} = \tau_2 \sum b_{ij} p^*_{2,j}, \tag{5.4}$$

for $i \in \{1, ..., N\}$, where $p^*_{1,i}$ and $p^*_{2,i}$ are respectively virus 1 and virus 2 equilibrium infection probabilities of node i. When $\tau_1 > 1/\lambda_1(A)$ and $\tau_2 > 1/\lambda_1(B)$, equilibrium equations (5.3-5.4) suggest that the SI_1SI_2S competitive spreading model have **at least** the following three equilibrium points:

1. Disease-free equilibrium $(p^*_{1,i} = 0, p^*_{2,i} = 0)$ $\forall i \in \{1, ..., N\}$ where all the nodes are healthy,

2. Virus-2-absolute-dominance equilibrium $(p^*_{1,i} = 0, p^*_{2,i} = y_i > 0)$ $\forall i \in \{1, ..., N\}$ where nodes are only infected by virus 2,

3. Virus-1-absolute-dominance equilibrium $(p^*_{1,i} = z_i > 0, p^*_{2,i} = 0)$ $\forall i \in \{1, ..., N\}$ where nodes are only infected by virus 1,

where z_i and y_i are steady-state infection probabilities in case of single-virus propagation (see [21]), satisfying

$$\frac{z_i}{1-z_i} = \tau_1 \sum a_{ij} z_j, \tag{5.5}$$

$$\frac{y_i}{1-y_i} = \tau_2 \sum b_{ij} y_j, \tag{5.6}$$

for $i \in \{1, ..., N\}$.

The disease-free equilibrium $(p^*_{1,i} = 0, p^*_{2,i} = 0)$ is always unstable for $\tau_1 > 1/\lambda_1(A)$ and $\tau_2 > 1/\lambda_1(B)$. Each of the above three solutions to the equilibrium equation (5.3-5.4) corresponds to the case that at least one of the viruses does not exist. In order to have coexistence of the two viruses, equilibriums 2 and 3 should also be unstable, and a fourth stable equilibrium should exist where $(p^*_{1,i} > 0, p^*_{2,i} > 0)$ $\forall i \in \{1, ..., N\}$. We refer to this equilibrium as *coexistence equilibrium* and show it only exists for multilayer contact network.

As explained in Problem Statements Section 5.2.3, we study this two-virus problem by analysis of virus 1 behavior, considering virus 2 as an external factor. Definitions of survival and absolute-dominance thresholds facilitate our analysis.

Definition: Given virus 2 effective infection rate $\tau_2 > 1/\lambda_1(B)$, the *survival threshold* τ_{1c} is the critical point such that virus 1 steady-state infection probability of each node is zero for $\tau_1 < \tau_{1c}$ and is positive for $\tau_1 > \tau_{1c}$, i.e.,

$$\begin{cases} p^{ss}_{1,i} = 0, & \text{for } \tau_1 < \tau_{1c}, \\ p^{ss}_{1,i} > 0, & \text{for } \tau_1 > \tau_{1c}, \end{cases}$$

Definition: Given virus 2 effective infection rate $\tau_2 > 1/\lambda_1(B)$, the *absolute-dominance threshold* $\tau_1^\dagger$ is the critical point such that not only virus 1 survives but also it removes the other virus. In other words, at absolute-dominance threshold virus 2 steady-state infection probability of each node becomes zero for $\tau_1 > \tau_1^\dagger$, i.e.,

$$\begin{cases} p_{2,i}^{ss} > 0 & \text{for } \tau_1 < \tau_1^{\dagger}, \\ p_{2,i}^{ss} = 0, & \text{for } \tau_1 > \tau_1^{\dagger}, \end{cases}$$

for $\forall i \in \{1, ..., N\}$.

For $\tau_2 \leq 1/\lambda_1(B)$, we survival and absolute-dominance conditions coincide and $\tau_{1c} = \tau_1^{\dagger} = \tau_1^0 = 1/\lambda_1(A)$. It is important to clearly distinguish the difference between no-spreading threshold and survival threshold. No-spreading threshold is the critical value of effective infection rate for which a virus cannot spread in the population, regardless of any competition with another virus. No-spreading threshold correspond to the transient dynamics of the spreading. The survival threshold on the other hand corresponds to the long-term behavior of a virus: whether it is going to eventually die-out or it will persist in the population. Survival threshold τ_{c1} is larger than the no-spreading threshold because competition with another virus reduces the susceptibility of the population, hence making it more difficult to survive. A virus which may initially spread in the population can die out eventually as the other virus grows. For virus 1 this scenario occurs if $\tau_1 > \tau_1^0 = 1/\lambda_1(A)$ and $\tau_1 < \tau_{1c}$.

Case of Single-Layer Network

If the two layers are identical, i.e., $B = A$, the survival threshold and the absolute-dominance threshold coincide, indicating that a surviving virus is also the absolute winner. Stability analysis of the equilibriums in case of identical network layers (see Appendix 5.5.1) proves virus-2-absolute-dominance equilibrium ($p_{1,i}^* = 0, p_{2,i}^* = y_i > 0$) is stable iff $\tau_1 < \tau_2$. Furthermore, virus-1-absolute-dominance equilibrium ($p_{1,i}^* = z_i > 0, p_{2,i}^* = 0$) is stable iff $\tau_2 < \tau_1$. Therefore, for $\tau_1 \neq \tau_2$ exactly one of the absolute-dominance equilibrium points is stable and the virus with larger effective infection rate is the sole survivor. According to the definitions of survival and absolute-dominance thresholds, $\tau_{1c} = \tau_1^{\dagger} = \tau_2$, denoting an abrupt transition for competitive spreading over a single-layer network. This is consistent with the previous result of [82]. FIG. 5.3 shows the sharp transition for the steady-state infection fractions in

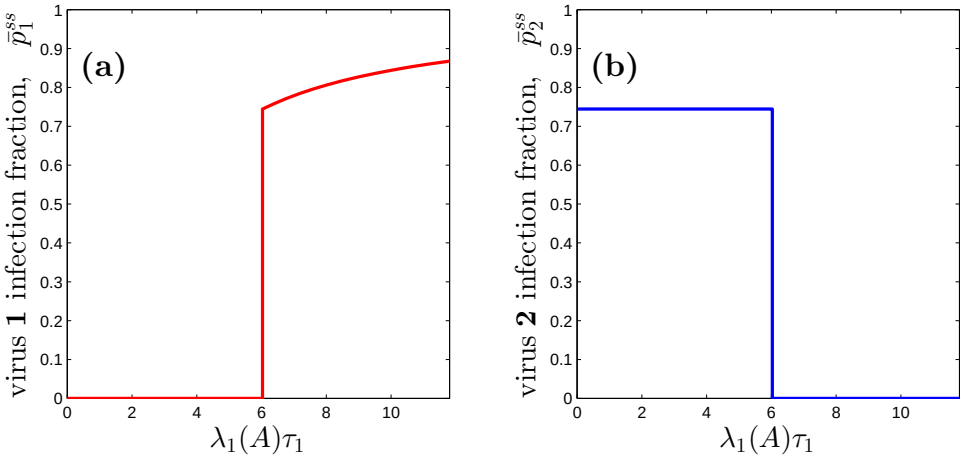

Figure 5.3: *Phase transition of competitive spreading model SI_1SI_2S for a **single-layer** network, i.e., $B = A$. Holding the effective infection rate of virus 2 constant at $\tau_2 = 6\frac{1}{\lambda_1(B)} = 6\frac{1}{\lambda_1(A)}$ and varying τ_1, (a) the steady-state infection fraction of virus 1, $\bar{p}_1^{ss} = \frac{1}{N}\sum p_{1,i}^{ss}$, and (b) the steady-state infection fraction of virus 2, $\bar{p}_2^{ss} = \frac{1}{N}\sum p_{2,i}^{ss}$, exhibit abrupt phase transition at $\tau_1 = 6\frac{1}{\lambda_1(A)} = \tau_2$. Specifically, (a) $\bar{p}_1^{ss}$ is zero for $\tau_1 < \tau_2$ and is positive for $\tau_1 > \tau_2$, denoting survival threshold of virus 1, and (b) $\bar{p}_2^{ss}$ is positive for $\tau_1 < \tau_2$ and becomes zero for $\tau_1 > \tau_2$, indicating absolute removal of virus 2 and thus the virus 1 absolute-dominance threshold.*

the SI_1SI_2S model as a function of τ_1, holding τ_2 fixed at a given value.

Case of Multilayer Network

In contrast to the case of single-layer networks, survival threshold and absolute-dominance threshold do not necessarily overlap for multilayer contact network. As a result, there is a non-trivial region for (τ_1, τ_2) values that both viruses exist, which we refer to as *coexistence region*. FIG. 5.4 shows the absolute-dominance and survival thresholds are distinct for a two-layer network (see Section 5.3.5 for details of network generation).

Given τ_2, plotting virus 1 steady-state infection fraction $\bar{p}_1^{ss} = \frac{1}{N}\sum_{j=1}^{N} p_{1,i}^{ss}$ as a function of τ_1 identifies the survival threshold τ_{1c} at which $\bar{p}_1^{ss}$ becomes positive. Interestingly, another alternative to identify the absolute-dominance threshold is to also plot the infection fraction of virus 1 in the absence of any competition with virus 2 ($\tau_2 = 0$). The two curves must coincide for τ_1 larger than the absolute-dominance threshold, because for $\tau_1 > \tau_1^{\dagger}$ virus 2

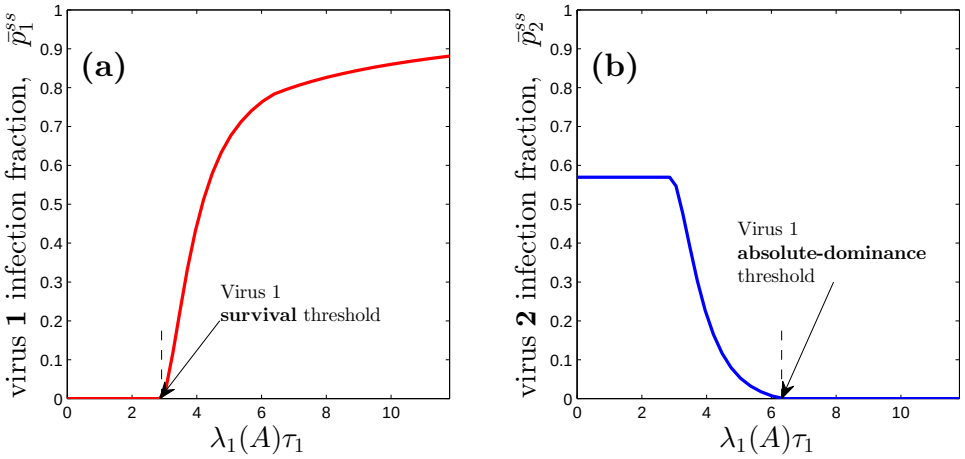

Figure 5.4: *Illustration of survival and absolute-dominance thresholds for virus* 1 *on a multilayer contact network. Holding the effective infection rate of virus* 2 *constant at* $\tau_2 = 6\frac{1}{\lambda_1(B)}$, *(a) the steady-state infection fraction of virus* 1, $\bar{p}_1^{ss} = \frac{1}{N}\sum p_{1,i}^{ss}$, *and (b) the steady-state infection fraction of virus* 2, $\bar{p}_2^{ss} = \frac{1}{N}\sum p_{2,i}^{ss}$, *exhibit phase transition at survival threshold* τ_{c1} *and absolute-dominance threshold* $\tau_1^\dagger$, *respectively. Specifically, (a)* $\bar{p}_1^{ss}$ *is zero for* $\tau_1 < \tau_{c1}$ *and becomes positive for* $\tau_1 > \tau_{c1}$, *denoting survival threshold of virus* 1, *and (b)* $\bar{p}_2^{ss}$ *is positive for* $\tau_1 < \tau_1^\dagger$ *and becomes zero for* $\tau_1 > \tau_1^\dagger$, *indicating absolute removal of virus* 2 *and thus the virus* 1 *absolute-dominance threshold. Additionally, it is interesting to observe that* $\bar{p}_2^{ss}$ *is constant when* $\tau_1 < \tau_{c1}$, *while it reduces gradually as* τ_1 *becomes larger than* τ_{c1}.

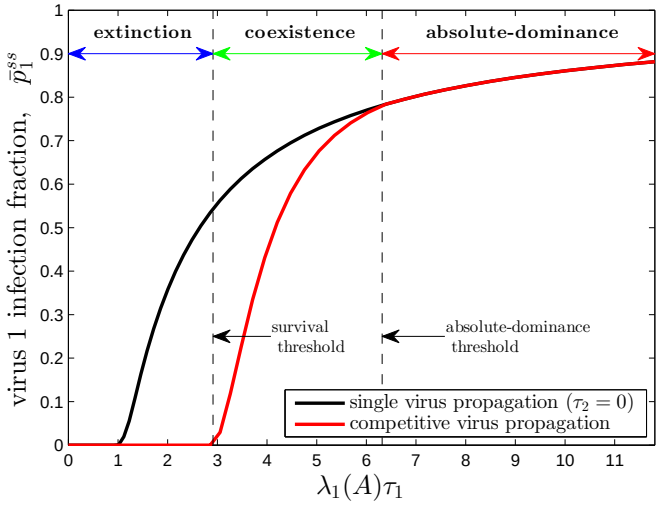

Figure 5.5: *Steady-state infection fraction curve of virus* 1 *in the* SI_1SI_2S *competing spreading model (red). While increasing* τ_1*, steady-state infection fraction of virus* 1 *in the the* SI_1SI_2S *model becomes nonzero at the survival threshold* τ_{1c}*, while it coincides with that of the* SIS *model (black curve) at the absolute-dominance threshold* $\tau_1^\dagger$*. In this simulation, the steady-state infection fraction of virus* 1 *(*$\bar{p}_1^{ss}$*) is zero for* $\tau_1 \leq \tau_{1c} \simeq 3\frac{1}{\lambda_1(A)}$*, an extinction region for virus* 1*. Interestingly, for* $\tau_1 > \tau_1^\dagger \simeq 6.6\frac{1}{\lambda_1(A)}$*,* $\bar{p}_1^{ss}$ *for the competitive scenario (red curve) is identical to the case of single-virus propagation (black curve), suggesting extinction of virus* 2*, hence marking this region as the absolute-dominance range for virus* 1*. For* $\tau_1 \in (\tau_{1c}, \tau_1^\dagger)$*, virus* 1 *and virus* 2 *both persist in the population, marking this range for coexistence region.*

infection probabilities are zero. FIG. 5.5 illustrates for extinction, coexistence, and absolute-dominance regions for virus 1.

Bifurcation analysis of the SI_1SI_2S equilibriums can determine the survival thresholds. The coexistence scenario corresponds to a coexistence equilibrium for SI_1SI_2S model (5.1-5.2) where $(p^*_{1,i} > 0, p^*_{2,i} > 0)\ \forall i \in \{1, ..., N\}$. Given τ_2, virus 1 survival threshold is the critical value that such coexistence equilibrium emerges. Exactly at the threshold value τ_{1c}, $p^*_{1,i}|_{\tau_1=\tau_{1c}} = 0$ and $\frac{dp^*_{1,i}}{d\tau_1}|_{\tau_1=\tau_{1c}} > 0$ for all $i \in \{1, ..., N\}$. Taking the derivative of equilibrium equations (5.3) with respect to τ_1, and defining

$$w_i \triangleq \frac{dp^*_{1,i}}{d\tau_1}|_{\tau_1=\tau_{1c}},\ y_i \triangleq p^*_{2,i}|_{\tau_1=\tau_{1c}}, \tag{5.7}$$

we find the survival threshold τ_{1c} is the value for which nontrivial solution exists for $w_i > 0$ in

$$w_i = \tau_{1c}(1 - y_i) \sum a_{ij} w_j, \tag{5.8}$$

where y_i is the solution of (5.6). Equation (5.8) is an eigenvalue problem (see Appendix 5.5.2). Among all the possible solutions, only

$$\tau_{1c} = \frac{1}{\lambda_1(diag\{1-y_i\}A)} \tag{5.9}$$

is acceptable; according to Perron-Frobenius Theorem, only the dominant eigenvector of the matrix $diag\{1 - y_i\}A$ has all positive entries, allowing $w_i = \frac{dp^*_{1,i}}{d\tau_1}|_{\tau_1=\tau_{1c}} > 0$. Having $w_i > 0$ at critical point τ_{1c} denotes emergence of the coexistence equilibrium.

As discussed earlier, the survival threshold for virus 1 must be larger than the no spreading threshold $1/\lambda_1(A)$ as the result of reduced susceptibility due to competition with virus 2. Above formula for the survival threshold of virus1 has intuitive interpretations. The expression in (5.9) demonstrates that the susceptibility is reduced by factor $(1 - y_i)$, where according to (5.6), y_i is the steady-state infection probability of virus 2 in the absence of virus 1 ($\tau_1 = 0$). Similar to the SIS epidemic threshold [21], the survival threshold (5.9) is inverse of spectral radius of the adjacency matrix A, however, scaled by the reduced susceptibility factor $(1 - y_i)$ for each node.

By duality of expressions, virus 2 survival threshold is $\tau_{2c} = 1/\lambda_1(diag\{1 - z_i\}B)$, where z_i is the solution of (5.5) denoting virus 1 infection fraction in the absence of any competition with virus 2 ($\tau_2 = 0$). The bifurcation analysis thus shows that if $\tau_1 > \tau_{1c}$ and $\tau_2 > \tau_{2c}$, then SI_1SI_2S model (5.1-5.2) has a coexistence equilibrium $(p^*_{1,i} > 0, p^*_{2,i} > 0)$ $\forall i \in \{1, ..., N\}$. In this case, all the other equilibriums of the system are unstable (see Appendix 5.5.2).

The bifurcation analysis for finding survival threshold for a two-layer network does not apply to the case of single-layer network, where the transition is abrupt. Though, we can show $\tau_{1c} = \tau_2$ and $w_i = cy_i$ solve the Perron-Frobenius problem (5.8). However, further

analysis shows $c = 0$, implying that coexistence equilibrium does not emerge in case of single-layer networks.

The survival and absolute-dominance thresholds of virus 1 are functions of τ_2, which we denote by $\tau_{1c} = \Phi_1(\tau_2)$ and $\tau_1^\dagger = \Psi_1(\tau_2)$. Similarly, for virus 2 we can define survival and absolute-dominance thresholds $\tau_{2c} = \Phi_2(\tau_1)$ and $\tau_2^\dagger = \Psi_2(\tau_1)$. Absolute-dominance threshold of one virus is closely related to the survival threshold of the other virus. Specifically, virus 1 absolute-dominance condition $\tau_1 > \tau_1^\dagger$ is equivalent to virus 2 extinction condition $\tau_2 < \tau_{2c}$. Therefore, for $\tau_1 > 1/\lambda_1(A)$ and $\tau_2 > 1/\lambda_1(B)$:

$$\Psi_1(\tau_2) = \Phi_2^{-1}(\tau_2). \tag{5.10}$$

FIG. 5.6 illustrate the survival and absolute-dominance threshold curves of the two viruses, clarifying the above relationship graphically.

The threshold curves identify four regions in (τ_1, τ_2) plane where: both viruses die-out, virus 1 survives only, virus 2 survives only, or both survive and coexist. FIG. 5.7 depicts a typical phase diagram of SI_1SI_2S competitive spreading on two-layer contact networks.

The eigenvalue problem (5.8) gives a mathematical way to find the survival threshold τ_{1c}, depending on the value of τ_2. Unfortunately, this implicit dependence hinders clear understanding of the propagation interplay between virus 1 and virus 2. Particularly, the role of the multilayer contact topology and layer interrelations on the competitive spreading is not apparent. In the following section, we employ eigenvalue perturbation techniques to unravel the multilayer network role.

5.3.2 Characterization of Threshold Curves

Complete analytical solution of survival threshold curves is not feasible. Instead, we quantitate interrelations of contact layers to formulate our analytical assertions. We describe conditions for viral coexistence through attaining explicit analytical quantities giving con-

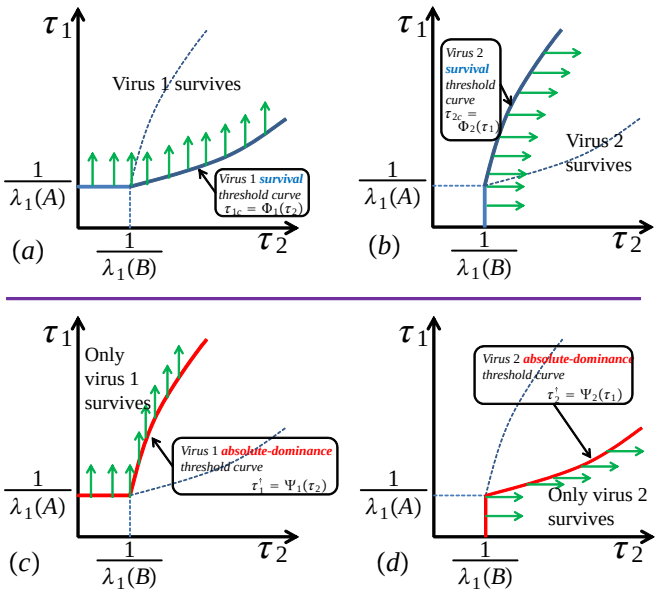

Figure 5.6: *Illustration of survival and absolute-dominance threshold curves in SI_1SI_2S model. (a) Virus 1 survives if its effective infection rates is larger than the survival threshold, i.e., $\tau_1 > \tau_{c1} = \Phi_1(\tau_2)$. Similar argument holds for survival threshold curve of virus 2, as depicted in (b). The absolute-dominance threshold curves can be obtained from the survival curves shown in (a) and (b). Specifically, the region virus 1 is the absolute winner is where virus 1 survives and virus 2 does not survive, as shown in (c). Likewise, the region virus 2 is the absolute winner is where virus 1 does not survive while virus 2 survives (d).*

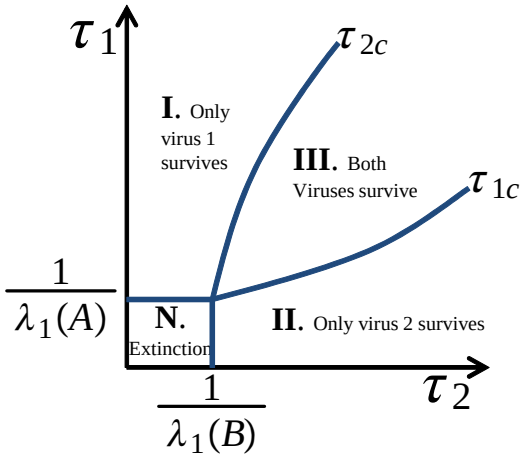

Figure 5.7: *The SI_1SI_2S model with two-layer contact topology exhibits four possibilities: extinction region N where both viruses die-out, absolute-dominance region I, where virus 1 survives and virus 2 dies out, absolute-dominance region II, where only virus 2 survives and virus 1 dies out, and finally coexistence region III, where both viruses survive and persist in the population.*

ditions for coexistence and absolute dominance of viruses. Our approach to this problem finds explicit solutions to (5.9) for values of τ_2 close to $1/\lambda_1(B)$ and for very large values of τ_2 to quantitate the survival epidemic curves. Since we know solution to (5.6) and the survival threshold value τ_{1c} at both extreme values, we can employ eigenvalue perturbation techniques to find explicit solutions for τ_2 close to $1/\lambda_1(B)$ and τ_2 very large. Results for τ_2 close to $1/\lambda_1(B)$ apply where competitive viruses are *non-aggressive*, whereas results for very large τ_2 corresponds to *aggressive*[4] competition. There is no sharp phase-transition between aggressive and non-aggressive competition. It qualitatively describes whether effective infection rates of the viruses are much larger than their respective no-spreading threshold or they are just moderately above the no-spreading thresholds. Behavior of competitive spreading processes is an interpolation of the extreme scenarios of non-aggressive and aggressive propagation.

First, we perform perturbation analysis to find τ_{c1} for values of τ_2 close to $1/\lambda_1(B)$. We know at $\tau_2 = 1/\lambda_1(B)$, $y_i = 0$ solves (5.6), thus $\tau_{c1} = 1/\lambda_1(A)$ is the survival threshold according to (5.9). For values of τ_2 close to $1/\lambda_1(B)$, we use eigenvalue perturbation technique and study sensitivity of threshold equation (5.8) respective to deviation in τ_2 from $1/\lambda_1(B)$. As detailed in the Appendix 5.5.3, we find

$$\frac{d\tau_{1c}}{d\tau_2}|_{\tau_2=\frac{1}{\lambda_1(B)}} = \frac{\lambda_1(B)}{\lambda_1(A)} \frac{\sum v_{A,i}^2 v_{B,i}}{\sum v_{B,i}^3}, \tag{5.11}$$

expressing the dependency of virus 1 survival threshold (τ_{1c}) to effective infection rate of virus 2 (τ_2) for values of τ_2 close to $1/\lambda_1(B)$. In the above equation, $v_{A,i}$ and $v_{B,i}$ are the i-th element of normalized dominant eigenvectors $\boldsymbol{v}_A$ and $\boldsymbol{v}_B$ of A and B, respectively. Among the terms in expression (5.11), $\lambda_1(B)$, $\lambda_1(A)$, and $\sum v_{B,i}^3$ are all graph properties of network layers in isolation, while $\sum v_{A,i}^2 v_{B,i}$ determines the influence of interrelations

[4]In the context of infectious disease propagation, 'highly contagious' is a common terminology to describe a virus with very large basic reproduction number. Since the cross-immunity assumption in our SI_1SI_2S model fits better to product competition interpretations, we describe competition between highly contagious viruses as 'aggressive'.

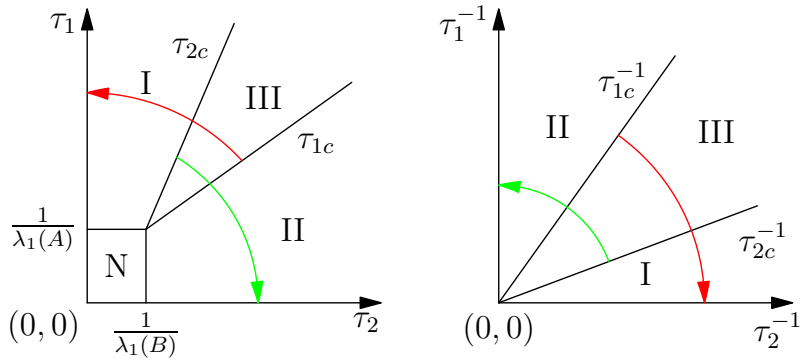

Figure 5.8: *The survival regions diagram in SI_1SI_2S model for values of (τ_1, τ_2) close to $(\frac{1}{\lambda_1(A)}, \frac{1}{\lambda_1(B)})$ (left) and for very large values of (τ_1, τ_2) (right). Regions N, I, II, and III are as defined in FIG. 5.7. The red arrow shows the survival region of virus 1 (regions I and III) and the green arrow shows the survival region of virus 2 (regions II and III). For aggressive viruses scenario, axes have inversed values of (τ_1, τ_2) so that the origin represents infinitely large values. Equations (5.11) and (5.13) analytically find the separating lines between the survival regions in explicit expressions.*

of the two layers. Significantly, if $\sum v_{A,i}^2 v_{B,i}$ is small, expression (5.11) suggests virus 1 survival threshold is minimally influenced by virus 2 infection rate. This has very interesting interpretations: when spectral central nodes of G_A (those nodes with larger element in dominant eigenvector of G_A) are spectrally insignificant in G_B, the virus 1 survival threshold does not increase much by τ_2. In other words, virus 2 does not compete over accessible resources of virus 1, therefore, virus 1 is not affected much by the co-propagation. On the other hand, if spectral central nodes of G_A have high spectral centrality in G_B, then $\sum v_{A,i}^2 v_{B,i}$ is maximal indicating considerable dependency of virus 1 survival threshold of contagiousness of the other virus. From (5.11), the die-out threshold curve $\Phi_1(\tau_2)$ can be approximated close to $(\tau_2, \tau_1) = (\frac{1}{\lambda_1(B)}, \frac{1}{\lambda_1(A)})$ as

$$\Phi_1(\tau_2) \simeq \frac{1}{\lambda_1(A)}\{1 + \frac{\sum v_{A,i}^2 v_{B,i}}{\sum v_{B,i}^3}(\lambda_1(B)\tau_2 - 1)\}. \tag{5.12}$$

Studying threshold equations (5.8)-(5.6) for $\tau_2 \to \infty$, we find $\frac{\tau_{1c}}{\tau_2}|_{\tau_2 \to \infty}$ is the inverse of

the spectral radius of $D_B^{-1}A$ (see Appendix 5.5.3 for detailed derivation):

$$\frac{\tau_{1c}}{\tau_2}|_{\tau_2\to\infty} = \frac{1}{\lambda_1(D_B^{-1}A)} = \frac{1}{\lambda_1(D_B^{-1/2}AD_B^{-1/2})}, \tag{5.13}$$

expressing the dependency of virus 1 survival threshold (τ_{1c}) on effective infection rate of virus 2 (τ_2) for large values of τ_2. This expression (5.13) directly highlights the influence of interrelations of the two layers. Significantly, if $\lambda_1(D_B^{-1}A)$ is large, expression (5.11) suggests that virus 1 survival threshold does not increase significantly by virus 2 infection rate. Similar arguments about interpretation of (5.11) apply to aggressive competitive viruses where τ_1 and τ_2 are relatively large. The main difference in case of aggressive competitive spreading is that node degree is the determinant of centrality. From (5.13), the die-out threshold curve $\Phi_1(\tau_2)$ asymptotically becomes

$$\Phi_1(\tau_2) \simeq \frac{1}{\lambda_1(D_B^{-1}A)}\tau_2, \tag{5.14}$$

for aggressive competitive propagation. FIG. 5.8 depicts survival threshold curves for non-aggressive (left) and aggressive (right) competitive spreading.

We prove conditions for coexistence by showing there is overlapping between regions where viruses survive.

Theorem 4. *In SI_1SI_2S model (5.1-5.2) for competitive epidemics over multi-layer networks, if the two network layers G_A and G_B are identical, coexistence is impossible, i.e., a virus with even a slightly larger effective infection rate dominates and completely removes the other virus. Otherwise, if node-degree vectors of G_A and G_B are not parallel, i.e., $\boldsymbol{d}_A \nparallel \boldsymbol{d}_B$, or normalized dominant eigenvectors of G_A and G_B do not completely overlap, i.e., $\boldsymbol{v}_A \neq \boldsymbol{v}_B$ the multi-layer structure of the underlying topology allows a nontrivial coexistence region.*

Proof. If $G_A = G_B$, we showed in Section 5.3.1 that survival and absolute-dominance thresholds coincide. Therefore, the virus with even a slightly larger effective infection rate domi-

nates and completely removes the other virus if the two network layers are identical.

To show possibility of coexistence for non-aggressive competitive viruses, we show the survival regions overlap by proving

$$\frac{d\tau_{1,c}}{d\tau_2}\frac{d\tau_{2,c}}{d\tau_1}\bigg|_{(\tau_1,\tau_2)=(\frac{1}{\lambda_1(A)},\frac{1}{\lambda_1(B)})} < 1. \tag{5.15}$$

Using expression (5.11) and its counterpart for $\frac{d\tau_{2,c}}{d\tau_1}$, we need to show

$$\frac{(\sum v_{B,i}v_{A,i}^2)(\sum v_{A,i}v_{B,i}^2)}{(\sum v_{B,i}^3)(\sum v_{A,i}^3)} < 1 \tag{5.16}$$

As proved in Appendix 5.5.4, we find condition (5.15) is always true except for the special case where dominant eigenvectors of G_A and G_B completely overlap, i.e., $\boldsymbol{v}_A = \boldsymbol{v}_B$.

In order to show possibility of coexistence for aggressive competitive viruses, we show the survival regions overlap by proving

$$\left(\frac{\tau_{1c}}{\tau_2}\bigg|_{\tau_2\to\infty}\right)\left(\frac{\tau_{2c}}{\tau_1}\bigg|_{\tau_2\to\infty}\right) < 1. \tag{5.17}$$

Using expression (5.13) and its counterpart for $\frac{\tau_{2c}}{\tau_1}|_{\tau_2\to\infty}$, we need to show

$$\left[\frac{1}{\lambda_1(D_B^{-1}A)}\right]\left[\frac{1}{\lambda_1(D_A^{-1}B)}\right] < 1 \tag{5.18}$$

As proved in Appendix 5.5.4, we find that condition (5.17) is always true except for the special case where node-degree vectors of G_A and G_B are parallel, i.e., $\boldsymbol{d}_A = c\boldsymbol{d}_B$. □

When dominant eigenvectors of G_A and G_B are not identical, condition (5.15) indicates non-aggressive viruses can coexist. When propagation of competitive viruses is aggressive, condition (5.17) indicates viruses can coexist if node-degree vectors of G_A and G_B are not parallel. However, the rare scenario where G_A and G_B are not identical and $\boldsymbol{d}_A = c\boldsymbol{d}_B$ and

$\boldsymbol{v}_A = \boldsymbol{v}_B$ hold simultaneously demands further exploration.

The above theorem and equations (5.11) and (5.13) prove the importance of interrelation of network layers. As will be discussed in the simulation section, one approach capturing only the effect of interrelation is generating multilayer networks from two graphs G_A and G_B through simple relabeling vertices of G_B. We thus have a set of multilayer networks whose layers have identical graph properties but correspondence of nodes in one layer to the nodes of the other varies.

In the context of competitive spreading, whether memes, opinions, or products, the population under study serves as the 'resource' for the competitive entities, relating nicely to the concept of 'competing species' in ecology. Long-term study of competing species in ecology centers on the 'competitive exclusion principle' [86]: *Two species competing for the same resources cannot coexist indefinitely under identical ecological factors. The species with the slightest advantage or edge over another will dominate eventually.* Our SI_1SI_2S model also predicts when the network layers are identical, coexistence is not possible. Significantly, different propagation routes break this 'ecological symmetry,' allowing coexistence. Not only have we rigorously proved a coexistence region, we quantitated this ecological asymmetry via interrelation of central nodes across the network layers. None or small overlapping of central nodes of each layer is the key determinant of coexistence. Excitingly, this conclusion nicely relates to 'niche differentiation' in ecology and yet is built upon network science rigor.

5.3.3 Standardized Threshold Diagram and a Global Approximate Formula

Exploring efficient characterization of threshold curves using extreme scenarios, we propose a standardized threshold diagram, where threshold curves are plotted in a $[0,1]\times[0,1]$ plane for $(x,y) = (\frac{1}{\lambda_1(B)\tau_2}, \frac{1}{\lambda_1(A)\tau_1})$, axes scaled by layer spectral radius and inverted. Curves in standardized threshold diagram start from origin and terminate at point $(1,1)$. From (5.11)

and (5.13) the slopes of the survival curve of virus 1 at $(0,0)$ and $(1,1)$ are

$$m_0 = \frac{\lambda_1(B)}{\lambda_1(A)}\lambda_1(D_B^{-1}A), \tag{5.19}$$

$$m_1 = \frac{\sum v_{A,i}^2 v_{B,i}}{\sum v_{B,i}^3}, \tag{5.20}$$

respectively. Importantly, these slopes help creating a parametric approximation for the survival threshold curve $\tau_{1c} = \Phi_1(\tau_2)$ for the full range of τ_2. We use a quadratic Bezier curve [87] as

$$\begin{bmatrix} x \\ y \end{bmatrix} = 2\sigma(1-\sigma)\begin{bmatrix} a \\ b \end{bmatrix} + \sigma^2 \begin{bmatrix} 1 \\ 1 \end{bmatrix}, \tag{5.21}$$

connecting $(x,y) = (0,0)$ to $(x,y) = (1,1)$ for $\sigma \in [0,1]$, and satisfying the slope constraints (5.19) and (5.20), if a and b are chosen as:

$$a = \frac{1-m_1}{m_0 - m_1},\ b = \frac{m_0(1-m_1)}{m_0 - m_1}. \tag{5.22}$$

Therefore, the Bezier curve (5.21) approximates the standardized threshold curve diagram for the whole range of $\tau_1 > 1/\lambda_1(A)$ and $\tau_2 > 1/\lambda_1(B)$ using only spectral information of a set of matrices.

5.3.4 Multi-layer Network Index for Competitive Spreading

Proving coexistence is one of the key contributions of this study. According to (5.16), we go further to define a topological index $\Gamma_s(\mathcal{G})$ quantifying possibility of coexistence in a multi-layer network $\mathcal{G} = (V, E_A, E_B)$ for the case of non-aggressive spreading as

$$\Gamma_s(\mathcal{G}) = 1 - \frac{(\sum v_{B,i}v_{A,i}^2)(\sum v_{A,i}v_{B,i}^2)}{(\sum v_{B,i}^3)(\sum v_{A,i}^3)}. \tag{5.23}$$

Values of $\Gamma_s(\mathcal{G})$ vary from 0 (corresponding to the case where $\boldsymbol{v}_A = \boldsymbol{v}_B$) to 1. Values of $\Gamma_s(\mathcal{G})$ close to zero imply coexistence is rare and any survived virus is indeed the absolute winner. $\Gamma_s(\mathcal{G})$ closer to 1 indicates coexistence is very possible on $\mathcal{G}$. Therefore, $\Gamma_s(\mathcal{G})$ can be used to discuss coexistence of non-aggressive competitive viruses.

Similar to non-aggressive competitive spreading, we can define a topological index $\Gamma_l(\mathcal{G})$ to quantify coexistence possibility in a multi-layer network $\mathcal{G} = (V, E_A, E_B)$ as

$$\Gamma_l(\mathcal{G}) = 1 - \left[\frac{1}{\lambda_1(D_B^{-1}A)}\right]\left[\frac{1}{\lambda_1(D_A^{-1}B)}\right], \tag{5.24}$$

according to (5.18).

Values of $\Gamma_l(\mathcal{G})$ vary from 0 (corresponding to the case where $\boldsymbol{d}_A = c\boldsymbol{d}_B$) to 1. Values of $\Gamma_l(\mathcal{G})$ close to zero imply coexistence is rare and any survived virus is indeed the absolute winner. $\Gamma_l(\mathcal{G})$ closer to 1 indicates coexistence is very possible on $\mathcal{G}$. Therefore, $\Gamma_l(\mathcal{G})$ can be used to discuss coexistence of aggressive competitive viruses.

5.3.5 Numerical Simulations

Multi-layer network generation: The objective of numerical simulations in this section is not only to test our analytical formulae, but also to investigate our prediction of cross-layer interrelation effect on competitive epidemics. This task demands a set of two-layer networks for which isolated layers have identical graph properties but how these layers are interrelated is different, hence capturing the *pure effect of interrelation*. Specifically, in the following numerical simulations, the contact network G_A through which virus 1 propagates is a random geometric graph with $N = 1000$ nodes, where pairs at distance less than $r_c = \sqrt{\frac{3\log(N)}{\pi N}}$ connect to ensure connectivity. For the contact graph of virus 2 (G_B), we first generated a scale-free network according to the Barabási–Albert model. We then used a randomized greedy algorithm to associate the nodes of this graph with the nodes of G_A, approaching a certain degree correlation coefficient ρ with G_A, i.e., each iteration step

permutates nodes when the degree correlation coefficient

$$\rho(\mathcal{G}) = \frac{\sum(d_{A,i} - \bar{d}_A)(d_{B,i} - \bar{d}_B)}{\sqrt{\sum(d_{A,i} - \bar{d}_A)^2}\sqrt{\sum(d_{B,i} - \bar{d}_B)^2}},$$

is closer to the desired value. Specifically, we obtained three different permutations where the generated graphs are negatively ($\rho = -0.47$), neutrally ($\rho = 0$), and positively ($\rho = 0.48$) correlated with G_A. These three graphs have *identical graph properties, yet they are distinct respective to* G_A. FIG. 5.9 depicts a graph G_A and three graphs of G_B with $N = 100$ nodes to improve conceptualization.

Steady-state infection fraction: When two viruses compete to spread, steady-state infection fraction $\bar{p}_1^{ss} = \frac{1}{N}\sum p_{1,i}$ of virus 1 in the SI_1SI_2S model exhibits a threshold behavior at $\tau_1 = \tau_{1c}$, for a given τ_2. Interestingly, aside from the survival threshold τ_{1c}, the absolute-dominance threshold $\tau_1^\dagger$ appears in the figure when plotted against a single virus case: $\bar{p}_1^{ss}$ takes the same values as the single virus case for effective infection rates larger than the absolute-dominance threshold $\tau_1^\dagger$, as was shown in FIG. 5.5.

FIG. 5.10 illustrates the dependency of steady-state infection fraction curve on network layer interrelation. When the contact network of virus 2 (G_B) is positively correlated with that of virus 1 (G_A), it is more difficult for virus 1 to survive, making the survival threshold τ_{1c} relatively larger for positively correlated G_B. Negatively correlated contact network layers impede virus 1 from completely suppressing virus 2, making absolute-dominance threshold $\tau_1^\dagger$ larger for negatively correlated G_B.

Survival diagram: Allowing variation of τ_2, the steady-state infection curve extends to the steady-state infection surface. FIG. 5.11 plots steady-state infection fraction for virus 1 and virus 2 as a function of τ_1 and τ_2. White curves represent theoretical threshold curves derived from the solution to (5.8), accurately separating the survival regions depicted in FIG. 5.7.

FIG. 5.12 plots standardized threshold diagram where G_B is negatively correlated with G_A (left) and G_B is positively correlated with G_A (right). Predictions from analytical

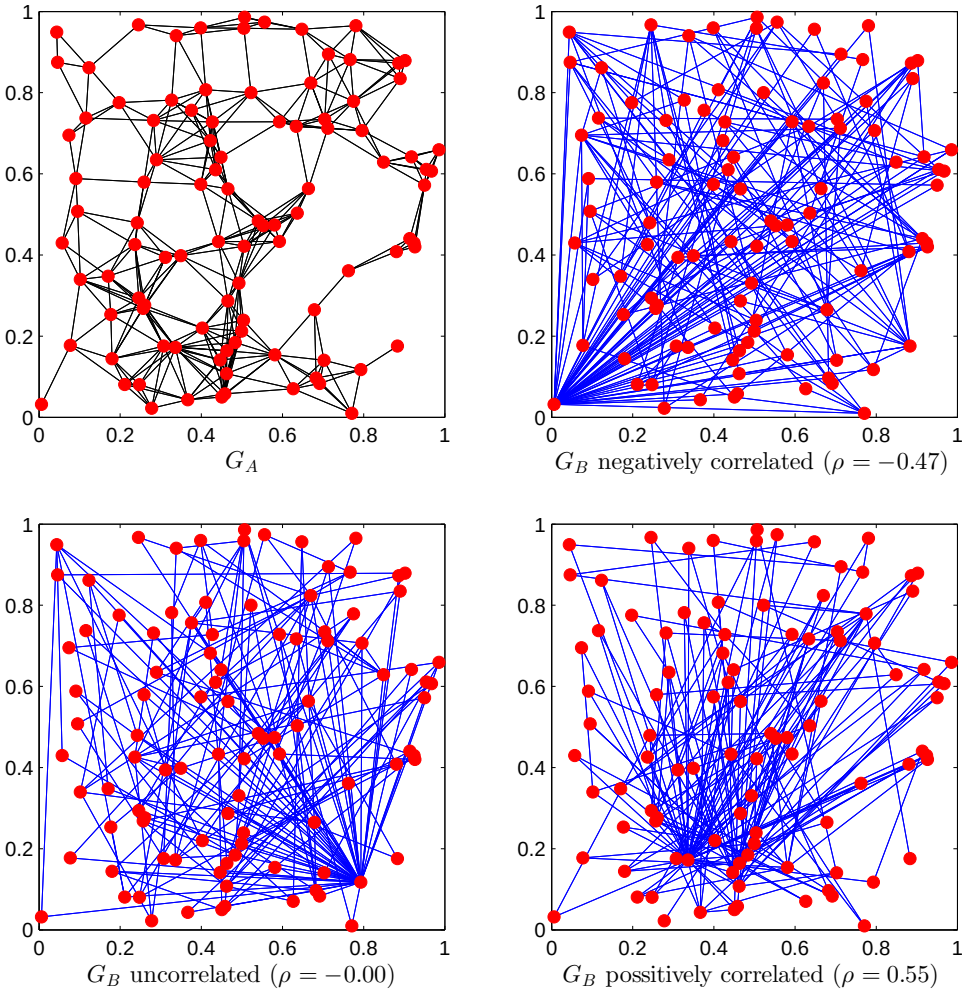

Figure 5.9: Two-layer network generation for numerical simulations is generated here. *The contact network G_A through which virus 1 propagates is a random geometric graph where pairs of nodes with a distance less than r_c are connected to each other. For visualization convenience, the number of nodes is $N = 100$, which is different from the actual $N = 1000$ used for numerical simulation results. For the contact graph of virus 2 (G_B), we first generated a scale-free network according to the B-A model, associating the nodes of this graph with the nodes of G_A to achieve a certain degree correlation coefficient with G_A. Specifically, we obtained three different permutations such that the generated graphs are negatively, neutrally, and positively correlated with G_A. These three graphs are the same if isolated, and distinct in their interrelation with G_A. The high-degree nodes in the positively correlated G_B (lower right) have also high degree in G_A (upper left), while the high-degree nodes in the negatively correlated G_B (upper right) have low degree size in G_A. The uncorrelated G_B (lower left) shows no clear association.*

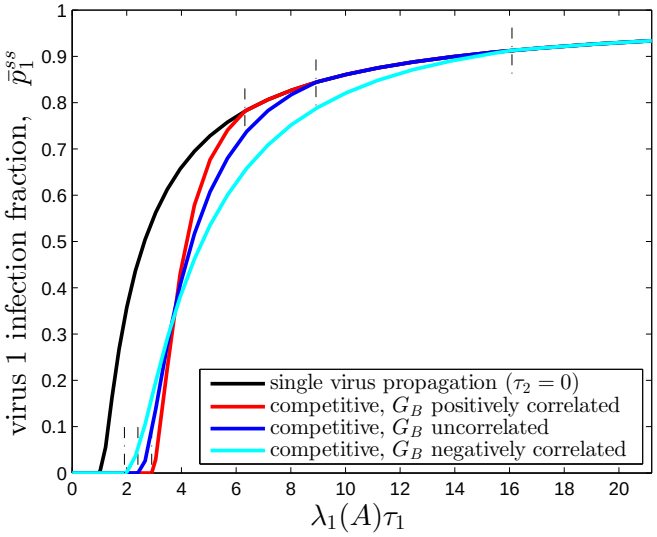

Figure 5.10: *Comparison of steady-state infection fraction curves of virus* 1 *in the* SI_1SI_2S *competitive spreading model. Survival threshold* τ_{1c} *is larger for positively correlated* G_B*, indicating it is more difficult to survive positively correlated* G_B*, while* $\tau_1^\dagger$ *is larger for negatively correlated* G_B*, indicating it is more difficult to completely suppress the other virus in negatively correlated* G_B*.*

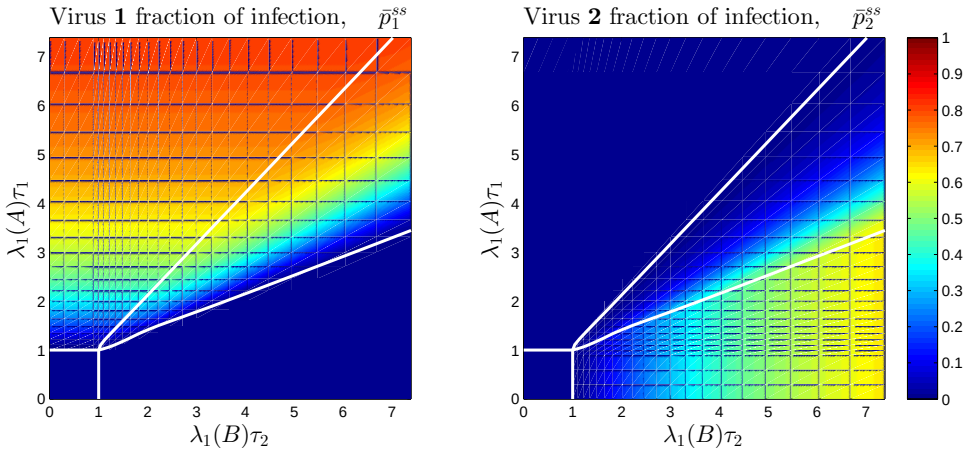

Figure 5.11: *Steady-state fraction of infection for virus* 1 *(left) and virus* 2 *(right) as a function of* τ_1 *and* τ_2*. The white lines are theoretical threshold curves accurately separating the survival regions.*

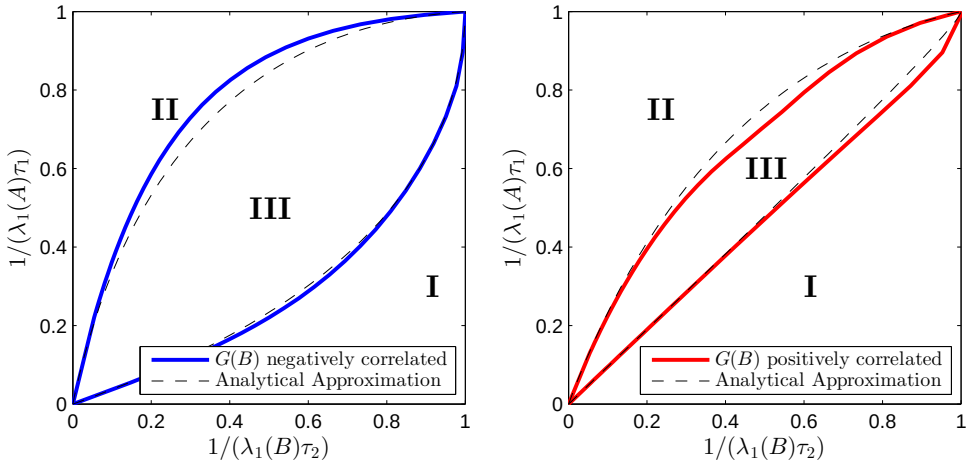

Figure 5.12: *Standardized threshold diagram for case where G_B is negatively correlated with G_A (left) and the case where G_B is positively correlated with G_A (right). Dashed lines are the predictions from analytical approximation formula explicitly expressed in (5.21). Standardized threshold diagram shows three survival regions: absolute-dominance region I, where only virus 1 survives and virus 2 dies out, absolute-dominance region II, where only virus 2 survives and virus 1 dies out, and finally, coexistence region III, where both viruses survive and persist in the population.*

approximation formula (5.21) find the threshold curves fairly accurately.

5.4 Discussion and Conclusion

Competitive multi-virus propagation shows very rich behaviors, beyond those of single-virus propagation. This type of modeling is suitable for co-propagation of exclusive entities, for example, opposing opinions about a subject, where people are for, against, or neutral; spreading of a disease through physical contact and viral propagation of antidote providing immunity to the disease, or marketing penetration of competitive products like Android versus Apple smart phones. Aside from its potential applications, the problem of competitive spreading over multilayer networks is technically challenging. In particular, compared to single layer networks, science of multilayer networks is still in its infancy. There are yet numerous unknowns about this complex problem.

Physics of Competitive Spreading on Multilayer Networks

Definition of survival and absolute-dominance thresholds facilitate articulation of all possible outcomes for the fate of competing viruses. Specifically, survival threshold of a virus determines the phase transition for that virus from extinction to existence in the competitive environment, while the absolute-dominance threshold denotes the critical point where the virus becomes the sole survivor/absolute winner. Our analytical results highlighted major differences between a single-layer contact network, where both viruses spread through same routes, and a multilayer contact network, where each virus has its own transmission route. Significantly, we showed in case of a single network contact, the phase transition is abrupt, while in case of the multilayer contact the phase transitions occurs continuously. The abrupt transition occurs because coexistence is not possible for single-layer contact network and a virus either completely dies out or its infection fraction jumps to the positive value of no competition (refer back to FIG. 5.3). Our results show the coexistence of exclusive, competitive viruses is an emergent phenomena due to multilayer structure of the underlying contact network. When network layers are identical, SI_1SI_2S model does not have a coexistence equilibrium point. This result exemplifies how promising it is to study phenomenology of dynamic processes on networks with more complex topologies than static, single-layer graphs. As an another example of coexistence, Antunovic et al. [88] demonstrated coexistence of competing products when product adoption and network formation would occur concurrently, demonstrating an emergent phenomena for preferential attachment-adoption network model.

How interrelation of graph layers of a multilayer network influence dynamical characteristics of processes is very intricate and still open. In case of the competitive spreading process, the threshold equations (5.6) and (5.9) shows an implicit and complex dependency between network layers. However, the eigenvalue perturbation techniques employed in (5.12) and (5.14) help unravelling the implicit interdependencies of the graph layers. These formulae elucidate that no or little overlapping of "central nodes" is a key determinant of coexistence

phase. Interestingly, which nodes are central depends on the dynamical characteristics of the viruses: when the effective infection rates are very large, the central nodes are mainly those with highest node degrees, and when effective infection rates are close to no-spreading thresholds, the central nodes are those with highest eigenvector centrality. How implication of nodes centrality changes depending on the effective infection rates is a promising future research direction.

The case of aggressive competitive spreading is very important from practical point of view, as it describes the situation where both viruses are highly contagious if alone, and the competition among the viruses to find available (susceptible) hosts is the limiting factor. The survival threshold for aggressive competitive spreading, (5.14), has a very simple and elegant expression. In particular, $\lambda_1(D_B^{-1}A)$ is a new measure for multilayer network structures. The normalized adjacency matrix $D_A^{-1}A$, where each rows are divided by the degree of its corresponding node, is well-known particularly in random walks over graphs. Matrix $D_B^{-1}A$ is likewise a normalized adjacency matrix, where each row of A is however divided by the degree of its corresponding node in layer B. Unlike, $D_A^{-1}A$, the matrix $D_B^{-1}A$ is not necessarily a row-stochastic matrix and henceforth does not posses well-known properties of stochastic matrices. In this study, we have shown that $\lambda_1(D_B^{-1}A)\lambda_1(D_A^{-1}B) > 1$. Studying the properties $D_B^{-1}A$ will further our understanding of competitive viruses, in particular in the more appealing region of aggressive viruses.

Scalability to Multivirus Competitive Spreading

A critical challenge regarding modeling and analysis of mulitvirus spreading is its scalability to higher number of viruses. Our competitive spreading model (5.1-5.2) for two viruses can be extended to multiple virus competitive spreading. In this case, the node state space size is $M+1$, i.e., each node is either susceptible or infected by one of the M viruses[5]. Considering

[5]In the general case of interacting multivirus problem, the problem setup is cumbersom because each node state has 2^M possibilities, as a node might be infected by multiple viruses simultanously. However, in the special case of competitive spreading, problem setup is no longer problematic as a node can only be infected by just one virus at any instance.

each virus has its own transmission route, the contact network will be an $M-$layer network. The $M-$virus competitive spreading dynamics can be expressed as the following:

$$\dot{p}_{m,i} = \beta_m(1 - \sum_{n=1}^{M} p_{n,i}) \sum_{j=1}^{N} a_{m,ij} p_{m,j} - \delta_m p_{m,i}, \quad m \in \{1, ..., M\} \tag{5.25}$$

where $p_{m,i}$ is the node i probability of infection by virus m, with infection rate β_m and recovery rate δ_m. $a_{m,ij}$ is the adjacency matrix elements of layer m.

Analysis of a competitive spreading scenario with multiple viruses and multiple network layers is technically challenging. This scalability issue directly emerges due to multilayer network structure. If the contact network has a single layer, then coexistence is not possible and the winner virus will be the one with largest effective infection rate. However, as coexistence is possible for the multilayer network scenario, for a system of M competitive viruses, the phase-space size is 2^M; each virus can either survive or die-out, and coexistence is possible in a multilayer network. This exponential explosion of phase-space imposes technical difficulties on the problem analysis. While this study develops novel analytical results for competitive spreading of two SIS viruses on a two-layer network, it does not solve the scalability issue upon extensions to multivirus-multilayer competitive spreading. Future research to address the scalability issue is a great contribution in better understanding spreading processes and machinery of dynamical processes over multilayer networks.

Conclusive Remarks

In this study, we study SI_1SI_2S model, the simplest extension of SIS model to competitive spreading over a two-layer network, focusing on long-term behaviors in relation to multilayer network topology. In brief, the major contributions of this study are: (a) identifying and quantifying extinction, coexistence, and absolute dominance via defining survival thresholds and absolute-dominance thresholds, (b) proving a region of coexistence and quantitating it through overlapping of layers central nodes, (c) developing an explicit approximate formula to globally find threshold values, and (d) proposing a novel multilayer network generation

scheme to capture influence of layers interrelation. We believe our methodology has great potentials for application to broader classes of multi-pathogen spreading over multi-layer and interconnected networks.

5.5 Appendix: Selected Proofs

5.5.1 Stability Analysis of Single-Layer Network

When $\tau_1 > 1/\lambda_1(A)$ and $\tau_2 > 1/\lambda_1(B)$, the disease-free equilibrium $(p^*_{1,i} = 0, p^*_{2,i} = 0)\ \forall i \in \{1, ..., N\}$ is unstable. Stability of virus-2-absolute-dominance equilibrium $(p^*_{1,i} = 0, p^*_{2,i} = y_i > 0)\ \forall i \in \{1, ..., N\}$ can be explored by linearizing (5.1) at this equilibrium. The linearized system is

$$\dot{\hat{p}}_{1,i} = \beta_1(1 - y_i)\sum a_{ij}\hat{p}_{1,j} - \delta_1\hat{p}_{1,i} \tag{5.26}$$

which is stable if all the eigenvalues of $\tau_1 diag\{1 - y_i\}A - I$ are negative. Rewriting (5.6) for $B = A$ as

$$y_i = \tau_2(1 - y_i)\sum a_{ij}y_j \tag{5.27}$$

suggests that zero is the largest eigenvalue of $\tau_2 diag\{1 - y_i\}A - I$. Therefore, for $\tau_1 < \tau_2$, all the eigenvalues of $\tau_1 diag\{1 - y_i\}A - I$ are negative, thus virus-2-absolute-dominance equilibrium is stable. Similarly, virus-1-absolute-dominance equilibrium is stable if $\tau_1 > \tau_2$. Therefore, for $\tau_1 \neq \tau_2$, exactly only one of the absolute-dominance equilibriums is stable.

5.5.2 Derivation of Threshold Equation

Differentiating equilibrium equation (5.3) with respect to τ_1 yields

$$\frac{\frac{dp^*_{1,i}}{d\tau_1}(1 - p^*_{2,i}) + p^*_{1,i}\frac{dp^*_{2,i}}{d\tau_1}}{(1 - p^*_{1,i} - p^*_{2,i})^2} = \tau_1\sum a_{ij}\frac{dp^*_{1,j}}{d\tau_1} + \sum a_{ij}p^*_{1,j}. \tag{5.28}$$

At the survival threshold value $\tau_1 = \tau_{1c}$, $p^*_{1,i} = 0$, and $p^*_{2,i} = y_i$ from (5.6). Substituting these values in (5.28),

$$\frac{1}{(1-y_i)}\frac{dp^*_{1,i}}{d\tau_1}\bigg|_{\tau_1=\tau_{1c}} = \tau_{1c}\sum a_{ij}\frac{dp^*_{1,j}}{d\tau_1}\bigg|_{\tau_1=\tau_{1c}}, \tag{5.29}$$

Re-expressing the above equation, we get

$$\frac{dp^*_{1,i}}{d\tau_1}\bigg|_{\tau_1=\tau_{1c}} = \tau_{1c}(1-y_i)\sum a_{ij}\frac{dp^*_{1,j}}{d\tau_1}\bigg|_{\tau_1=\tau_{1c}} \tag{5.30}$$

which is equivalent to (5.8) according to definitions (5.7). Similar stability analysis technique of Section 5.5.1 proves virus-2-absolute-dominance equilibrium is unstable if $\tau_1 > \tau_{1c}$. Therefore, if $\tau_1 > \tau_{1c}$ and $\tau_2 > \tau_{2c}$, disease-free and absolute-dominance equilibriums are all unstable and the system will go to the coexistence equilibrium.

5.5.3 Derivation of Eigenvalue Perturbation Formulae

Here, we detail the derivations of (5.11) and (5.13).

At $\tau_2 = 1/\lambda_1(B)$, (5.6) finds $y_i = 0$ for all nodes. Equation (5.6) is indeed the steady-state equation for infection probabilities in NIMFA model. Van Mieghem [21] found for SIS model the derivative with respect to effective infection rate, suggesting

$$\frac{dy_i}{d\tau_2}|_{\tau_2=\frac{1}{\lambda_1(B)}} = c_B v_{B,i}, \tag{5.31}$$

$$w_i|_{\tau_2=\frac{1}{\lambda_1(B)}} = c_A v_{A,i} \tag{5.32}$$

where

$$c_A = \frac{\lambda_1(A)}{\sum v^3_{A,i}},\ c_B = \frac{\lambda_1(B)}{\sum v^3_{B,i}}, \tag{5.33}$$

where v_A and v_B are the normalized dominant eigenvectors of A and B, respectively.

Differentiating (5.8) with respect to τ_2 yields

$$\begin{aligned}\frac{dw_i}{d\tau_2} &= \frac{d\tau_{1c}}{d\tau_2}(1-y_i)\sum a_{ij}w_j \\ &+ \tau_{1c}(-\frac{dy_i}{d\tau_2})\sum a_{ij}w_j \\ &+ \tau_{1c}(1-y_i)\sum a_{ij}\frac{dw_j}{d\tau_2}.\end{aligned} \tag{5.34}$$

Inserting $\tau_{1c} = 1/\lambda_1(A)$, $w_i = c_A v_{A,i}$, $y_i = 0$, and $dy_i/d\tau_2 = c_B v_{B,i}$ into the above equation changes it to

$$(I - \frac{1}{\lambda_1(A)}A)\frac{d\boldsymbol{w}}{d\tau_2} = (\frac{d\tau_{1c}}{d\tau_2})\lambda_1(A)c_A\boldsymbol{v}_A - c_B c_A(\boldsymbol{v}_B \circ \boldsymbol{v}_A) \tag{5.35}$$

in the collective form, where the Hadamard product $\circ$ acts entry-wise. Multiplying both sides by v_A^T from the left yields:

$$\begin{aligned}\frac{d\tau_{1c}}{d\tau_2}|_{\tau_2=\frac{1}{\lambda_1(B)}} &= \frac{1}{\lambda_1(A)}c_B\boldsymbol{v}_A^T(\boldsymbol{v}_B \circ \boldsymbol{v}_A) \\ &= \frac{\lambda_1(B)}{\lambda_1(A)}\frac{\sum v_{A,i}^2 v_{B,i}}{\sum v_{B,i}^3},\end{aligned} \tag{5.36}$$

obtaining (5.11). Finding $\dfrac{d\tau_{1c}}{d\tau_2}$ at $\tau_2 = 1/\lambda_1(B)$ obtains the dependence of τ_{1c} on τ_2 close to $1/\lambda_1(B)$.

Replacing for $1 - y_i = \dfrac{\tau_2^{-1}}{\tau_2^{-1} + \sum b_{ij}y_j}$ from (5.6) into (5.8) yields

$$w_i = (\frac{\tau_{1c}}{\tau_2})(\frac{1}{\tau_2^{-1} + \sum b_{ij}y_j})\sum a_{ij}w_j. \tag{5.37}$$

When effective infection rate τ_2 is enormous $\tau_2^{-1} \to 0$ and $y_i \to 1$, suggesting

$$w_i = (\frac{\tau_{1c}}{\tau_2}|_{\tau_2\to\infty})\frac{1}{d_{B,i}}\sum a_{ij}w_j, \tag{5.38}$$

where $d_{B,i}$ is the $B-$degree of node i. Therefore, $\frac{\tau_{1c}}{\tau_2}|_{\tau_2\to\infty}$ is the inverse of the spectral

radius of $D_B^{-1}A$, proving (5.13) for large values of τ_2.

5.5.4 Coexistence Proofs

Coexistent region non-aggressive competitive viruses:

To investigate the coexistence region for non-aggressive viruses we show that (5.15) is true. From (5.11), we find

$$\frac{d\tau_{1c}}{d\tau_2}\frac{d\tau_{2c}}{d\tau_1}|_{(\tau_1,\tau_2)=(\frac{1}{\lambda_1(A)},\frac{1}{\lambda_1(B)})} = \frac{(\sum v_{B,i}v_{A,i}^2)(\sum v_{A,i}v_{B,i}^2)}{(\sum v_{B,i}^3)(\sum v_{A,i}^3)} \tag{5.39}$$

Proposition 1. *(Hölder's inequality [89]) For $p, q > 0$ satisfying $\frac{1}{p} + \frac{1}{q} = 1$, the following is always true*

$$\sum_{i=1}^{n} |x_i y_i| \leq \left(\sum_{i=1}^{n} |x_i|^p\right)^{1/p} \left(\sum_{i=1}^{n} |y_i|^q\right)^{1/q}$$

for $x, y \in \mathbb{R}^n$. The equality happens iff $x = y$.

Selecting $p = 3, q = 3/2$, we apply the Hölder's inequality to get

$$\begin{aligned} \sum v_{B,i}v_{A,i}^2 &\leq \left(\sum v_{B,i}^3\right)^{1/3} \left(\sum (v_{A,i}^2)^{3/2}\right)^{1/\frac{3}{2}} \\ &= \left(\sum v_{B,i}^3\right)^{1/3} \left(\sum v_{A,i}^3\right)^{2/3}, \end{aligned} \tag{5.40}$$

and similarly for $p = 3/2, q = 3$, we obtain

$$\sum v_{A,i}v_{B,i}^2 \leq \left(\sum v_{B,i}^3\right)^{2/3} \left(\sum v_{A,i}^3\right)^{1/3}, \tag{5.41}$$

and the equality happens iff $\boldsymbol{v}_A = \boldsymbol{v}_B$. Multiplying sides of (5.40) and (5.41) yields

$$(\sum v_{B,i}v_{A,i}^2)(\sum v_{A,i}v_{B,i}^2) \leq (\sum v_{B,i}^3)(\sum v_{A,i}^3), \tag{5.42}$$

proving (5.15) is true if $\boldsymbol{v}_A \neq \boldsymbol{v}_B$.

Coexistent region for aggressive competitive viruses:

To investigate the coexistence region for non-aggressive viruses we shown that (5.15) is true. Substituting from (5.13) yields

$$\begin{aligned}\left(\frac{\tau_{1c}}{\tau_2}|_{\tau_2\to\infty}\right)\left(\frac{\tau_{2c}}{\tau_1}|_{\tau_1\to\infty}\right) &= \frac{1}{\lambda_1(D_B^{-1}A)}.\frac{1}{\lambda_1(D_A^{-1}B)} \\ &= \frac{1}{\lambda_1(D_B^{-1}A\otimes D_A^{-1}B)} \\ &= \frac{1}{\lambda_1[(D_B^{-1}\otimes D_A^{-1})(A\otimes B)]} \\ &= \frac{1}{\lambda_1[(D_B\otimes D_A)^{-1}(A\otimes B)]},\end{aligned} \tag{5.43}$$

according to properties of Kronecker product (see, [90]).

The degree diagonal matrix of $(A\otimes B)$ is $(D_A\otimes D_B)$. Therefore, $(D_B\otimes D_A)$ is a diagonal permutation of the degree diagonal matrix of $(A\otimes B)$. According to Lemma 1, presented in the following, $\lambda_1[(D_B\otimes D_A)^{-1}(A\otimes B)]\geq 1$; thus,

$$\left(\frac{\tau_{1c}}{\tau_2}|_{\tau_2\to\infty}\right)\left(\frac{\tau_{2c}}{\tau_1}|_{\tau_1\to\infty}\right)\leq 1, \tag{5.44}$$

and equality holds only if $D_B\otimes D_A = D_A\otimes D_B$, which holds only if the ratio of $B-$degree and $A-$degree of each node is the same for all nodes.

Lemma 3. *If $H=\pi(D_C)^{-1}C$, where $\pi(D_C)$ is a diagonal permutation of degree diagonal matrix of symmetric matrix C, then $\lambda_1(H)\geq 1$. Furthermore, equality holds only if $\pi(D_C)=D_c$.*

Proof. The largest eigenvalue maximizes Rayleigh quotient, therefore,

$$\begin{aligned}\lambda_1(H) &= \lambda_1(\pi(D_C)^{-1}C) = \lambda_1(\pi(D_C)^{-1/2}C\pi(D_C)^{-1/2}) \\ &= \max_x \frac{x^T\pi(D_C)^{-1/2}C\pi(D_C)^{-1/2}x}{x^Tx} \\ &\geq \frac{1^TC1}{1^T\pi(D_C)1} = \frac{\sum d_{C,i}}{\sum d_{C,\pi_i}} = 1,\end{aligned}$$

where d_{C,π_i} is the degree of node i map. Therefore, $\lambda_1(H) \geq 1$. Equality holds only if $x = \pi(D_C)^{1/2}1$ is the dominant eigenvector of $\pi(D_C)^{-1/2}C\pi(D_C)^{-1/2}$, i.e., $\pi(D_C)^{-1/2}C1 = \pi(D_C)^{1/2}1$, which only holds if $d_{C,\pi_i} = d_{C,i}$. □

5.5.5 Steady-State Numerical Solution

Given $\tau_2 > 1/\lambda_1(B)$, (5.8) and (5.6) numerically find $\tau_{1,c}$. We now define $x_i \triangleq \frac{y_i}{1-y_i}$, given the recursive iteration law:

$$x_i(k+1) = \tau_2 \sum b_{ij} \frac{x_j(k)}{1+x_j(k)} \tag{5.45}$$

to prove they converge exponentially, numerically solving (5.6) as $\frac{x_i(k)}{1+x_i(k)} \to y_i$. The main advantage of finding equilibrium values using recursive law (5.45) instead of solving the ordinary differential equations of the model is recursive law (5.45) does not require incremental time increase, making computations drastically faster.

Furthermore, the steady-state infection probabilities in (5.3)-(5.4) can be found via the recursive iteration law:

$$x_{1,i}(k+1) = \tau_1 \sum a_{ij} \frac{x_{1,j}(k)}{1+x_{1,j}(k)+x_{2,j}(k)}, \tag{5.46}$$

$$x_{2,i}(k+1) = \tau_2 \sum b_{ij} \frac{x_{2,j}(k)}{1+x_{1,j}(k)+x_{2,j}(k)}, \tag{5.47}$$

for which $\dfrac{x_{1,j}(k)}{1+x_{1,j}(k)+x_{2,j}(k)} \to p^*_{1,i}$ and $\dfrac{x_{2,j}(k)}{1+x_{1,j}(k)+x_{2,j}(k)} \to p^*_{2,i}$ as $k \to \infty$.

Part III

Modeling Behaviors in Social Epidemic Networks

Chapter 6

Epidemic Spread in Social Networks

6.1 Introduction

Modeling human reactions to the spread of infectious disease is an important topic in current epidemiology [91], and has recently attracted a substantial attention [92–98]. The challenges in this topic concern not only how to model human reactions to the presence of epidemics, but also how these reactions affect the spread of the disease itself. In general, human response to an epidemic spread can be categorized in three main types: (1) Change in the system state. For example, in a vaccination scenario individuals go directly from susceptible state to recovered without going through infected state. (2) Change in system parameters as the result of an adopted cautious behavior. For example, as in [97], individuals might choose to use masks, therefore, have a smaller infection rate parameter. (3) Change in the contact topology. For example, due to the perception of a serious danger, individuals reduce or change their contacts with other people who can potentially be infectious [92].

A good review on the existing results studying the interaction of the epidemic spreading and the human behavior can be found in [92]. Poletti et al. [99] developed a population-based model where susceptible individuals could choose between two behaviors in response to presence of infection. Funk et al. [94] showed that awareness of individuals about the

presence of a disease can help reducing the size of the epidemic outbreak. In their paper, awareness and disease have interconnected dynamics. Theodorakopoulos et al. [98] formulated the problem so that individuals could make decision based on the perception of the epidemic size. Perra et al. [100] considered the case where individuals go to a '*feared*' state when they sense infection. Since most of the existing results are for population-based models, they are suitable for a society of well-mixed individuals. To the best of the authors' knowledge, individual-based results have not been reported for this problem so far.

The contribution of this chapter is two-fold: (1) Unlike most of the previous results, no homogeneity assumption is made on the contact network, and the human-disease interaction in this study is modeled on a generic contact graph. (2) We show through analytical approaches that two distinct critical values exist for the effective infection rate. The two are explicitly computed. The existence of two distinct thresholds is reported for the first time in this study, providing a fundamental progress on previous results.

6.2 Model Development

In this chapter, we have built our modeling based on the NIMFA model. Specifically, we add a new compartment to the classic SIS model for epidemic spread modeling to propose a susceptible-alert-infected-susceptible (SAIS) model.

The contact topology in this formulation is considered as a generic graph. Each node is allowed to be in one of the three states *'susceptible'*, *'infected'*, and *'alert'*. For each agent $i \in \{1, ..., N\}$, let the random variable $x_i(t) = e_1$ if the agent i is susceptible at time t, $x_i(t) = e_2$ if alert, and $x_i(t) = e_3$ if infected, where $e_1 = [1, 0, 0]^T$, $e_2 = [0, 1, 0]^T$, and $e_3 = [0, 1, 0]^T$ are the standard unit vectors of $\mathbb{R}^3$. There are four stochastic transitions in the SAIS model:

1. A susceptible agent becomes infected by the infection rate β times the number of its

infected neighbors, i.e.,

$$\Pr[x_i(t+\Delta t) = e_3 | x_i(t) = e_1, X(t)] = \beta Y_i(t)\Delta t + o(\Delta t), \tag{6.1}$$

for $i \in \{1, ..., N\}$ and $Y_i(t) \triangleq \sum_{j=1}^{N} a_{ij} 1_{\{x_j(t)=e_1\}}$.

2. An infected agent recovers back to the susceptible state by the curing rate δ, i.e.,

$$P(x_i(t+\Delta t) = e_1 | x_i(t) = e_3, X(t)) = \delta \Delta t + o(\Delta t). \tag{6.2}$$

3. A susceptible agent might go to the alert state if surrounded by infected individuals. Specifically, a susceptible node becomes alert with the alerting rate $\kappa \in \mathbb{R}^+$ times the number of infected neighbors, i.e.,

$$P(x_i(t+\Delta t) = e_2 | x_i(t) = e_1, X(t)) = \kappa Y_i(t)\Delta t + o(\Delta t). \tag{6.3}$$

4. An alert agent can get infected in a process similar to a susceptible agent but with a smaller infection rate $0 < \beta_a < \beta$, i.e.,

$$P(x_i(t+\Delta t) = e_3 | x_i(t) = e_2, X(t)) = \beta_a Y_i(t)\Delta t + o(\Delta t). \tag{6.4}$$

In above equations, $\Pr[\cdot]$ denotes probability, $X(t) \triangleq \{x_i(t), i = 1, ..., N\}$ is the joint state of the network, $\Delta t > 0$ is a time step, and the indicator function $1_{\{\mathcal{X}\}}$ is one if $\mathcal{X}$ is true and zero otherwise. A function $f(\Delta t)$ is said to be $o(\Delta t)$ if $\lim_{\Delta t \to 0} \frac{f(\Delta t)}{\Delta t} = 0$.

The stochastic compartmental transitions of a node in SAIS model are depicted in Fig. 6.1.

A common approach for studying a continuous-time Markov process is to derive the corresponding Kolmogorov forward (backward) differential equations (see [47]). As can be seen

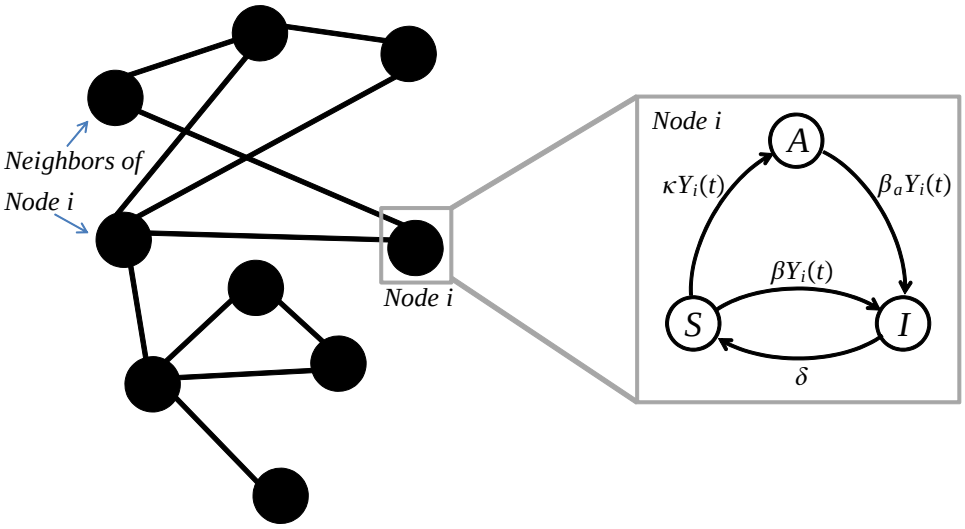

Figure 6.1: *Schematics of agent-level stochastic transitions in the SAIS model. Parameters β, δ, β_a, and κ denote the infection rate, curing rate, alert infection rate, and alerting rate, respectively. $Y_i(t)$ is the number of the neighbors of agent i that are infected at time t.*

from the above equations, the conditional transition probabilities of a node are expressed in terms of the current state of its neighboring nodes. Therefore, each state of the Kolmogorov differential equations corresponding to the Markov process will be the probability of being in a specific joint state. In this case, we will end up with a set of first order ordinary differential equations of the order 3^N. Hence, the analysis will become dramatically complicated as the network size grows. Using a first-order mean-field approximation, as described in [1] (see Chapter 3), we get a system of nonlinear differential equations with $2N$ states. Specifically, let p_i and q_i denote the probabilities of agent i to be infected and alert, respectively. The SAIS spreading model is obtained as

$$\dot{p}_i = \beta(1 - p_i - q_i) \sum_{j=1}^{N} a_{ij} p_j + \beta_a q_i \sum_{j=1}^{N} a_{ij} p_j - \delta p_i, \tag{6.5}$$

$$\dot{q}_i = \kappa(1 - p_i - q_i) \sum_{j=1}^{N} a_{ij} p_j - \beta_a q_i \sum_{j=1}^{N} a_{ij} p_j, \tag{6.6}$$

for $i \in \{1, ..., N\}$.

6.3 Analysis of SAIS Spreading Model

In this section, the SAIS spreading model (6.5) and (6.6) derived in the previous section is analyzed.

6.3.1 Comparison between SAIS and SIS

As a first step, we compare the SAIS model and the SIS model with respect to the infection probabilities. Specifically, we are interested in comparing $p_i(t)$, the response of (6.5) and (6.6), with infection probability $p'_i(t)$ in the N-intertwined SIS model (see Chapter 2), which is the solution of the system

$$\dot{p'_i} = \beta(1 - p'_i) \sum_{j=1}^{N} a_{ij} p'_j - \delta p'_i. \tag{6.7}$$

The following theorem shows that alertness decreases the probability of infection for each individual.

Theorem 5. *Starting with the same initial conditions $p_i(t_0) = p'_i(t_0)$, $i = \{1, ..., N\}$, the infection probabilities of individuals in SIS model (6.7) always dominate those of the SAIS model (6.5) and (6.6), i.e.,*

$$p_i(t) \leq p'_i(t), i = \{1, ..., N\} \ \forall t \in [t_0, \infty). \tag{6.8}$$

Proof. Rewrite the equation (6.5) as

$$\dot{p}_i = \beta(1 - p_i) \sum_{j=1}^{N} a_{ij} p_j - \delta p_i - (\beta - \beta_a) q_i \sum_{j=1}^{N} a_{ij} p_j. \tag{6.9}$$

Starting with the same initial conditions $p_i(t_0) = p'_i(t_0)$ for $i \in \{1, ..., N\}$, it is concluded

that

$$p_i(t_0) = p_i'(t_0) \Rightarrow \dot{p}_i(t_0) \leq \dot{p}_i'(t_0), \tag{6.10}$$

since $(\beta - \beta_a)q_i(t_0)\sum_{j=1}^{N} a_{ij}p_j(t_0)$ is a non-negative term having $\beta_a < \beta$ by definition. According to (6.10), there exists $t_f > t_0$ so that

$$p_i(t) \leq p_i'(t), i \in \{1, ..., N\} \ \forall t \in [t_0, t_f]. \tag{6.11}$$

The theorem is proved if we show that inequality (6.11) holds for every $t_f \in (t_0, \infty)$. Assume that there exists $t_1 > t_0$, so that (6.11) holds for $t_f = t_1$ but it is not true for any $t_f > t_1$. Obviously, at $t = t_1$,

$$\exists i \in \{1, ..., N\} \text{ s.t. } p_i(t_1) = p_i'(t_1) \text{ and } \dot{p}_i(t_1) > \dot{p}_i'(t_1). \tag{6.12}$$

In the subsequent arguments, it is shown that no such t_1 exists. From (6.9), $\dot{p}_i(t_1)$ is found to satisfy

$$\begin{aligned}
\dot{p}_i(t_1) &= \beta(1 - p_i(t_1)) \sum_{j=1}^{N} a_{ij}p_j(t_1) \\
&\quad - (\beta - \beta_a)q_i(t_1) \sum_{j=1}^{N} a_{ij}p_j(t_1) - \delta p_i(t_1) \\
&\leq \beta(1 - p_i(t_1)) \sum_{j=1}^{N} a_{ij}p_j(t_1) - \delta p_i(t_1) \\
&= \beta(1 - p_i'(t_1)) \sum_{j=1}^{N} a_{ij}p_j(t_1) - \delta p_i'(t_1),
\end{aligned} \tag{6.13}$$

according to (6.12) and the fact that $(\beta - \beta_a)q_i(t_1)\sum_{j=1}^{N} a_{ij}p_j(t_1)$ is a non-negative term. Based on (6.11), $\forall j \in \{1, ..., N\}$ we have $p_j(t_1) \leq p_j'(t_1)$. Therefore, the inequality (6.13) is

further simplified as

$$\dot{p}_i(t_1) \leq \beta(1 - p'_i(t_1)) \sum_{j=1}^{N} a_{ij} p'_j(t_1) - \delta p'_i(t_1) = \dot{p}'_i(t_1). \tag{6.14}$$

Having $\dot{p}_i(t_1) \leq \dot{p}'_i(t_1)$ contradicts (6.12). Hence, no such t_1 exists so that (6.12) is true. As a result, the inequality (6.11) holds for every $t_f \in (t_0, \infty)$. This completes the proof. □

6.3.2 Exponential Epidemic Die-Out

Theorem 6. *Consider the SAIS spreading model (6.5) and (6.6). Assume that the effective infection rate satisfies*

$$\tau = \frac{\beta}{\delta} < \frac{1}{\lambda_1(A)}. \tag{6.15}$$

Then, initial infections will die out exponentially.

Proof. The solution of $p_i(t)$ was proved in Theorem 5 to be upper-bounded by $p'_i(t)$. According to earlier results in Section 2.3, the NIMFA model (6.7) is exponentially stable if (6.15) is satisfied. As a consequence, $p_i(t)$ in (6.9) is also exponentially stable if (6.15) is satisfied. □

6.3.3 Asymptotically Epidemic Die-Out

According to (6.6),

$$q_i^e = \frac{1 - p_i}{1 + \frac{\beta_a}{\kappa}}, \ i \in \{1, ..., N\}, \tag{6.16}$$

is an equilibrium for (6.6). To facilitate the subsequent analysis, define a new state r_i as

$$r_i \triangleq q_i - q_i^e = q_i - \frac{1 - p_i}{1 + \frac{\beta_a}{\kappa}}. \tag{6.17}$$

Substituting $q_i = r_i + \frac{1}{1+\frac{\beta_a}{\kappa}} - \frac{p_i}{1+\frac{\beta_a}{\kappa}}$ from (6.17) in (6.5) and (6.6), the derivatives $\dot{p}_i$ and $\dot{r}_i$ in the new coordinate are derived as

$$\begin{aligned}\dot{p}_i = &\{\beta\frac{\frac{\beta_a}{\kappa}}{1+\frac{\beta_a}{\kappa}} + \beta_a\frac{1}{1+\frac{\beta_a}{\kappa}}\}\sum_{j=1}^{N} a_{ij}p_j \\ &- \{\beta + \frac{\beta+\beta_a}{1+\frac{\beta_a}{\kappa}}\}p_i\sum_{j=1}^{N} a_{ij}p_j \\ &- (\beta-\beta_a)r_i\sum_{j=1}^{N} a_{ij}p_j - \delta p_i, \qquad (6.18)\end{aligned}$$

$$\dot{r}_i = -\kappa(1+\frac{\beta_a}{\kappa})r_i\sum_{j=1}^{N} a_{ij}p_j. \qquad (6.19)$$

To facilitate the subsequent analysis, define

$$\mathbf{p} \triangleq [p_1, ..., p_N]^T \in \mathbb{R}^N, \ \mathbf{r} \triangleq [r_1, ..., r_N]^T \in \mathbb{R}^N. \qquad (6.20)$$

According to (6.18) and (6.19) and the definitions (6.20), the followings are true

$$\dot{\mathbf{p}} = (\beta_{eff}A - \delta I)\mathbf{p} + \boldsymbol{g}_1(\mathbf{p}, \mathbf{r}), \qquad (6.21)$$

$$\dot{\mathbf{r}} = \mathbf{0}\mathbf{r} + \boldsymbol{g}_2(\mathbf{p}, \mathbf{r}), \qquad (6.22)$$

where $\mathbf{0}$ is a matrix or vector of appropriate dimensions,

$$\beta_{eff} \triangleq \beta\frac{\frac{\beta_a}{\kappa}}{1+\frac{\beta_a}{\kappa}} + \beta_a\frac{1}{1+\frac{\beta_a}{\kappa}}, \qquad (6.23)$$

and

$$\boldsymbol{g}_k(\cdot) \triangleq [g_{k,1}(\cdot), ..., g_{k,N}(\cdot)]^T, \qquad (6.24)$$

for $k \in \{1, 2\}$ with

$$g_{1,i}(\mathbf{p}, \mathbf{r}) \triangleq -\{\beta + \frac{\beta + \beta_a}{1 + \frac{\beta_a}{\kappa}}\} p_i \sum_{j=1}^{N} a_{ij} p_j$$
$$- (\beta - \beta_a) r_i \sum_{j=1}^{N} a_{ij} p_j, \tag{6.25}$$

$$g_{2,i}(\mathbf{p}, \mathbf{r}) \triangleq -\kappa(1 + \frac{\beta_a}{\kappa}) r_i \sum_{j=1}^{N} a_{ij} p_j. \tag{6.26}$$

If we linearize the system (6.21) and (6.22) at the origin, the resulting system has N zero eigenvalues. Therefore, linearization technique fails to investigate the stability properties of (6.21) and (6.22). In the following arguments, we show that center manifold theory can be employed here.

The eigenvalues of matrix $(\beta_{eff} A - \delta I)$ are $\beta_{eff} \lambda_i - \delta, i \in \{1, ...N\}$, where λ_i's are the eigenvalues of the adjacency matrix A. Therefore, assuming that

$$\frac{\beta_{eff}}{\delta} < \frac{1}{\lambda_1(A)}, \tag{6.27}$$

the matrix $(\beta_{eff} A - \delta I)$ is Hurwitz (i.e., a matrix that all of its eigenvalues have negative real parts). In addition, the two nonlinear functions $\boldsymbol{g}_1$ and $\boldsymbol{g}_2$ defined in (6.24) satisfy

$$\boldsymbol{g}_k(\mathbf{0}, \mathbf{0}) = \mathbf{0}, \ \nabla \boldsymbol{g}_k(\mathbf{0}, \mathbf{0}) = \mathbf{0}, \tag{6.28}$$

for $k \in \{1, 2\}$, where ∇ is the gradient operator. The center manifold theorem (see [101] for more details) suggests that there exists a function $H(\cdot) : \mathbb{R}^N \to \mathbb{R}^N$ where the dynamics (6.21) and (6.22) can be determined by

$$\dot{\hat{\mathbf{r}}} = \boldsymbol{g}_2(H(\hat{\mathbf{r}}), \hat{\mathbf{r}}). \tag{6.29}$$

Differential equation (6.29) can be written in terms of its entries as

$$\dot{\hat{r}}_i = -\kappa(1 + \frac{\beta_a}{\kappa})\hat{r}_i \sum_{j=1}^{N} a_{ij} h_j(\hat{\mathbf{r}}), \tag{6.30}$$

for $i \in \{1, ..., N\}$, where $h_i(\cdot)$ is the i-th component of $H(\cdot) \triangleq [h_1(\cdot), ..., h_N(\cdot)]^T$.

Remark 2. *Usually, it is not feasible to find $h_i(\cdot)$ explicitly. However, we know that each function $h_i(\cdot)$ is necessarily non-negative since the probability p_i is non-negative.*

Lemma 4. *The trajectories of (6.30) will asymptotically converge to the set defined by*

$$\Omega = \{\hat{\mathbf{r}} \in \mathbb{R}^N | \hat{r}_i \sum_{j=1}^{N} a_{ij} h_j(\hat{\mathbf{r}}) = 0, i = 1, ..., N\}. \tag{6.31}$$

Proof. Define a continuously differentiable function V as

$$V \triangleq \frac{1}{2}\hat{\mathbf{r}}^T\hat{\mathbf{r}}. \tag{6.32}$$

Taking the derivative of V with respect to time, we have

$$\dot{V} = \sum_{i=1}^{N} \hat{r}_i\dot{\hat{r}}_i = -\kappa(1 + \frac{\beta_a}{\kappa}) \sum_{i=1}^{N} \left(\hat{r}_i^2 \sum_{j=1}^{N} a_{ij} h_j(\hat{\mathbf{r}}) \right). \tag{6.33}$$

It can be seen that the time derivative $\dot{V}$ is negative semi-definite according to Remark 2. According to the LaSalle's invariance theorem (see [101]) the trajectories of (6.30) will asymptotically converge to the set $\dot{V} \equiv 0$, i.e., Ω in (6.31). □

Theorem 7. *Consider the SAIS spreading model (6.5) and (6.6). Assume that the effective infection rate satisfies (6.27) where β_{eff} is defined in (6.23). Small initial infections die out asymptotically as $t \to \infty$.*

Proof. Since the effective infection rate satisfies (6.27), the matrix $(\beta_{eff}A - \delta I)$ is Hurwitz.

According to the property (6.28) of $\boldsymbol{g}_1(\mathbf{p}, \mathbf{r})$, the system

$$\dot{\mathbf{p}} = (\beta_{eff} A - \delta I)\mathbf{p} + \boldsymbol{g}_1(\mathbf{p}, \mathbf{0}),$$

which is system (6.21) with $\mathbf{r} = \mathbf{0}$, is exponentially stable. In addition, according to Lemma 4, $\hat{r}_i \sum_{j=1}^{N} a_{ij} h_j(\hat{\mathbf{r}}) \to \infty$ as $t \to \infty$. Therefore, the term $r_i \sum_{j=1}^{N} a_{ij} p_j$ in (6.18) can be considered as a vanishing disturbance for (6.21). Therefore, $p_i \to 0$ asymptotically as $t \to \infty$. □

Remark 3. *From Theorem 6, the first epidemic threshold is*

$$\tau_{c_1} = \frac{1}{\lambda_1(A)}, \tag{6.34}$$

which is equal to the epidemic threshold in the N-intertwined SIS epidemic model. If the infection rate β_a is such that

$$\frac{\beta_a}{\delta} < \frac{1}{\lambda_1(A)}, \tag{6.35}$$

the ratio $\frac{\beta_{eff}}{\delta}$ can be larger or smaller than $\frac{1}{\lambda_1(A)}$, depending on the value of β. Therefore, if (6.35) holds, Theorem 7 suggests that there exists another epidemic threshold τ_{c_2}. Using the definition of β_{eff} in (6.23), the condition (6.27) in Theorem 7 can be expressed as

$$\frac{\beta_{eff}}{\delta} = \frac{\beta}{\delta} \frac{\frac{\beta_a}{\kappa}}{1 + \frac{\beta_a}{\kappa}} + \frac{\beta_a}{\delta} \frac{1}{1 + \frac{\beta_a}{\kappa}} \leq \frac{1}{\lambda_1(A)}, \tag{6.36}$$

which is equivalent to

$$\frac{\beta}{\delta} \leq \frac{1}{\lambda_1(A)} + \frac{\kappa}{\beta_a}\left(\frac{1}{\lambda_1(A)} - \frac{\beta_a}{\delta}\right). \tag{6.37}$$

From (6.37), the second epidemic threshold τ_{c_2} is

$$\tau_{c_2} = \tau_{c_1} + \frac{\kappa}{\beta_a}\left(\frac{1}{\lambda_1(A)} - \frac{\beta_a}{\delta}\right). \tag{6.38}$$

Notice that, according to (6.35), $\tau_{c_2} > \tau_{c_1}$.

6.3.4 Epidemic Persistence in the Steady-State

The steady-state is studied by letting the time derivatives $\dot{p}_i$ and $\dot{q}_i$ equal to zero, namely,

$$0 = \beta(1 - p_i^{ss} - q_i^{ss})y_i^{ss} + \beta_a q_i^{ss} y_i^{ss} - \delta p_i^{ss}, \tag{6.39}$$

$$0 = \kappa(1 - p_i^{ss} - q_i^{ss})y_i^{ss} - \beta_a q_i^{ss} y_i^{ss}, \tag{6.40}$$

where $y_i^{ss} \triangleq \sum_{j=1}^{N} a_{ij} p_j^{ss}$.

From (6.40), it is inferred that

$$q_i^{ss} \sum_{j=1}^{N} a_{ij} p_j^{ss} = \frac{1 - p_i^{ss}}{1 + \frac{\beta_a}{\kappa}} \sum_{j=1}^{N} a_{ij} p_j^{ss}. \tag{6.41}$$

Now, substitute for $q_i^{ss} \sum_{j=1}^{N} a_{ij} p_j^{ss}$ terms in (6.39) using (6.41) to get

$$\left(\beta \frac{\frac{\beta_a}{\kappa}}{1 + \frac{\beta_a}{\kappa}} + \beta_a \frac{1}{1 + \frac{\beta_a}{\kappa}} \right) (1 - p_i^{ss}) \sum_{j=1}^{N} a_{ij} p_j^{ss} - \delta p_i^{ss} = 0. \tag{6.42}$$

Theorem 8. *Consider the SAIS spreading model (6.5) and (6.6). The steady-state values of the infection probability of each individual in the SAIS model is similar to those of the NIMFA model (2.6) with an effective infection rate β_{eff}.*

Proof. Based on the definition of β_{eff} in (6.23), the equation (6.42) is simplified to

$$\beta_{eff}(1 - p_i^{ss}) \sum_{j=1}^{N} a_{ij} p_j^{ss} - \delta p_i^{ss} = 0,$$

which can be expressed as

$$\frac{\beta_{eff}}{\delta} \sum_{j=1}^{N} a_{ij} p_j^{ss} = \frac{p_i^{ss}}{1 - p_i^{ss}}. \tag{6.43}$$

Comparing (6.43) with (2.7), it is observed that the steady-state values of the infection probabilities in an SAIS epidemic network is equal to those of a SIS epidemic network with effective infection rate β_{eff}. □

6.4 Simulation Results

In order to examine the analytical results developed for the SAIS spreading model, three examples are provided in this section. In all of the simulations, the curing rate is fixed at $\delta = 1$ so that the dimensionless time $\bar{t} = \delta t$ is the same as the simulation time.

Example 1. *We consider an arbitrary contact graph with* 11 *nodes and* 16 *links. For this network, the spectral radius is found to be* $\lambda_1(A) = 3.1385$. *For the simulation purpose, three nodes are initialized in the infected state while others are all susceptible. In Fig. 6.2, three trajectories of the total infection fraction* $\bar{p}(t) = \frac{1}{N}\sum_{i=1}^{N} p_i(t)$ *are plotted. For all the three,* $\kappa = 0.1$ *and* $\beta_a = 0.1$. *The trajectories (a) and (b) correspond to the NIMFA model 2.6 and the SAIS spreading model (6.5) and (6.6), respectively, with* $\beta = 2$. *Trajectory (c) is the solution of the SIS model with the infection rate* β_{eff} *defined in (6.23). As is expected from Theorem 5, the infected fraction in SIS model always dominates the SAIS model. In addition, as proved in Theorem 8, the steady-state infection fraction in the SAIS is equal to that of the SIS model with the effective infection rate* β_{eff}. *In Fig. 6.2, it can be observed that the infection probabilities in the SAIS model spread similar to the SIS model at the first stage. Then, the size of the epidemics is reduced due to increased alertness in the network.*

Example 2. *In this example, for the same network in the previous example, (1) the steady-state value of the infected fraction and (2) the maximum value of the infected fraction are plotted as a function of the effective infection rate* $\tau = \beta/\delta$. *The simulation parameters are chosen as* $\kappa = 1$, $\beta_a = 0.1$. *Since* $\beta_a/\delta = 0.1 < 1/\lambda_1(A) = 0.3186$, *there exists two distinct thresholds* τ_{c_1} *and* τ_{c_2} *presented in (6.34) and (6.38), respectively, as discussed in Remark 3. Simulation results for this example are shown in Fig. 6.3. As is observed in Fig. 6.3,*

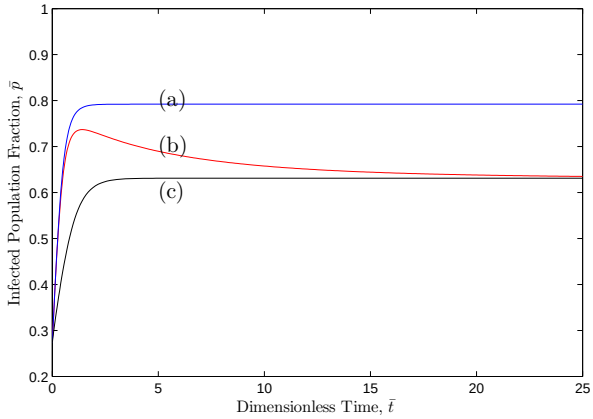

Figure 6.2: *The infected population fraction in Example 1. (a) SIS model. (b) SAIS model. (c) SIS model with reduced infection rate* β_{eff}.

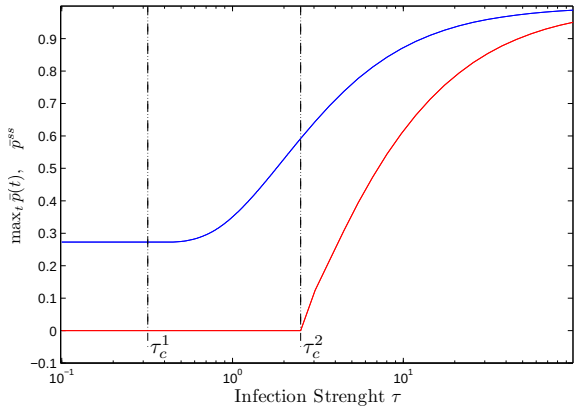

Figure 6.3: *The maximum infected fraction and the steady-state value for the infected fraction in Example 2.*

the steady-state values of the infected fraction $\bar{p}$ *is zero before the second epidemic threshold* τ_{c_2}. *In addition, the maximum of the infected fraction is equal to the initial infected fraction before* τ_{c_1}, *because before* τ_{c_1}, *the epidemics dies out exponentially; as stated in Theorem 6. Between the two thresholds,* $\max_t \bar{p}(t)$ *is greater than* $\bar{p}(0)$ *but steady-state value* $\bar{p}^{ss} = 0$. *Therefore, in this region the epidemic spreads at the first stage but then completely dies out as a result of increased alertness. After the second threshold,* $\bar{p}^{ss} < \max_t \bar{p}(t)$, *i.e., alertness reduced the infection size.*

Example 3. *Consider an epidemic network where the contact graph is an Erdos-Reyni random graph with* $N = 320$ *nodes and connection probability* $p = 0.2$. *The initial infected*

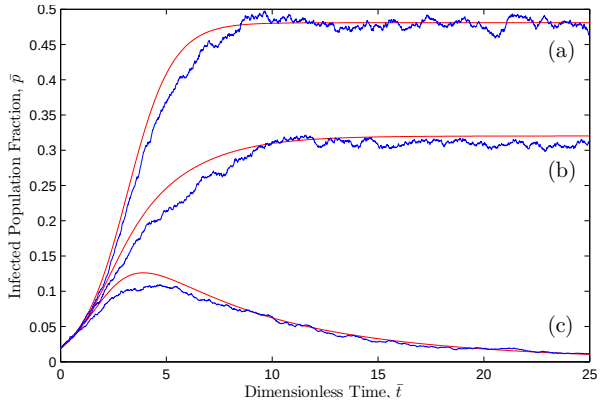

Figure 6.4: *The infected population fraction in Example 3. (a) SIS model. (b) SAIS model with* $\beta_a = 0.02$. *(c) SAIS model with* $\beta_a = 0.01$.

population is %2 of the whole population. The simulation parameters are $\beta = 0.03$, $\kappa = 0.05$. *Three trajectories (a), (b), and (c) are presented in Fig. 6.4 corresponding to* $\beta_a = \beta$, $\beta_a = 0.02$, $\beta_a = 0.01$. *For the sake of evaluating the model development in Section 6.2, a Monte-Carlo simulation is also provided for each trajectory, shown in Fig. 6.4 in blue. As can be seen, there is a reasonable agreement between the proposed model (6.5) and (6.6) and the actual SAIS Markov process. It can be observed that lowering* β_a *reduces the steady state infection probability. For a sufficiently small value of* β_a *infection is mitigated totally at the steady state.*

Chapter 7

Optimal Information Dissemination in Epidemic Networks

7.1 Introduction

In this study, built upon the SAIS model [5], we investigate how information dissemination can help boosting the resilience of the agent population against the spreading. The role of information about the infection on the behavior of individuals has attracted a substantial attention [94,96,102]. Information dissemination policies can potentially be used to promote the public health. In our formulation, the information dissemination is realized through an additional network among agents, which has the same nodes (agents) but different links with respect to the contact network. Each link in the information dissemination network is a directed link which provides the health status of the source agent to the end agent. The contributions of this study are: (1) Unlike most of the existing results in the literature, the contact network and the information dissemination network are generic graphs. (2) An information dissemination metric is introduced which is explicitly related to the effect of the information dissemination on the resilience of the epidemic network. The metric has a simple and elegant expression. It is a quadratic form of the adjacency matrix of the information

dissemination network and the dominant eigenvector of the adjacency matrix of the contact graph. (3) Given the contact network and some design constraint, the optimal topology of the information dissemination network is found. It is proven that the spectral centrality of the nodes and edges determines the optimal information dissemination network. Up to the authors' knowledge these results for epidemic networks are reported for the first time in this study, providing a fundamental progress w.r.t. the literature. Additionally, these results have the potential to be applied to mitigate epidemics in several different complex systems, from human and animal infectious diseases, to malware propagation in computer and sensor networks.

7.2 Model Development

This study proposes an extension to the SAIS model developed in [5] (see Chapter 6), promoting the alerting process using an information dissemination mechanism. Specifically, an information dissemination mechanism is developed so that the health information of some agents in the population is provided to some other agents. We denote the adjacency matrix of the information dissemination network by matrix $B = [b_{ij}]_{N\times N}$. The entry b_{ij} is such that if the information of the agent j is provided to agent i, $b_{ij} = 1$, otherwise, $b_{ij} = 0$. The information dissemination network is a *directed* network which is not required to be connected. The transition from the susceptible to the alert state (6.3) in the original SAIS model is modified to be

$$P(x_i(t+\Delta t) = e_2 | x_i(t) = e_1, X(t)) = (\kappa Y_i(t) + kZ_i(t))\Delta t + o(\Delta t), \tag{7.1}$$

where $Z_i(t) \triangleq \sum_{j=1}^{N} b_{ij} 1_{\{x_j(t)=e_1\}}$ is the number of infected agents whose health status is provided to agent i through the information dissemination network. The coefficient $k > 0$ determines the rate that susceptible agents become alert when they learn about existence of infection through the information dissemination network. The stochastic compartmental

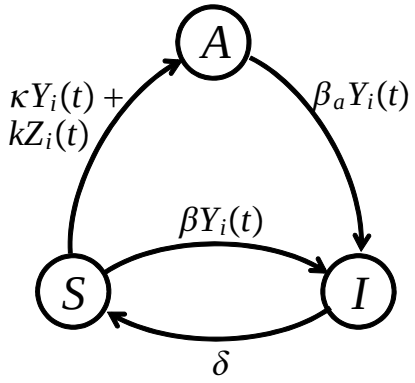

Figure 7.1: *Compartmental transition graph according to the SAIS model with information dissemination. Y_i and Z_i are the number of infected neighbors of agent i in contact network and information dissemination network, respectively.*

transitions of a node are depicted in Fig. 7.1. An illustrative schematics of the contact network and the information dissemination network is shown in 7.2.

Let p_i, and q_i denote the probabilities of agent i to be infected and alert, respectively. Using the same procedures as in [5], the SAIS model with information dissemination is obtained as:

$$\dot{p}_i = \beta(1 - p_i - q_i) \sum_{j=1}^{N} a_{ij} p_j + \beta_a q_i \sum_{j=1}^{N} a_{ij} p_j - \delta p_i, \tag{7.2}$$

$$\dot{q}_i = (1 - p_i - q_i)\{\kappa \sum_{j=1}^{N} a_{ij} p_j + k \sum_{j=1}^{N} b_{ij} p_j\} - \beta_a q_i \sum_{j=1}^{N} a_{ij} p_j, \tag{7.3}$$

for $i \in \{1, ..., N\}$.

7.3 Analysis of the SAIS Model with Information Dissemination

In this section, the dynamic system (7.2) and (7.3) derived in the previous section is analyzed. First, we review the basic results for the case where there is no information dis-

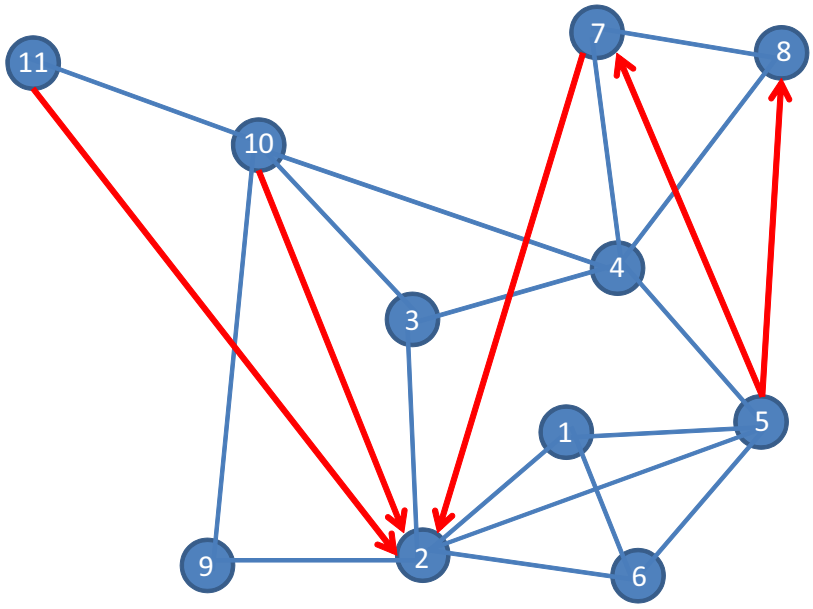

Figure 7.2: *Contact network (blue links) and the information dissemination network (red directed links).*

semination. Throughout this study, the alerted infection rate β_a is assumed to satisfy the following assumption to ensure that the cautious behavior is strong enough to mitigate the infection.

Assumption 3. *The infection rate is β_a satisfies*

$$0 < \frac{\beta_a}{\delta} < \frac{1}{\lambda_1}. \tag{7.4}$$

7.3.1 Case of No Information Dissemination

When there is not information, $k = 0$ in the dynamical system (7.2) and (7.3). The equations (7.2) and (7.3) with $k = 0$ are actually the original SAIS model developed and studied in [5]. It was shown in [5] that the SAIS model with no information dissemination exhibits two distinct thresholds in the dynamics of epidemic spread. Below the first threshold τ_{c_1}, infection dies out exponentially. Beyond the second threshold $\tau_{c_2}(0)$, infection persists in the steady state. Between the two thresholds, infection spreads at the first stage but then

dies out asymptotically as the result of increased alertness in the network. It was shown that the first threshold τ_{c_1} does not depend on behavioral parameters, while the second threshold $\tau_{c_2}(0)$ is directly influenced by the behavioral parameters. More discussion about the second threshold and its practical importance are available in [3].The main results of the analysis are provided in the following.

Theorem 9. *Consider the SAIS epidemic spread model (7.2) and (7.3) with no information dissemination (i.e. $k = 0$). Under the Assumption 3,*

- *initial infections will die out exponentially if the effective infection rate $\tau \triangleq \beta/\delta$ satisfies*

$$\tau < \tau_{c_1} \triangleq \frac{1}{\lambda_1}, \tag{7.5}$$

- *initial infections die out asymptotically if*

$$\tau_{c_1} < \tau < \tau_{c_2}(0) \triangleq \frac{1}{\lambda_1} + \frac{\kappa}{\beta_a}(\frac{1}{\lambda_1} - \frac{\beta_a}{\delta}), \tag{7.6}$$

- *infection probabilities will reach to nonzero steady-state values if*

$$\tau > \tau_{c_2}(0).$$

Proof. See [5] for the proof. □

7.3.2 SAIS with Information Dissemination

Theorem 10. *For the SAIS model with information dissemination (7.2-7.3), under the Assumption 3, initial infection with will die out if the effective infection rate is less than $\tau_{c_1} = \lambda_1^{-1}$. Furthermore, there exists a second threshold $\tau_{c_2}(k)$, such that if $\tau_{c_1} < \tau < \tau_{c_2}(k)$, initial infection dies out asymptotically. In addition, the second threshold $\tau_{c_2}(k)$ is a monotonically increasing function of k.*

Proof. If $\tau < \tau_{c_1}$, the infection probability dies out exponentially according to Theorem 9 for the SAIS model. It is straightforward to show that the infection probability of the SAIS model (7.2-7.3) with no information dissemination is never less than the case with information dissemination. Therefore, the infection probability in the SAIS model with information dissemination also dies out exponentially. Similar argument can be made for the asymptotically die out.

If the effective infection rate is very strong, i.e., $\tau \to \infty$, all of the agents will be infected in the steady state. Therefore, there must be a second threshold $\tau_{c_2}(k)$ such that for $\tau < \tau_{c_2}(k)$ infection dies out and for $\tau > \tau_{c_2}(k)$ infection persist in the steady state. Also, the information dissemination contributes positively to reducing the infection size. Therefore, $\tau_{c_2}(k)$ should increase monotonically by k. □

Lemma 5. *If the contact network is connected, the steady-state values of the infection probabilities are either zero for all of the agents or absolutely positive for all the agents.*

Proof. The idea of the proof is inspired from [21]. The steady-state values for the infection and alertness probabilities, denoted by p_i^* and q_i^*, satisfies

$$\beta(1 - p_i^* - q_i^*) \sum_{j=1}^{N} a_{ij} p_j^* + \beta_a q_i^* \sum_{j=1}^{N} a_{ij} p_j^* - \delta p_i^* = 0. \tag{7.7}$$

According to (7.7), $p_i^* = 0$, for $\forall i \in \{1, ..., N\}$ is a solution for the steady-state infection probabilities. Suppose there exists a node j such that $p_j^* > 0$. For any node i that is a neighbor of node j, i.e., $a_{ij} \neq 0$, the probability of infection is

$$p_i^* = \frac{\beta(1 - q_i^*) \sum_{j=1}^{N} a_{ij} p_j^* + \beta_a q_i^* \sum_{j=1}^{N} a_{ij} p_j^*}{\beta \sum_{j=1}^{N} a_{ij} p_j^* + \delta}. \tag{7.8}$$

The steady-state value p_i^* is positive because $\sum_{j=1}^{N} a_{ij} p_j^* \geq a_{ij} p_j^* > 0$, $0 \leq q_i^* \leq 1$, and $\beta, \beta_a > 0$. Same procedure can be applied to the neighbors of node i, and so on. Hence, if the contact network is connected and at least one of the agents have nonzero infection

probability, then $p_i^* > 0$, for all $i \in \{1, ..., N\}$. □

After the second threshold, i.e., $\tau > \tau_{c_2}(k)$, the the steady-state values p_i^* start to obtain positive values. Therefore, the value for $\tau_{c_2}(k)$ can be determined by studying the solution of the steady-state values. At the steady-state, according to (7.3),

$$(1-p_i^*)\{\kappa\sum_{j=1}^{N}a_{ij}p_j^*+k\sum_{j=1}^{N}b_{ij}p_j^*\}-q_i^*\{\kappa\sum_{j=1}^{N}a_{ij}p_j^*+k\sum_{j=1}^{N}b_{ij}p_j^*\}-\beta_a q_i^*\sum_{j=1}^{N}a_{ij}p_j^*=0. \quad (7.9)$$

Therefore, if the values of p_i^* are positive, then

$$q_i^* = (1-p_i^*)f_i(\mathbf{p}^*, \bar{k}),$$

where $\bar{k} \triangleq \frac{k}{\beta_a}$ and $\mathbf{p}^* \triangleq [p_1^*, ..., p_N^*]^T$, and $f_i(\mathbf{p}^*, \bar{k})$ is defined as

$$f_i(\mathbf{p}^*, \bar{k}) \triangleq \frac{\frac{\kappa}{\beta_a}\sum_{j=1}^{N}a_{ij}p_j^*+\bar{k}\sum_{j=1}^{N}b_{ij}p_j^*}{(1+\frac{\kappa}{\beta_a})\sum_{j=1}^{N}a_{ij}p_j^*+\bar{k}\sum_{j=1}^{N}b_{ij}p_j^*}. \quad (7.10)$$

Also, to facilitate the subsequent analysis, we make the convention that $f_i(\mathbf{0}, \bar{k})$ is some positive real number.

Substituting for q_i^* in (7.7) and dividing the both sides by δ,

$$\tau(1-p_i^*)\sum_{j=1}^{N}a_{ij}p_j^*-(\tau-\frac{\beta_a}{\delta})(1-p_i^*)f_i(\mathbf{p}^*,\bar{k})\sum_{j=1}^{N}a_{ij}p_j^*-p_i^*=0, \quad (7.11)$$

for $i \in \{1, ..., N\}$, where $\tau = \beta/\delta$. The above equation gives the steady-state value of the infection probabilities.

Theorem 11. *Second threshold τ_{c_2} is such that the set of equations*

$$\tau_{c_2}\sum_{j=1}^{N}a_{ij}w_j-(\tau_{c_2}-\frac{\beta_a}{\delta})f_i(\mathbf{w},\bar{k})\sum_{j=1}^{N}a_{ij}w_j-w_i=0, \quad (7.12)$$

where $\mathbf{w} = [w_1, ..., w_N]^T$*, has a nontrivial solution with all* $w_i > 0$*.*

Proof. Define $\tilde{\tau} \triangleq \tau - \tau_{c_2}$. Close to the second threshold, i.e., as $\tilde{\tau} \to 0^+$, $p_i^* = \tilde{\tau} \frac{\partial p_i^*}{\partial \tau}|_{\tau=\tau_{c_2}} + o(\tilde{\tau})$. Therefore, $f_i(\mathbf{p}^*, \bar{k}) \to f_i(\frac{\partial \mathbf{p}^*}{\partial \tau}|_{\tau=\tau_{c_2}}, \bar{k})$. Letting $\tau \to \tau_{c_2}^+$ in (7.11),

$$\tau_{c_2} \sum_{j=1}^{N} a_{ij} \frac{\partial p_j^*}{\partial \tau}|_{\tau=\tau_{c_2}} - (\tau_{c_2} - \frac{\beta_a}{\delta}) f_i(\frac{\partial \mathbf{p}^*}{\partial \tau}|_{\tau=\tau_{c_2}}, \bar{k}) \sum_{j=1}^{N} a_{ij} \frac{\partial p_j^*}{\partial \tau}|_{\tau=\tau_{c_2}} - \frac{\partial p_i^*}{\partial \tau}|_{\tau=\tau_{c_2}} = 0. \quad (7.13)$$

Since τ_{c_2} is the second threshold, $\frac{\partial p_i^*}{\partial \tau}|_{\tau=\tau_{c_2}}$ must be positive for every $i \in \{1, ..., N\}$. Hence, τ_{c_2} is such that the set of algebraic equations (7.12) has positive solutions. □

Remark 4. *The set of algebraic equations (7.12) is a nonlinear eigenvalue-type problem. If* $\mathbf{w}$ *is a solution then* $\alpha\mathbf{w}$ *is also a solution for any* $\alpha > 0$*, because* $f_i(\alpha\mathbf{w}, \bar{k}) = f_i(\mathbf{w}, \bar{k})$*. The trivial solution* $\mathbf{w} = \mathbf{0}$ *always satisfies (7.12). However, we are interested in non-trivial solutions and specifically the ones with all positive entries.*

Remark 5. *The second threshold* τ_{c_2} *is a function of* $\bar{k}$*. For* $\bar{k} = 0$*,* $f_i(\mathbf{w}, \bar{k})$ *is*

$$f_i(\mathbf{w}, 0) = \frac{\frac{\kappa}{\beta_a}}{1 + \frac{\kappa}{\beta_a}}. \quad (7.14)$$

Therefore, for $\bar{k} = 0$*, the set of algebraic equations (7.12) becomes*

$$(\tau_{c_2} \frac{1}{1 + \frac{\kappa}{\beta_a}} - \frac{\beta_a}{\delta} \frac{\frac{\kappa}{\beta_a}}{1 + \frac{\kappa}{\beta_a}}) \sum_{j=1}^{N} a_{ij} w_j - w_i = 0, \quad (7.15)$$

which can be expressed in the collective form,

$$(\tau_{c_2} \frac{1}{1 + \frac{\kappa}{\beta_a}} - \frac{\beta_a}{\delta} \frac{\frac{\kappa}{\beta_a}}{1 + \frac{\kappa}{\beta_a}}) A\mathbf{w} = \mathbf{w}. \quad (7.16)$$

The above equation has nontrivial solution if $(\tau_{c_2} \frac{1}{1+\frac{\kappa}{\beta_a}} - \frac{\beta_a}{\delta} \frac{\frac{\kappa}{\beta_a}}{1+\frac{\kappa}{\beta_a}})^{-1}$ *is an eigenvalue of* A*. In this case,* $\mathbf{w}$ *is the corresponding eigenvector. However, all the elements of* $\mathbf{w}$ *are strictly*

positive only if $\mathbf{w}$ *is the eigenvector of* A *corresponding to the largest eigenvalue, i.e.,* $\mathbf{w} = v_1$. *Letting* $(\tau_{c_2}\frac{1}{1+\frac{\kappa}{\beta_a}} - \frac{\beta_a}{\delta}\frac{\frac{\kappa}{\beta_a}}{1+\frac{\kappa}{\beta_a}}) = \lambda_1^{-1}$, *the second threshold* $\tau_{c_2}(0)$ *is found to be*

$$\tau_{c_2}(0) = \frac{1}{\lambda_1} + \frac{\kappa}{\beta_a}(\frac{1}{\lambda_1} - \frac{\beta_a}{\delta}), \tag{7.17}$$

which is actually equal to the second threshold for SAIS model with no information dissemination defined in (7.6).

7.4 Optimal Information Dissemination

7.4.1 Information Dissemination Metric

In general, it is very difficult, if not impossible, to find analytic solution to the set of algebraic equations (7.12). The epidemic threshold τ_{c_2} is a function of $\bar{k}$. We propose to use perturbation theory to find approximate solutions for the second threshold. As shown in Remark 5, for $\bar{k} = 0$, $\tau_{c_2}(0) = \frac{1}{\lambda_1} + \frac{\kappa}{\beta_a}(\frac{1}{\lambda_1} - \frac{\beta_a}{\delta})$ and $\mathbf{w} = v_1$. Taking the partial derivative from both sides of (7.12) at $\bar{k} = 0$ yields

$$\begin{aligned}
&\frac{\partial \tau_{c_2}}{\partial \bar{k}} \sum_{j=1}^{N} a_{ij} v_{1,j} + \tau_{c_2}(0) \sum_{j=1}^{N} a_{ij} \frac{\partial w_j}{\partial \bar{k}} - \frac{\partial \tau_{c_2}}{\partial \bar{k}} f_i(v_1, 0) \sum_{j=1}^{N} a_{ij} v_{1,j} \\
&- (\tau_{c_2}(0) - \frac{\beta_a}{\delta}) \frac{\partial f_i}{\partial \bar{k}}(v_1, 0) \sum_{j=1}^{N} a_{ij} v_{1,j} - (\tau_{c_2}(0) - \frac{\beta_a}{\delta}) f_i(v_1, 0) \sum_{j=1}^{N} a_{ij} \frac{\partial w_j}{\partial \bar{k}} - \frac{\partial w_i}{\partial \bar{k}} = 0.
\end{aligned} \tag{7.18}$$

In the above equation, the expression for $\tau_{c_2}(0)$ is known from (7.6). The expression for $\frac{\partial f_i}{\partial \bar{k}}(v_1, 0)$ can also be obtained from (7.10) as

$$\begin{aligned}\frac{\partial f_i}{\partial \bar{k}}(v_1,0) &= \frac{\partial}{\partial \bar{k}} \frac{\frac{\kappa}{\beta_a}\sum_{j=1}^{N} a_{ij}w_j + \bar{k}\sum_{j=1}^{N} b_{ij}w_j}{(1+\frac{\kappa}{\beta_a})\sum_{j=1}^{N} a_{ij}w_j + \bar{k}\sum_{j=1}^{N} b_{ij}w_j}\Big|_{\substack{\mathbf{w}=v_1,\\ \bar{k}=0}} \\ &= \frac{\partial}{\partial \bar{k}}\{\frac{\frac{\kappa}{\beta_a}}{1+\frac{\kappa}{\beta_a}} + \\ &\quad \frac{\bar{k}(1+\frac{\kappa}{\beta_a})^{-1}\sum_{j=1}^{N} b_{ij}w_j}{(1+\frac{\kappa}{\beta_a})\sum_{j=1}^{N} a_{ij}w_j + \bar{k}\sum_{j=1}^{N} b_{ij}w_j}\}\Big|_{\substack{\mathbf{w}=v_1,\\ \bar{k}=0}} \\ &= \frac{\sum_{j=1}^{N} b_{ij}v_{1,j}}{(1+\frac{\kappa}{\beta_a})^2\sum_{j=1}^{N} a_{ij}v_{1,j}}. \end{aligned} \tag{7.19}$$

Substituting for $\tau_{c_2}(0)$ and $\frac{\partial f_i}{\partial \bar{k}}(v_1, 0)$ in (7.18) leads to

$$\frac{\partial \tau_{c_2}}{\partial \bar{k}}\frac{1}{1+\frac{\kappa}{\beta_a}}\sum_{j=1}^{N} a_{ij}v_{1,j} - \frac{1}{1+\frac{\kappa}{\beta_a}}(\frac{1}{\lambda_1} - \frac{\beta_a}{\delta})\sum_{j=1}^{N} b_{ij}v_{1,j} + \frac{1}{\lambda_1}\sum_{j=1}^{N} a_{ij}\frac{\partial w_j}{\partial \bar{k}} - \frac{\partial w_i}{\partial \bar{k}} = 0. \tag{7.20}$$

In the collective form,

$$\frac{\partial \tau_{c_2}}{\partial \bar{k}}\frac{1}{1+\frac{\kappa}{\beta_a}}\lambda_1 v_1 - \frac{1}{1+\frac{\kappa}{\beta_a}}(\frac{1}{\lambda_1} - \frac{\beta_a}{\delta})Bv_1 + (\frac{1}{\lambda_1}A - I)\frac{\partial \mathbf{w}}{\partial \bar{k}} = 0. \tag{7.21}$$

Theorem 12. *The second threshold $\tau_{c_2}(\bar{k})$ for which the set of equations (7.12) has positive solutions for w_i is*

$$\begin{aligned}\tau_{c_2}(\bar{k}) &= \frac{1}{\lambda_1} + \frac{\kappa}{\beta_a}(\frac{1}{\lambda_1} - \frac{\beta_a}{\delta}) \\ &\quad + \bar{k}\frac{v_1^T B v_1}{\lambda_1}(\frac{1}{\lambda_1} - \frac{\beta_a}{\delta}) + o(\bar{k}).\end{aligned} \tag{7.22}$$

Proof. Multiplying v_1^T from right to the both sides of (7.21) yields

$$\frac{\partial \tau_{c_2}}{\partial \bar{k}}\frac{1}{1+\frac{\kappa}{\beta_a}}\lambda_1 v_1^T v_1 - \frac{1}{1+\frac{\kappa}{\beta_a}}(\frac{1}{\lambda_1} - \frac{\beta_a}{\delta})v_1^T B v_1 + v_1^T(\frac{1}{\lambda_1}A - I)\frac{\partial \mathbf{w}}{\partial \bar{k}} = 0. \tag{7.23}$$

Since v_1 is the eigenvector of matrix A corresponding to λ_1 and A is symmetric, $v_1^T(\frac{1}{\lambda_1}A - I) = 0$. Furthermore, v_1 is normalized so $v_1^T v_1 = 1$. Substituting in the above equation, $\frac{\partial \tau_{c_2}}{\partial \bar{k}}$ is obtained as

$$\frac{\partial \tau_{c_2}}{\partial \bar{k}}|_{\bar{k}=0} = \frac{v_1^T B v_1}{\lambda_1}(\frac{1}{\lambda_1} - \frac{\beta_a}{\delta}). \tag{7.24}$$

Therefore, $\tau_{c_2}(\bar{k})$ can be expressed as

$$\begin{aligned}\tau_{c_2}(\bar{k}) &= \tau_{c_2}(0) + \frac{\partial \tau_{c_2}}{\partial k}(0)\bar{k} + o(\bar{k}) \\ &= \frac{1}{\lambda_1} + \frac{\kappa}{\beta_a}(\frac{1}{\lambda_1} - \frac{\beta_a}{\delta}) \\ &+ \frac{k}{\beta_a}\frac{v_1^T B v_1}{\lambda_1}(\frac{1}{\lambda_1} - \frac{\beta_a}{\delta}) + o(\bar{k}).\end{aligned} \tag{7.25}$$

□

Remark 6. *The expression (7.25) provides an elegant expression for the value of second threshold $\tau_{c_2}(\bar{k})$. However, this expression is only useful for small values of $\bar{k}$. As a consequence, all the subsequent analysis and result are valid for small values of $\bar{k}$.*

Remark 7. *As a special case, assume that the information dissemination network is the same as the contact network, i.e., $B = A$. This case is similar to the case where there is no information dissemination, but the alerting rate is $\kappa + k$. In this case,*

$$\frac{v_1^T B v_1}{\lambda_1} = \frac{v_1^T A v_1}{\lambda_1} = \frac{\lambda_1 v_1^T v_1}{\lambda_1} = v_1^T v_1 = 1.$$

From (7.22), $\tau_{c_2}(\bar{k}) = \frac{1}{\lambda_1} + \frac{\kappa+k}{\beta_a}(\frac{1}{\lambda_1} - \frac{\beta_a}{\delta}) + o(\bar{k})$.

Remark 8. *From (7.22), it is observed that if the information dissemination network is designed such that*

$$\phi(A, B) \triangleq \frac{v_1^T B v_1}{\lambda_1} \tag{7.26}$$

is maximized, the value for $\tau_{c_2}(\bar{k})$ is bigger. Therefore, the resilience of the network against

the spreading process is enhanced. We refer to the metric $\phi(A, B)$ as the information dissemination metric. *The information dissemination metric $\phi(A, B)$ can be easily computed from (7.26) once the spectral radius λ_1 and the dominant eigenvector v_1 of the contact network A are found.*

7.4.2 Optimal Topology of the Information Dissemination Network

From both application and theoretical aspects, a very interesting problem is to find the optimal topology of the information dissemination network. The optimal information dissemination network generates the maximal value for the second threshold τ_{c2}, discussed in Theorem 10 and Theorem 11. Based the arguments in Remark 8, for small values of $\bar{k}$, the optimal information dissemination network is associated with finding the best adjacency matrix B such that for a given A and some design constraints, the information dissemination metric $\phi(A, B)$ defined in (7.26) is maximized.

If there is no constraint on the B matrix, then the maximal value for $\phi(A, B)$ is obtained for the case where the information dissemination network is a complete graph, i.e., $B = \mathbf{1}\mathbf{1}^T - I$. In this case, the value of the information dissemination metric is

$$\phi^* = \phi(A, \mathbf{1}\mathbf{1}^T - I) = \lambda_1^{-1}\{(\mathbf{1}^T v_1)^2 - 1\}. \tag{7.27}$$

The above value is the maximal effect that can be expected from the information dissemination network. The worst case trivially is the case where there is no information dissemination, i.e., $\phi(A, \mathbf{0}) = 0$. In this section, we consider two types of constraint on the information dissemination network.

Constraint on the Degree Distribution

Assume that each agent i can only receive the health status of d_i other agents.

Theorem 13. *Given the degree distribution* $\mathbf{d} = (d_1, ..., d_N)$*, the optimal topology of the information dissemination network is such that each agent receives the health status of the* d_i *agents that have the largest element in the eigenvector* v_1 *with respect to other agents.*

Proof. From (7.26), the information dissemination metric can be expressed as

$$\phi(A, B) = \sum_{i=1}^{N} \sum_{j=1}^{N} b_{ij} v_{1,i} v_{1,j}. \tag{7.28}$$

If the degree d_i of agent i is fixed, the following set of constraints should be imposed on B:

$$\sum_{j=1}^{N} b_{ij} = d_i, \ i \in \{1, ..., N\}. \tag{7.29}$$

The optimal choice of b_{ij}'s in this case is such that $\sum_{j=1}^{N} b_{ij} v_{1,j}$ is maximized for each node i with the constraint $\sum_{j=1}^{N} b_{ij} = d_i$. Therefore, the optimal solution is to set $b_{ij} = 1$ for the d_i agents that have the largest value of $v_{1,j}$. □

Remark 9. *As can be seen, the elements of the dominant eigenvector* v_1 *of the contact network provides a measure of centrality for the nodes in the information dissemination network.*

Remark 10. *Consider the case where* d_i *are actually the degree of the nodes in the contact network, i.e.,* $d_i = \sum_{j=1}^{N} a_{ij}$*. It is interesting to note that the optimal topology for the information dissemination network is very different from the contact network. In other words, it is of more benefit to know the health information of the nodes with high eigenvector centrality rather that the health information of the nodes in immediate contact.*

Constraint on Number of Links

Consider the case where the number of the links in the information dissemination network is given and fixed.

Theorem 14. *Given the number of the links L, the optimal topology of the information dissemination network is such that $b_{ij} = 1$ for the first L pairs (i, j) with highest value of $v_{1,i}v_{1,j}$ and $b_{ij} = 0$ for the rest.*

Proof. Let $\mathcal{E}_B$ be the set of directed links in the information dissemination network. The information dissemination metric (7.26) can be expressed as

$$\phi(A, B) = \sum_{j=1}^{N} 1_{\{(i,j)\in\mathcal{E}_B\}} v_{1,i}v_{1,j}. \tag{7.30}$$

Given the number of the links L, the constraint is $\sum_{j=1}^{N} 1_{\{(i,j)\in\mathcal{E}_B\}} = L$. Therefore, the optimal solution is to set $(i, j) \in \mathcal{E}_B$ for the first L pairs (i, j) with highest value of $v_{1,i}v_{1,j}$. Having $(i, j) \in \mathcal{E}_B$ is equivalent to $b_{ij} = 1$. □

Remark 11. *As can be seen the product $v_{1,i}v_{1,j}$ provides a measure of centrality for the links in the information dissemination network. The eigenvector centrality measure of links, $v_{1,i}v_{1,j}$, is symmetric with respect to i and j. Therefore, if L is an even number, the optimal dissemination network is undirected.*

7.5 Conclusion and Future Work

This chapter studied the impact of information dissemination network on enhancing the resilience of a population against epidemic spreading. In particular, our modeling and analysis was to answer this question: "given a contact network, through which infection spreads, what is the optimal information dissemination network which boosts the system resilience the most?" We found elegant expressions and solutions to the optimal information dissemination problem. However, results reported here are only valid for small values of alerting rate since a perturbation method was used to solve (7.12). It is a very promising research work to look for possible analytical or numerical solutions for the optimal information dissemination problem for wider range of the alerting rate. This problem has multiple potential

areas of applications, from infectious diseases mitigation to malware impact reduction.

Chapter 8

Epidemic Spreading in State-Dependent Locally-Adaptive Networks

8.1 Introduction

Control of infectious disease spreading in social networks is very critical for public health purposes, and mitigation strategies include vaccination, quarantine, and preventive behaviors. Incorporating individuals' preventive behaviors into epidemic models has recently attracted substantial attention [92, 103]. Individuals tend to respond to emergence of an epidemic by (1) adopting hygiene/pharmaceutical actions [5, 94, 95, 99, 100, 104], e.g., wearing masks, following more hygiene, and taking vaccinations, or by (2) reducing or changing contacts to avoid infection [51, 105–112].

Recently, Sahneh et al. [5] proposed a model to implement self-initiated preventive response to infections. The key idea is to introduce an '*Alert*' state where individuals can still become infected, however, they adopt some preventive measures. Alert individuals adopt hygienic behavior modeled by a reduction in their infection rate [5]. This model was later

used to show importance of individuals' responsiveness to perceived infection [3], suggesting an optimization framework for investments on social awareness [113]. Built upon this model, authors investigated the effect of information dissemination on social alertness promotion, increasing the resilience of the population to infectious disease propagation [6]. In this chapter, we study the SAIS model where alert individuals adopt the preventive behavioral type 2, i.e., they change the contact network.

While various problems about dynamics on networks, such as synchronization and viral spreading, and dynamics of networks, such as rewiring processes, have been studied separately, synergistic development of models considering both dynamics has begun and provided some initial contributions. Gross et al. [107] is one of the first contributions on the topic of dynamic coevolving networks, where infected individuals rewire their links from infected individuals toward susceptible ones forming two loosely connected clusters. Marceau et al. [108] improved the compartmental formalism of this model to simultaneously track the evolution of the spreading process and the contact network structure. Risau-Gusman [109] showed simple rewiring of susceptible individuals from infected neighbors to other randomly chosen nodes can completely suppress the epidemic spreading.

Some models consider the reduction of contact on a weighted network as reduction of the weights of the contact links [51]. Other approaches consider a rewiring process, where individuals change their neighbors in an unweighted direct network when sensing infection. Such rewiring of local contacts can have a strong effect on the dynamics of the disease, which in turn influences the rewiring process. Thus, a complicated mutual interaction between a time-varying network topology and the dynamics of the nodes emerges. Guo et al. [114] studied an SIS epidemic model where contact between susceptible and infected nodes is removed at some rate. They showed the epidemic threshold increases as a function of the link removal rate, while the network topology exhibits binomial-like degree distribution, assortative mixing, and modularity. A thorough review of relevant results in this field can be found in [106]. It has been observed that adaptation of a contact network

does not always help in suppressing the infection. For example, previous models consider scenarios where individuals act as vectors for transmitting the infection to their new contacts. Meloni et al. [112] considered self-initiated behavioral changes for the mobility patterns of individuals. When travelers decide to avoid locations with high levels of infection and travel through locations with low levels of infections, this behavioral change may facilitate disease spreading.

We study a case where individuals myopically change their contact neighborhood when moving to the alert state as a response to sensing infection. We refer to this model as SAIS-LAC, where LAC stands for '**l**ocally **a**daptive **c**ontact.' In particular, each individual i has the myopic neighborhood $\mathcal{N}_i^A$ at normal time. However, once she becomes alert, she switches her neighbor set to $\mathcal{N}_i^B$. In the SAIS-LAC model, the transition to the alert state happens to susceptible individuals as a function of the infection state of the neighborhood $\mathcal{N}_i^A$, while the new neighbor set $\mathcal{N}_i^B$ is predetermined and the infection state of these new neighbors is not influencing the switching. As a result, overall contact topology switches among 2^N possible configurations. We show this state-dependent, locally switching network can be formulated as a two-layer network $\mathcal{G} = (V, E_A, E_B)$, where V is the node set, and E_A and E_B are the edge sets of susceptible and alert nodes, respectively. Employing the bifurcation theory, we show the epidemic threshold in this model is the solution of a nonlinear Perron-Frobenius (NPF) problem [115]. Finally, we provide analytical results to characterize solutions of the epidemic threshold in terms of the spectral quantities of two *auxiliary* graphs $G_A = (V, E_A)$ and $G_B = (V, E_B)$, corresponding to the two extreme cases of no switching contact and fully switched contact, respectively. The contribution of our work is two-fold. First, we propose a spectral study of a spreading scenario for an adaptive contact network. To the best of the authors' knowledge, this contribution is novel for the emerging research field of multilayer networks [55]. Second, we show that when $\mathcal{N}_i^B$ is a subset of $\mathcal{N}_i^A$, alertness always helps in reducing the infection impact. Additionally, according to our simple model, it is possible that contact change may worsen the spreading scenario. While the possible negative impact

of contact adaptation has been detected in previous research [112], the importance of our result is that in our model, switching individuals do not act as vectors for transmitting the disease and this counterintuitive observation is purely the consequence of topological complexities of the underlying adaptive hybrid contact. Therefore, our results complement and advance existing results on epidemic spreading over social networks.

8.2 Model Development

In this chapter, we model and study an SIS-type spreading on an adaptive contact network. The contact network is not fixed through time and is indeed a function of the states of the individuals. In general, the contact among a pair of individuals can depend on the joint state of two. For example, when an individual learns he is in risk of receiving infection from an infected individual, the tendency is to remove contact with that infected individual and possibly make a new contact with another healthy one. The adaptive contact network scheme in this study is technically simpler: if an individual becomes alert about existence of infection, he switches his myopic neighborhood to another set of nodes. This can reflect the case where people tend to avoid particular locations, and as a result change their neighborhood. In our formulation, we only consider two, fixed myopic neighborhoods for each individual. In practice, people vary the level of contact based on the perceived severity of infection risk/cost. Therefore, more realistic modeling would be to consider several choices of myopic neighborhood, depending on level of alertness.

8.2.1 Locally Switching Contact Network

In a networked SIS model [21, 22], each individual is a node of a graph and the (i, j) represents the contact between individuals i and j. Specifically, if j can potentially infect i, then $a_{ij} > 0$, otherwise $a_{ij} = 0$. According to this definition, existence of a contact between two individuals is independent of their states. A key concept in developing the

switching contact of this chapter is *state-dependent contact*, where the contact between a pair of individuals depends on the individuals' states. Specifically, we let a_{ij} denote the contact between susceptible individual i and infected individual j, and we let b_{ij} denote the contact between alert individual i and infected individual j. Generally, we can denote contact between susceptible-susceptible pairs, susceptible-alert pairs, and so on. However, since we are only interested in contacts capable of virus transmission, this chapter only models susceptible-infected and alert-infected contacts. In this interpretation, *if j is not infected, a_{ij} does not have any physical meaning.*

Remark 12. *In this view, susceptible node i receives infection from infected node j with rate βa_{ij}; with component β adjusting for the potency of infection globally, and component a_{ij} incorporating heterogeneity of infection process between pairs. When an individual becomes alert, here the rate of infection changes from the normal value of βa_{ij}. In the case of hygienic behavior, the β component changes to $\beta_a < \beta$ [5]. Therefore, as in the original SAIS model in [5], an alert node i receives the infection from infected node j at rate $\beta_a a_{ij}$. In order to model contact change, the a_{ij} component is changed to b_{ij}. Therefore, in the SAIS-LAC model, an alert node i receives the infection from infected node j at rate βb_{ij}.*

Remark 13. *Our contact switching scheme can also be viewed from another perspective. A very common approach for modeling switching networks is to relate network switching dynamics to an exogenous Markov chain process. In our proposed scheme, network switching corresponds not to an exogenous Markov process but instead to the epidemic spreading process on top, which is itself a Markov process. In particular, upon transition of an individual to alert state or to susceptible, her contact neighborhood switches. In this view, the overall contact topology is a directed graph switching among 2^N possible configurations.*

We show that our switching contact network can be effectively modeled as a two-layer network $\mathcal{G} = (V, E_A, E_B)$, where V is the node set, and E_A and E_B are the edge sets of susceptible and alert nodes, respectively. Therefore, $(i, j) \in E_A$ iff $a_{ij} > 0$, and $(i, j) \in E_B$ iff $b_{ij} > 0$. The layers of $\mathcal{G}$ are two *auxiliary* graphs $G_A = (V, E_A)$ and $G_B = (V, E_B)$,

corresponding to the two extreme cases of no switching contact and fully switched contact, respectively. In Section 8.4.2, we show it is possible to characterize the behavior of the SAIS-LAC model using spectral properties of G_A and G_B, and their interrelation.

8.2.2 SAIS-LAC Markov Model

Consider a population of N individuals, where each individual is either '*Susceptible*,' '*Infected*,' or '*Alert*.' For each individual $i \in \{1, ..., N\}$, let the random variable $x_i(t) = e_1$ if the individual i is susceptible at time t, $x_i(t) = e_2$ if alert, and $x_i(t) = e_3$ if infected, where $e_1 = [1, 0, 0]^T$, $e_2 = [0, 1, 0]^T$, and $e_3 = [0, 0, 1]^T$ are the standard unit vectors of $\mathbb{R}^3$. There are four stochastic transitions in the SAIS model with switching contact:

1. A susceptible individual becomes infected by the infection rate β times the number of its infected $A-$neighbors, i.e.,

$$\Pr[x_i(t + \Delta t) = e_3 | x_i(t) = e_1, X(t)] = \beta Y_i(t)\Delta t + o(\Delta t), \tag{8.1}$$

   for $i \in \{1, ..., N\}$ and $Y_i(t) \triangleq \sum_{j=1}^{N} a_{ij} 1_{\{x_j(t)=e_3\}}$.

2. An infected individual recovers back to the susceptible state by the curing rate δ, i.e.,

$$P(x_i(t + \Delta t) = e_1 | x_i(t) = e_3, X(t)) = \delta\Delta t + o(\Delta t). \tag{8.2}$$

3. A susceptible individual might go to the alert state if surrounded by infected individuals. Specifically, a susceptible node becomes alert with the alerting rate $\kappa \in \mathbb{R}^+$ times the number of infected $A-$neighbors, i.e.,

$$P(x_i(t + \Delta t) = e_2 | x_i(t) = e_1, X(t)) = \kappa Y_i(t)\Delta t + o(\Delta t). \tag{8.3}$$

4. An alert individual switches her myopic contact, and becomes infected with rate β

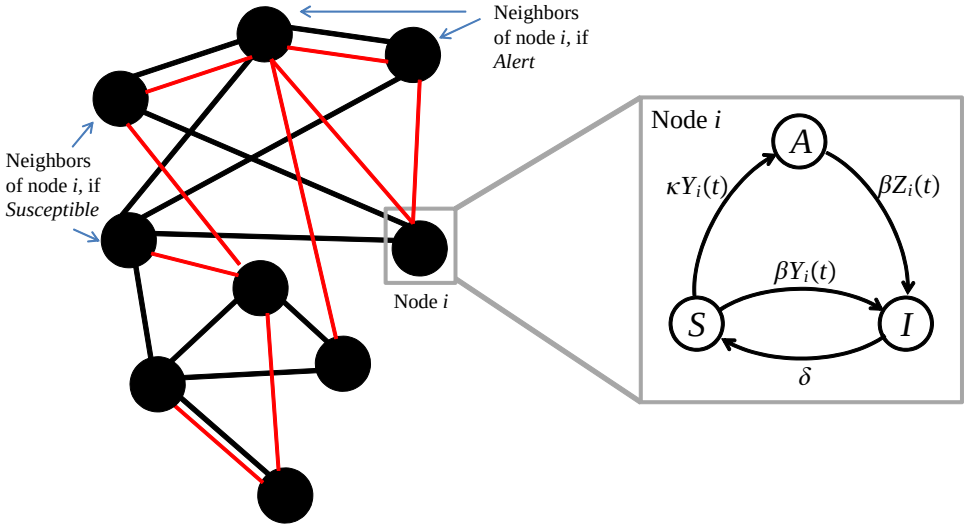

Figure 8.1: *Schematics of the SAIS-LAC model. Black edges correspond to neighborhood* $\mathcal{N}_i^A$ *of a susceptible agent* i*, while red edges represent the neighborhood* $\mathcal{N}_i^B$ *of an alert agent* i*. Here,* β*,* δ*, and* k *are the infection rate, curing rate, and alerting rate, respectively.* $Y_i(t)$ *is the number of infected neighbors of* i *in* $\mathcal{N}_i^A$ *at time* t*, and* $Z_i(t)$ *is the number of infected neighbors of* i *in* $\mathcal{N}_i^B$ *at time* t*.*

times the number of infected $B-$neighbors, i.e.,

$$P(x_i(t+\Delta t) = e_3 | x_i(t) = e_2, X(t)) = \beta Z_i(t)\Delta t + o(\Delta t), \tag{8.4}$$

for $i \in \{1, ..., N\}$ and $Z_i(t) \triangleq \sum_{j=1}^{N} b_{ij} 1_{\{x_j(t)=e_3\}}$.

In the above equations, $\Pr[\cdot]$ denotes probability, $X(t) \triangleq \{x_i(t), i = 1, ..., N\}$ is the joint state of the network, $\Delta t > 0$ is a time step, and the indicator function $1_{\{\mathcal{X}\}}$ is one if $\mathcal{X}$ is true and is zero otherwise. A function $f(\Delta t)$ is said to be $o(\Delta t)$ if $\lim_{\Delta t \to 0} \frac{f(\Delta t)}{\Delta t} = 0$.

Fig. 8.1 depicts a schematic of the networked dynamics of the SAIS-LAC model.

8.2.3 Mean-Field SAIS-LAC Model

According to node-level description of the stochastic transitions in Section 8.2.2, the joint network state $X(t)$ is a Markov process. However, this Markov process is both analytically and numerically intractable due to its exponential state space size of 3^N. A common approach to overcome this issue is to use closure techniques. In particular, a first-order, mean-field-type approximation derives a set of nonlinear differential equations of size $2N$, describing the time evolution of state occupancy probabilities. Recently, Sahneh et al. [1] have introduced a class of epidemic models on multilayer graphs, finding a general expression for the corresponding first-order, mean-filed model. Interestingly, the node-level stochastic transition of the SAIS-LAC model explained in 8.2.2 is equivalent to a spreading process over a two-layer network $\mathcal{G} = (V, E_A, E_B)$. Thus, we find the first-order mean-field-type approximate model according to the generalized epidemic mean-field model (GEMF) developed in [1], as

$$\dot{p}_i = -\delta p_i + \beta(1 - q_i - p_i) \sum_{j=1}^{N} a_{ij} p_j + \beta q_i \sum_{j=1}^{N} b_{ij} p_j, \tag{8.5}$$

$$\dot{q}_i = \kappa(1 - q_i - p_i) \sum_{j=1}^{N} a_{ij} p_j - \beta q_i \sum_{j=1}^{N} b_{ij} p_j, \tag{8.6}$$

for $i \in \{1, ..., N\}$, where p_i is the probability that individual i is '*Infected*,' and q_i is the probability that she is '*Alert*.'

8.3 Epidemic Threshold Equation

Given the contact topology, the value of the effective infection rate $\tau \triangleq \frac{\beta}{\delta}$ determines the dynamical behavior of the epidemic spreading process in SIS model [22]. For small values of τ, initial infections die out exponentially, while for large values of the effective infection rate τ, small initial infections invade the population and persist for a "*long*" time. The

mean-field SIS epidemic model shows a threshold phenomena [21]: a critical value τ_c of the effective infection rate exists such that for any effective infection rate $\tau < \tau_c$ initial infections die out; while for effective infection rate $\tau > \tau_c$, initial infections converge to an endemic (i.e. $\forall i\ p_i^* > 0$) equilibrium.

The epidemic threshold value τ_c is a measure of robustness of a population against epidemic spreading. The objective of our analysis in this chapter is to derive and study the epidemic threshold in our SAIS-LAC model.

8.3.1 Analysis of Equilibrium State

In the subsequent analysis, we repeatedly make use of the two auxiliary graphs $G_A = (V, E_A)$ and $G_B = (V, E_B)$, corresponding to the two extreme cases of no switching contact and fully switched contact, respectively. In order to avoid unnecessary complexities, we make the following assumption:

Assumption 4. *G_A and G_B are undirected connected graphs.*

According to (8.5), the equilibrium infection probabilities p_i^* satisfy

$$p_i^* = \beta \frac{(1 - q_i^*) \sum_{j=1}^N a_{ij} p_j^* + q_i^* \sum_{j=1}^N b_{ij} p_j^*}{\delta + \beta \sum_{j=1}^N a_{ij} p_j^*}. \tag{8.7}$$

If the contact graphs G_A and G_B are connected, the equilibrium value of the infection probability p_i^* is either zero for all individuals, or strictly positive for all individuals. From (8.6), the equilibrium value q_i^* is not definite if the population is disease free. However, if the infection probabilities are nonzero, then q_i^* becomes

$$q_i^* = \frac{\bar{\kappa} \sum_{j=1}^N a_{ij} p_j^*}{\bar{\kappa} \sum_{j=1}^N a_{ij} p_j^* + \sum_{j=1}^N b_{ij} p_j^*} (1 - p_i^*). \tag{8.8}$$

where $\bar{\kappa}$ is the relative alerting rate defined as

$$\bar{\kappa} \triangleq \frac{\kappa}{\beta}. \tag{8.9}$$

According to (8.5), and substituting for q_i^* from (8.7), we get the following equation for p_i^*:

$$\begin{aligned} &-\delta p_i^* + \beta(1-p_i^*)\sum_{j=1}^{N} a_{ij}p_j^* \\ &\qquad + \beta\frac{\bar{\kappa}\sum_{j=1}^{N} a_{ij}p_j^*}{\bar{\kappa}\sum_{j=1}^{N} a_{ij}p_j^* + \sum_{j=1}^{N} b_{ij}p_j^*}(1-p_i^*)(\sum_{j=1}^{N} b_{ij}p_j^* - \sum_{j=1}^{N} a_{ij}p_j^*) = 0. \end{aligned} \tag{8.10}$$

Rearranging the terms, we have

$$\frac{p_i^*}{1-p_i^*} = \tau\{\frac{(\bar{\kappa}+1)\sum_{j=1}^{N} b_{ij}p_j^*}{\bar{\kappa}\sum_{j=1}^{N} a_{ij}p_j^* + \sum_{j=1}^{N} b_{ij}p_j^*}\}\sum_{j=1}^{N} a_{ij}p_j^*, \tag{8.11}$$

with effective infection rate τ defined as

$$\tau \triangleq \beta/\delta. \tag{8.12}$$

8.3.2 Derivation of Epidemic Threshold Equation

We can find the epidemic threshold by studying the location of the equilibrium points. For $\tau < \tau_c$, the disease-free state is the equilibrium. However, for $\tau > \tau_c$, another equilibrium point $P^* \triangleq [p_1^*, ..., p_N^*]^T$ also exists in the positive orthant, i.e., $p_i^* > 0$ for all $i \in \{1, ..., N\}$. Therefore, the threshold value of τ_c is such that $p_i^*|_{\tau=\tau_c} = 0$ for all $i \in \{1, ..., N\}$; however, $\frac{dp_i^*}{d\tau}|_{\tau=\tau_c} > 0$ for all $i \in \{1, ..., N\}$ is a solution. Taking a *right* derivative of both sides of (8.11) with respect to τ yields

$$\frac{1}{(1-p_i^*)^2}\frac{d}{d\tau}p_i^* = \{\frac{(\bar{\kappa}+1)\sum_{j=1}^N b_{ij}p_j^*}{\bar{\kappa}\sum_{j=1}^N a_{ij}p_j^* + \sum_{j=1}^N b_{ij}p_j^*}\}\sum_{j=1}^N a_{ij}p_j^* + \tau\frac{d}{d\tau}\left[\{\frac{(\bar{\kappa}+1)\sum_{j=1}^N b_{ij}p_j^*}{\bar{\kappa}\sum_{j=1}^N a_{ij}p_j^* + \sum_{j=1}^N b_{ij}p_j^*}\}\sum_{j=1}^N a_{ij}p_j^*\right]. \quad (8.13)$$

Since we are only interested in the derivative at $\tau = \tau_c$, for which $p_i^*|_{\tau=\tau_c} = 0$, we can directly use the definition of derivative to compute the last term. Specifically, according to the derivative definition, if $f(x)$ is (right) differentiable at $x = 0$ and $f(a) = 0$, then

$$\frac{d}{dx}\{f(x)g(x)\}|_{x=a} = f'(a)\lim_{x\to a} g(x). \quad (8.14)$$

Therefore, the derivative $w_i \triangleq \frac{d}{d\tau}p_i^*|_{\tau=\tau_c}$ satisfies

$$w_i = \tau_c\{\frac{(\bar{\kappa}+1)\sum_{j=1}^N b_{ij}w_j}{\bar{\kappa}\sum_{j=1}^N a_{ij}w_j + \sum_{j=1}^N b_{ij}w_j}\}\sum_{j=1}^N a_{ij}w_j, \quad (8.15)$$

where we have used

$$\lim_{\tau\to\tau_c^+}\{\frac{(\bar{\kappa}+1)\sum_{j=1}^N b_{ij}p_j^*}{\bar{\kappa}\sum_{j=1}^N a_{ij}p_j^* + \sum_{j=1}^N b_{ij}p_j^*}\} = \{\frac{(\bar{\kappa}+1)(\sum_{j=1}^N b_{ij}p_j^{*\prime}|_{\tau=\tau_c})}{\bar{\kappa}\sum_{j=1}^N a_{ij}p_j^{*\prime}|_{\tau=\tau_c} + \sum_{j=1}^N b_{ij}p_j^{*\prime}|_{\tau=\tau_c}}\}. \quad (8.16)$$

Theorem 15. *The threshold value τ_c for the SAIS-LAC model (8.5-8.6) is such that the equation (8.15) has a nontrivial solution $W \triangleq [w_1, ..., w_N]^T$ with $w_i > 0$ for all $i \in \{1, ..., N\}$.*

Proof. The value of τ_c that solves (8.15) is the critical value for which $p_i^* = 0$; however, $dp_i^*/d\tau > 0$, denoting a second-order phase transition at $\tau = \tau_c$. Therefore, τ_c is the epidemic threshold for SAIS-LAC model (8.5-8.6). □

Remark 14. *For the SIS model, the epidemic threshold is the critical value τ_c such that $w_i = \tau_c\sum_{j=1}^N a_{ij}w_j$ has a nontrivial positive solution for w_i (let $\bar{\kappa} = 0$ in (8.15)). In the*

collective form, $W = \tau_c AW$ is a Perron-Frobenius problem, suggesting that $\tau_c = 1/\lambda_1(A)$ for the SIS model. For the SAIS-LAC model, the epidemic threshold condition reduces to solving the nonlinear Perron-Frobenius (NPF) problem (8.15).

8.4 Solution to Threshold Equation

8.4.1 Exact Numerical Solution

The threshold equation (8.15) is an NPF problem, perhaps with no analytical solution. The solution W discussed in Theorem 15 is in fact an extension of the Perron-Frobenius problem for nonlinear maps. Hence, we seek numerical solution for (8.15) through application of a nonlinear map iteration. Specifically, we can define the update law

$$W_{k+1} \triangleq \frac{F(W_k)}{\|F(W_k)\|_2}, \tag{8.17}$$

where

$$F(W)_i \triangleq \{\frac{\sum_{j=1}^N b_{ij} w_j}{\bar{\kappa} \sum_{j=1}^N a_{ij} w_j + \sum_{j=1}^N b_{ij} w_j}\} \sum_{j=1}^N a_{ij} w_j, \tag{8.18}$$

and the initial state $W_0 \in S_{>0}^{N-1} \triangleq \{\boldsymbol{x} \in \mathbb{R}^N \text{ st } \|\boldsymbol{x}\|_2 = 1, \ \forall i \ x_i > 0\}$. The following theorem gives a numerical solution to the threshold equation (8.15).

Theorem 16. *For the update law (8.17) $W_k \to \zeta$ as $k \to \infty$, given the initial state $W_0 \in S_{>0}^{N-1}$. Moreover, $W = \zeta$ and $\tau_c = \frac{1}{(\bar{\kappa}+1)\zeta^T F(\zeta)}$ solves the NPF problem (8.15).*

Proof. Suppose τ_c and $\zeta = [\zeta_1, \cdots, \zeta_N]^T \in \mathbb{R}^N$ solve the threshold equation (8.15). Define the auxiliary matrix $Q \triangleq [Q_{ij}] \in \mathbb{R}^{N \times N}$, where

$$Q_{ij} \triangleq \{\frac{\sum_{j=1}^N b_{ij} \zeta_j}{\bar{\kappa} \sum_{j=1}^N a_{ij} \zeta_j + \sum_{j=1}^N b_{ij} \zeta_j}\} a_{ij}. \tag{8.19}$$

Therefore, $\mu_1 \triangleq \frac{1}{(\bar{\kappa}+1)\tau_c}$ and ζ are an eigenvalue and the corresponding eigenvector of matrix

Q. Moreover, τ_c and ζ are the dominant eigenvalue and the corresponding eigenvector of matrix Q, because Q is in fact an irreducible non-negative matrix and ζ has strictly positive elements. Matrix Q is irreducible because it has the form $Q = DA$, where A is the adjacency matrix and D is a diagonal matrix with positive diagonal entries. Therefore, since A is irreducible, so is Q. According to the Perron–Frobenius theorem, there is only a single eigenvector with all positive entries, so it should be ζ. In order to prove the convergence, we show that all eigenvalues of the Jacobian matrix

$$J \triangleq \frac{d}{dW} \frac{F(W)}{\|F(W)\|_2}\bigg|_{W=\zeta} \tag{8.20}$$

lie inside the unit circle, i.e., have a magnitudes less than one. Since ζ is an eigenvalue of Q, $F(\zeta) = \mu_1 \zeta$. Therefore, the Jacobian matrix can be computed as

$$\begin{aligned} J &= \frac{1}{\|F(W)\|_2} \frac{dF(W)}{dW} \\ &\quad - \frac{1}{\|F(W)\|_2^3} F(W)F(W)^T \frac{dF(W)}{dW}\bigg|_{W=\zeta} \\ &= \frac{1}{\mu_1} H - \frac{1}{\mu_1} \zeta\zeta^T H = \frac{1}{\mu_1}(I - \zeta\zeta^T)H \end{aligned} \tag{8.21}$$

where the matrix H is

$$H \triangleq \frac{dF(W)}{dW}\bigg|_{W=\zeta}. \tag{8.22}$$

After some rather tedious calculations, we find $\frac{\partial F(W)_i}{\partial w_j}$ as

$$\begin{aligned} \frac{\partial F(W)_i}{\partial w_j} &= \{\frac{\sum_{j=1}^N b_{ij} w_j}{\bar{\kappa} \sum_{j=1}^N a_{ij} w_j + \sum_{j=1}^N b_{ij} w_j}\} a_{ij} + \\ &\left(\frac{b_{ij}}{\sum_{j=1}^N b_{ij} w_j} - \frac{\bar{\kappa} a_{ij} + b_{ij}}{\bar{\kappa} \sum_{j=1}^N a_{ij} w_j + \sum_{j=1}^N b_{ij} w_j} \right) \times \sum_{j=1}^N \{\frac{\sum_{j=1}^N b_{ij} w_j}{\bar{\kappa} \sum_{j=1}^N a_{ij} w_j + \sum_{j=1}^N b_{ij} w_j}\} a_{ij} w_j \end{aligned} \tag{8.23}$$

Hence,

$$H_{ij} = Q_{ij} + \mu_1 \zeta_i \left(\frac{b_{ij}}{\sum_{j=1}^{N} b_{ij}\zeta_j} - \frac{\bar{\kappa} a_{ij} + b_{ij}}{\bar{\kappa} \sum_{j=1}^{N} a_{ij}\zeta_j + \sum_{j=1}^{N} b_{ij}\zeta_j} \right).$$

We claim that μ_1 and ζ are also eigenvalue and eigenvector of $H \triangleq [H_{ij}] \in \mathbb{R}^{N \times N}$ because

$$\begin{aligned}
(H\zeta)_i &= (Q\zeta)_i \\
&\quad + \mu_1 \zeta_i \sum_{j=1}^{N} \left(\frac{b_{ij}}{\sum_{j=1}^{N} b_{ij}\zeta_j} - \frac{\bar{\kappa} a_{ij} + b_{ij}}{\bar{\kappa} \sum_{j=1}^{N} a_{ij}\zeta_j + \sum_{j=1}^{N} b_{ij}\zeta_j} \right) \zeta_j \\
&= (Q\zeta)_i \\
&\quad + \mu_1 \zeta_i \left(\frac{\sum_{j=1}^{N} b_{ij}\zeta_j}{\sum_{j=1}^{N} b_{ij}\zeta_j} - \frac{\bar{\kappa} \sum_{j=1}^{N} a_{ij}\zeta_j + \sum_{j=1}^{N} b_{ij}\zeta_j}{\bar{\kappa} \sum_{j=1}^{N} a_{ij}\zeta_j + \sum_{j=1}^{N} b_{ij}\zeta_j} \right) \\
&= (Q\zeta)_i + 0 = \mu_1 \zeta_i.
\end{aligned}$$

Using definition of Q and the fact that μ_1 and ζ are its eigenvalue and eigenvector, we can further simplify H_{ij} as

$$H_{ij} = \mu_1 \zeta_i \left(\frac{\kappa a_{ij}}{\kappa \sum_{j=1}^{N} a_{ij}\zeta_j} + \frac{b_{ij}}{\sum_{j=1}^{N} b_{ij}\zeta_j} - \frac{\kappa a_{ij} + b_{ij}}{\kappa \sum_{j=1}^{N} a_{ij} + \sum_{j=1}^{N} b_{ij}\zeta_j} \right). \tag{8.24}$$

Therefore, H is a non-negative matrix. Furthermore, it is irreducible if A and B are also irreducible. Since H is a non-negative, irreducible matrix, and ζ is a positive vector, μ_1 is the largest eigenvalue of H. Therefore, H can be expressed as

$$H = \mu_1 \zeta \eta^T + \tilde{H}, \tag{8.25}$$

where $\eta^T \tilde{H} = \mathbf{0}$, $\tilde{H}\zeta = \mathbf{0}$, $\eta^T \zeta = 1$, and all the eigenvalues of $\tilde{H}$ have a magnitude less than

μ_1. Therefore, the Jacobian matrix J (8.21) becomes

$$\begin{aligned} J &= \frac{1}{\mu_1}(I - \zeta\zeta^T)(\mu_1\zeta\eta^T + \tilde{H}) \\ &= \frac{1}{\mu_1}(I - \zeta\zeta^T)\mu_1\zeta\eta^T + \frac{1}{\mu_1}(I - \zeta\zeta^T)\tilde{H} \\ &= \zeta\eta^T - \zeta\eta^T + \frac{1}{\mu_1}(I - \zeta\zeta^T)\tilde{H} = \frac{1}{\mu_1}(I - \zeta\zeta^T)\tilde{H} \end{aligned} \tag{8.26}$$

Eigenvalues of Jacobian matrix J are the eigenvalues of $\tilde{H}$ divided by μ_1. In fact, if r_i is an eigenvector of $\tilde{H}$, then $(I - \zeta\zeta^T)r_i$ is an eigenvalue of J. Since, all eigenvalues of $\tilde{H}$ have a magnitude less than μ_1, all the eigenvalues of J lie inside the unit circle. This proves the local convergence of the iteration method. If the initial W_0 lies in $S_{>0}^{N-1}$, the iteration method converges to the fixed point $W = \zeta$. Starting from W_0 on $S_{>0}^{N-1}$, the iteration law always keeps W_k on on $S_{>0}^{N-1}$. Therefore, since there is only a single equilibrium point on $S_{>0}^{N-1}$, which is locally exponentially stable, any initial values of W_0 on $S_{>0}^{N-1}$ will converge to ζ. □

8.4.2 Approximate Analytical Solution

In the previous section, we showed a power iteration method can solve the threshold equation (8.15) numerically. However, finding analytical solutions is much more challenging. In this section, we propose to use perturbation methods to get approximate analytical solutions. The idea is that we know the exact solution of the threshold equation (8.15) in two specific cases: 1) for $\bar{\kappa} = 0$, the epidemic threshold is $\tau_c|_{\bar{\kappa}=0} = \frac{1}{\lambda_1(A)}$ and $W|_{\bar{\kappa}=0} = V$ is a solution, where $V \triangleq [v_1, ..., v_N]^T > 0$ is the dominant eigenvector of matrix A; and 2) for $\bar{\kappa} \to \infty$, the epidemic threshold is $\tau_c|_{\bar{\kappa}\to\infty} = \frac{1}{\lambda_1(B)}$ and $W|_{\bar{\kappa}=0} = U$ is a solution, where $U \triangleq [u_1, ..., u_N]^T > 0$ is the dominant eigenvector of matrix B. Thus, perturbation techniques approximate the threshold value for small and large values of relative alerting rate $\bar{\kappa}$.

Case I: Slow Alerting Process

For small values of $\bar{\kappa}$, we can find the solution to the threshold equation (8.15) by perturbation at $\bar{\kappa} = 0$. Taking the right derivative of threshold equation (8.15) with respect to $\bar{\kappa}$ at $\bar{\kappa} = 0$ and $W = V$, yields

$$\begin{aligned}\frac{dw_i}{d\bar{\kappa}} &= \frac{d\tau_c}{d\bar{\kappa}} \sum_{j=1}^{N} a_{ij} v_j + \frac{1}{\lambda_1(A)} \sum_{j=1}^{N} a_{ij} \frac{dw_j}{d\bar{\kappa}} + \frac{1}{\lambda_1(A)} \{1 - \frac{\sum_{j=1}^{N} a_{ij} v_j}{\sum_{j=1}^{N} b_{ij} v_j}\} \sum_{j=1}^{N} a_{ij} v_j \\ &= \lambda_1(A) \frac{d\tau_c}{d\bar{\kappa}} - \frac{\lambda_1(A) v_i^2}{\sum_{j=1}^{N} b_{ij} v_j} + v_i + \frac{1}{\lambda_1(A)} \sum_{j=1}^{N} a_{ij} \frac{dw_j}{d\bar{\kappa}} \end{aligned} \tag{8.27}$$

Theorem 17. *The value of the epidemic threshold solving (8.15) has the form*

$$\tau_c = \frac{1}{\lambda_1(A)} (1 + \bar{\kappa}(\Psi(A, B) - 1)) + o(\bar{\kappa}), \tag{8.28}$$

where $\Psi(A, B)$ *is*

$$\Psi(A, B) \triangleq \sum_{j=1}^{N} v_i^2 \frac{\sum_{j=1}^{N} a_{ij} v_j}{\sum_{j=1}^{N} b_{ij} v_j} \tag{8.29}$$

Proof. The collective form of (8.27) is

$$\frac{dW}{d\bar{\kappa}} = \lambda_1(A) \frac{d\tau_c}{d\bar{\kappa}} V + (I - D_0) V + \frac{1}{\lambda_1(A)} A \frac{dW}{d\bar{\kappa}}, \tag{8.30}$$

where D_0 is the diagonal matrix

$$D_0 \triangleq diag\{\frac{\sum_{j=1}^{N} a_{ij} v_j}{\sum_{j=1}^{N} b_{ij} v_j}\}. \tag{8.31}$$

Therefore, the following is also true:

$$(I - \frac{1}{\lambda_1(A)} A) \frac{dW}{d\bar{\kappa}} = \lambda_1(A) \frac{d\tau_c}{d\bar{\kappa}} V - D_0 V + V. \tag{8.32}$$

Multiplying both sides by V^T from the right gives

$$0 = \lambda_1(A)\frac{d\tau_c}{d\bar{\kappa}} - V^T D_0 V + 1, \tag{8.33}$$

because A is symmetric and V is the normalized dominant eigenvector of A. From (8.33), we get

$$\frac{d\tau_c}{d\bar{\kappa}} = \frac{1}{\lambda_1(A)}(\Psi(A,B) - 1),$$

because $V^T D_0 V = \Psi(A,B)$ according to (8.29). Formula (8.28) is the first-order Taylor expansion of τ_c at $\bar{\kappa} = 0$. □

Case II: Fast Alertness Process

For large values of $\bar{\kappa}$, we can find the solution to the threshold equation (8.15) by perturbation at $s = 0$, where $s \triangleq \bar{\kappa}^{-1}$.

The threshold equation in (8.15) in terms of the new parameter s, is

$$\begin{aligned} w_i &= \tau_c\{\frac{\bar{\kappa}^{-1}}{\bar{\kappa}^{-1}}\frac{(\bar{\kappa}+1)\sum_{j=1}^N b_{ij}w_j}{\bar{\kappa}\sum_{j=1}^N a_{ij}w_j + \sum_{j=1}^N b_{ij}w_j}\} \\ &= \tau_c\{\frac{(1+s)\sum_{j=1}^N b_{ij}w_j}{\sum_{j=1}^N a_{ij}w_j + s\sum_{j=1}^N b_{ij}w_j}\}\sum_{j=1}^N a_{ij}w_j \\ &= \tau_c\{\frac{(s+1)\sum_{j=1}^N a_{ij}w_j}{s\sum_{j=1}^N b_{ij}w_j + \sum_{j=1}^N a_{ij}w_j}\}\sum_{j=1}^N b_{ij}w_j. \end{aligned} \tag{8.34}$$

Theorem 18. *The value of the epidemic threshold solving (8.15) has the form of*

$$\tau_c = \frac{1}{\lambda_1(B)}(1 + \bar{\kappa}^{-1}(\Psi(B,A) - 1)) + o(\bar{\kappa}^{-1}), \tag{8.35}$$

where $\Psi(A,B)$ is defined in (8.29).

Proof. As can be seen, (8.34) has exactly the form of the threshold equation (8.15), where

A and B matrices have changed roles, and $\bar{\kappa}$ is replaced by s. Therefore, similar to the proof of Theorem 17, the threshold can be found around $s = 0$, as by switching A and B matrices and replacing $\bar{\kappa}$ by $s = \bar{\kappa}^{-1}$. The result is (8.35), which is in fact the first-order Taylor expansion of τ_c at $s = 0$. □

8.4.3 Discussion of Possible Solutions

We developed the algebraic equation for the value of the epidemic threshold (8.15) in the case of the SAIS model with adaptive contact network. This equation is a nonlinear eigenvalue-type algebraic equation and possibly, no explicit closed-form solution exists for it. In Section 8.4.1, we developed a numerical iteration method that proved to solve the epidemic threshold equation. Then, in Section 8.4.2, we derived analytical results for extreme cases with $\bar{\kappa}$ very small or very large. In this section, we investigate how the analytical expressions (8.28) and (8.35) help to characterize and understand the dependency of the threshold value on $\bar{\kappa}$. In particular, we are interested to realize how the epidemic threshold moves from $\tau_c(0) = 1/\lambda_1(A)$ for small values of $\bar{\kappa}$ to $\tau_c(\infty) = 1/\lambda_1(B)$.

To reflect more realistic scenarios, we only consider cases where $\lambda_1(B) < \lambda_1(A)$, that is the alert contact network is more resilient than the normal contact graph G_A. If, as in many practical cases, B is a subgraph of A or its link weights are lower, then we have $\sum_{j=1}^{N} a_{ij}v_j > \sum_{j=1}^{N} b_{ij}v_j$ and $\sum_{j=1}^{N} a_{ij}u_j > \sum_{j=1}^{N} b_{ij}u_j$; therefore, according to the definition (8.29), $\Psi(A, B) > 1$ and $\Psi(B, A) < 1$. This is the simplest case where the value of the epidemic threshold increases monotonically by $\bar{\kappa}$. Such a scenario has been simulated in Section 8.5 and shown in Fig. 8.3 by the blue curve. An interesting and important scenario is when $\Psi(A, B) < 1$. In this case, the value of the epidemic threshold decreases for small values of $\bar{\kappa}$, i.e., and the alerting process worsens the infection spreading. The green curve in Fig. 8.3 depicts such a scenario. Another counterintuitive scenario is when $\Psi(B, A) > 1$. In this case, there is an optimal alerting rate $\bar{\kappa}$ for which the adaptive network is most resilient with respect to spreading infection. The red curve in Fig. 8.3 corresponds to this case.

8.5 Numerical Simulation

In this section, we perform a numerical study to evaluate the results of this chapter. We consider a simple contact graph for G_A illustrated in Fig. 8.2. Given this graph, we synthesize three contact graphs G_{B_1}, G_{B_2}, and G_{B_3}, such that

- The spectral radius of these graphs are all equal to $\frac{2}{3}$ of the spectral radius of G_A, i.e., $\lambda_1(B_i) = \frac{2}{3}\lambda_1(A)$. In this way, the contact switching is towards a more resilient network, and comparing the three cases is reasonable.

- For the graph G_{B_1}, $\Psi(A, B_1) < 1$, i.e., our analytical result in (8.28) predicts that for small values of $\bar{\kappa}$ there is a decrease in the epidemic threshold, even though the threshold increases for larger values of $\bar{\kappa}$. In this case, we expect an undershoot in $\tau_c(\bar{\kappa})$ as a function of $\bar{\kappa}$.

- For the graph G_{B_2}, $\Psi(A, B_2) > 1$ and $\Psi(B_2, A) > 1$, i.e., there is a value for $\bar{\kappa}$ for which $\tau_c(\bar{\kappa})$ is maximum.

- Graph G_{B_3} is constructed by decreasing link weights and removing links from A. As discussed in the previous section, we expect to see a monotonic increase in the epidemic threshold as normalized alerting rate $\bar{\kappa}$ increases.

The further the effective infection rate τ is from the epidemic threshold, the larger the size of the final infection fraction. For the case of G_{B_1}, as shown in Fig. 8.4, we have simulated the time evolution of the infection fraction for $\tau = 1.4/\lambda_1(A)$, which is still less than $1/\lambda_1(B_1) = 1.5/\lambda_1(A)$. By increasing the normalized alerting rate $\bar{\kappa}$ from zero, we observed that for a small value $\bar{\kappa} = 0.7$, the initial infection invades the population more severely. However, by increasing $\bar{\kappa}$, the size of the infection fraction decreases and finally goes to zero for large enough $\bar{\kappa}$.

We repeat the simulation for graph G_{B_2} in two scenarios. For $\tau = 1.4/\lambda_1(A)$, shown in Fig. 8.5, we observe that increasing the alerting rate suppresses the infection. A very

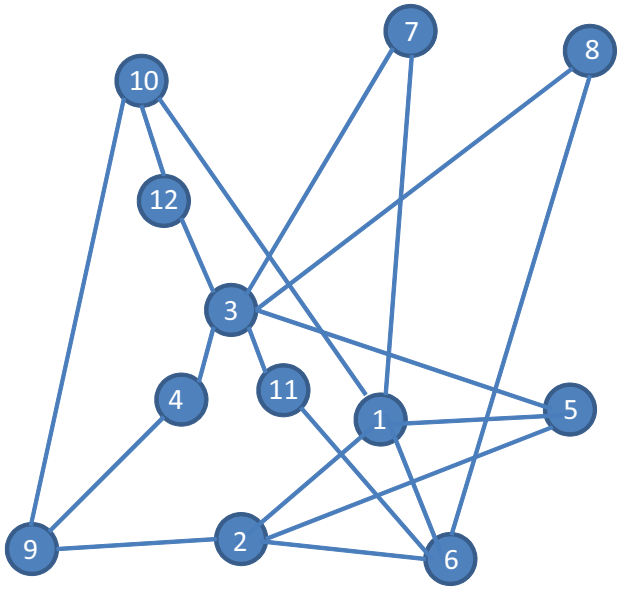

Figure 8.2: *Schematics of contact graph G_A of susceptible agents for numerical simulations. Nodes represent individuals and links represent contact.*

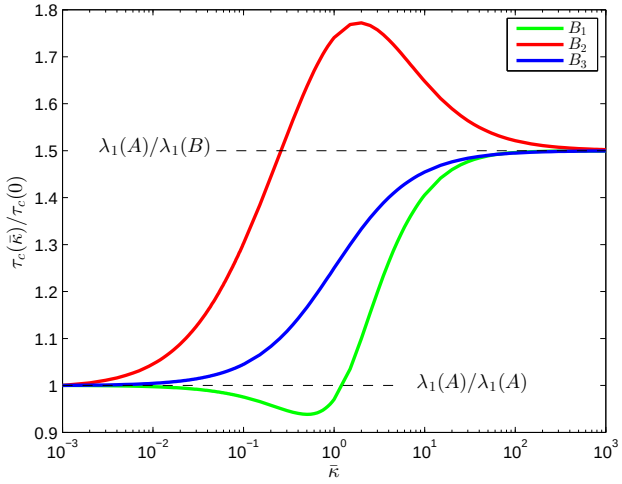

Figure 8.3: *Epidemic threshold $\tau_c(\bar{\kappa})$ as a function of normalized alerting rate $\bar{\kappa}$, for different contact graphs G_{B_i} of alert agents. All three graphs have the same spectral radius and $\lambda_1(A)/\lambda_1(B_i) = 1.5$. Graph G_{B_1} is synthesized such that $\Psi(A, B_1) < 1$. As can be seen (green curve), $\tau_c(\bar{\kappa})$ initially decreases and then increases as $\bar{\kappa}$ increases. Graph G_{B_2} is synthesized such that both $\Psi(A, B_2) > 1$ and $\Psi(B_2, A) > 1$. In this case (red curve), $\tau_c(\bar{\kappa})$ is maximal around $\bar{\kappa} \approx 2$. Topology of graph G_{B_3} is similar to G_A with reduced weights and some removed links. In this case, epidemic threshold $\tau_c(\bar{\kappa})$ (blue curve) increases monotonically by normalized alerting rate $\bar{\kappa}$.*

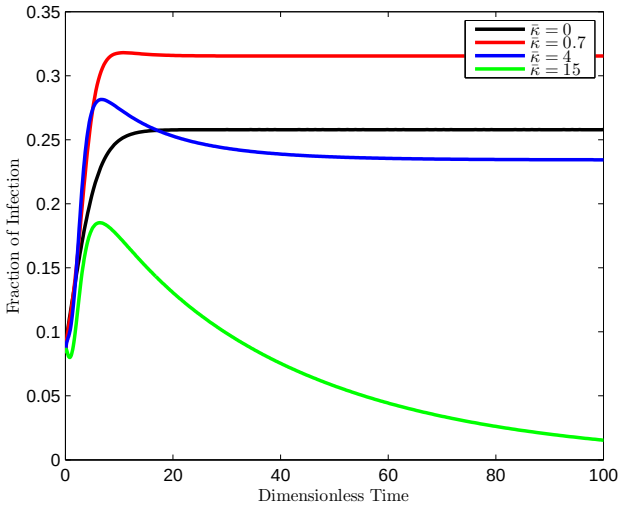

Figure 8.4: *Evolution of the fraction of infected individuals in the population with G_{B_1} at $\tau = 1.4/\lambda_1(A)$ for different values of $\bar{\kappa}$. The black curve represents the case where there is no alertness process ($\bar{\kappa} = 0$). It can be seen (red curve) that for $\bar{\kappa} = 0.7$, the infection size grows. However, by increasing $\bar{\kappa}$ further, we observe (blue and green curves) that infection size diminishes.*

interesting observation is when $\tau = 1.65/\lambda_1(A)$. In this case, the effective infection rate τ is even larger than $1/\lambda_1(B_1) = 1.5/\lambda_1(A)$. Therefore, for very large values of $\bar{\kappa}$, initial infections do not die out completely. However, as predicted in Fig. 8.3, for $\bar{\kappa}$ close to 3, the threshold value is $1.75/\lambda_1(A)$. As a result, by increasing $\bar{\kappa}$ from zero, we observe in Fig. 8.6 that the infection size diminishes and is fully suppressed for $\bar{\kappa} = 3$, but later on, for larger values of $\bar{\kappa}$, the infection size increases.

8.6 Conclusion

We extend the susceptible-infected-susceptible (SIS) epidemic model on a fixed static graph to the case where individuals myopically change their contact neighborhood as a response to sensing infection. In our model, the contact topology switches among 2^N possible configurations. The state-dependent switching contact network leads to very rich dynamics for the epidemic-spreading process. We show how the locally switching topology of the contact network is different from fixed, static graphs and can lead to counterintuitive conclusions.

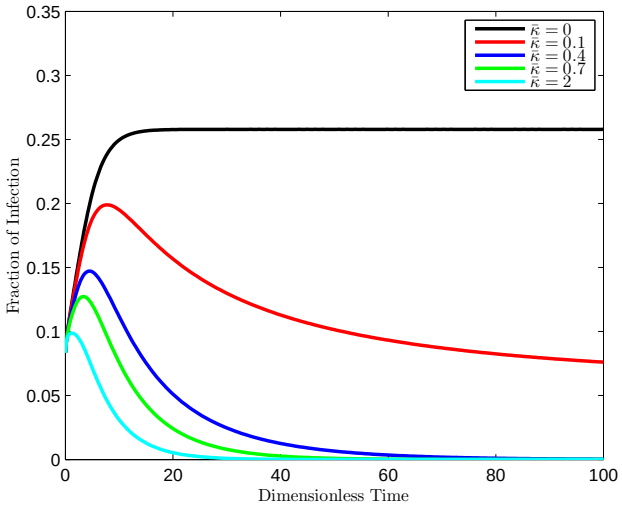

Figure 8.5: *Evolution of the fraction of infected individuals in the population with G_{B_2} at $\tau = 1.4/\lambda_1(A)$ for different values of $\bar{\kappa}$. The black curve represents the case where there is no alertness process ($\bar{\kappa} = 0$). It can be seen that by increasing $\bar{\kappa}$, infection size diminishes.*

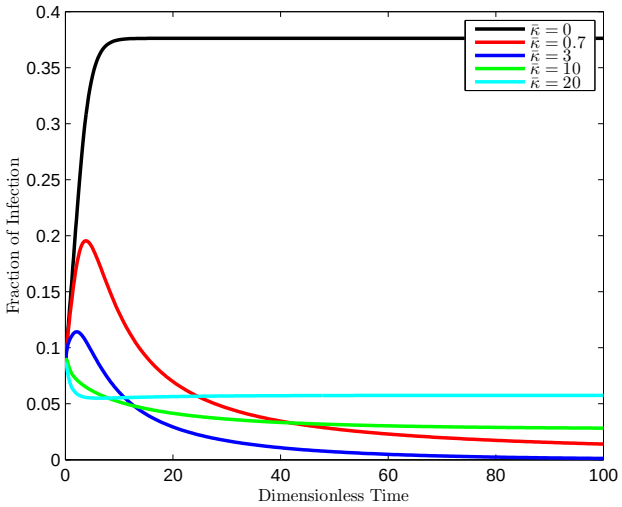

Figure 8.6: *Evolution of the fraction of infected individuals in the population with G_{B_2} at $\tau = 1.65/\lambda_1(A)$ for different values of $\bar{\kappa}$. The black curve represents the case where there is no alertness process ($\bar{\kappa} = 0$). It can be seen (red curve) that by increasing $\bar{\kappa}$ from zero, infection size diminishes and is fully suppressed for $\bar{\kappa} = 3$, but later on, for larger values of $\bar{\kappa}$, infection size increases.*

In particular, it is possible that local switching towards a supposedly more resilient network (i.e., having smaller spectral radius) can in fact worsen the spreading scenario. It is very important to highlight the difference of the underlying mechanism for such counterintuitive behavior with other formerly reported results. In most existing scenarios, an individual may transmit the infection upon switching to a new individual. However, in our model, such a scenario does not occur because those who switch do not carry infection. This signifies the importance of analysis of adaptive networks. Finally, even though we were able to characterize the complex behavior of the spreading scenario of this study in terms of spectral quantities of the two extreme cases, non-switching graph G_A, and fully-switched graph G_B, there are yet several unknowns regarding this problem which demand future research.

Chapter 9

Conclusion

This dissertation studies epidemic spreading processes over multilayer and interconnected networks. Multilayer and interconnected networks are relatively new mathematical objects, with behaviors very different from conventional single networks. This demands a fresh bottom-up approach for analysis to avoid being biased by previous established results for single networks. In this dissertation, I have avoided problem formulations which basically reduce to a larger, but single, network problem. Additionally, I have tried to avoid naive extension of single-network concepts to interconnected and multilayer networks. For example, while it is possible to generalize the concept of epidemic threshold value from single network to multilayer/interconnected networks, Chapter 4 takes into account multiple degrees of freedom in such networks by proposing a threshold curve instead of a single value.

Analysis of spreading processes on multilayer networks is much more challenging than on single-layer networks. Similar to simple networks, bifurcation analysis finds conditions for epidemic outbreak. However, the outbreak condition for the case of a single network is the solution of an eigenvalue problem, thus isolating the role of contact topology with clear structural characterization of an epidemic threshold. In contrast to single networks, the conditions for an epidemic threshold in multilayer networks suffer from an implicit, mixed effect of network layers and epidemic parameters. For example, for the competitive

spreading of two viruses in Chapter 5, the critical value of infection rate of one virus depends implicitly on the other virus infection rate, as well as its associated network layer. As another example, the epidemic threshold condition for the SAIS model with an information dissemination network in Chapter 7 is a nonlinear Perron–Frobenius (NPF) problem, for which no explicit analytical solution exists. Even though the NPF equations are numerically solvable, structural implications of the multilayer network topology are absent. In this dissertation, we have developed techniques based on eigenvalue perturbation to overcome this issue. While eigenvalue perturbation still does not exactly find the threshold values, it does facilitate characterizing the solutions with respect to structural properties of multilayer networks. For example, in the competitive spreading problem, we detected that overlapping of central nodes across network layers determines conditions for coexistence of competing viruses. I expect this methodology can be applied to much broader problems on multi-layer networks.

An important message of our results in Chapter 5 is that individual layers' graph properties do not possess enough information to characterize the spreading dynamics in multilayer networks, and some interrelation metrics are needed. This dissertation introduces several such interrelation metrics. This is particularly important because conventional metrics for single networks (e.g., average node degree, spectral radius, average clustering coefficient) are graph properties, and hence by definition do not depend on node relabeling. In contrast, for interconnected and multilayer networks, node labels matter, as it is very important which node in one layer corresponds to which node in another layer. Interrelation metrics complement the set of conventional network metrics to better describe multilayer and interconnected networks.

It is important to acknowledge that most of the developments are based on first-order mean-field approximations of the stochastic epidemic processes. Therefore, all possible limitations of the mean-field approximation for epidemic processes on single networks, also apply to multilayer and interconnected networks. As discussed in Chapter 3, mean-field

approximate models can exhibit considerable deviation from the true epidemic progression for sparse, structured networks and for epidemic parameters close to critical values. Despite this limitation, mean-field models are strong, tractable tools to study an intricate, complex process. In particular, network structural results from mean-field models are very compatible with the true spreading process.

Future Research Directions

From a design perspective, a very important problem is the optimal design of an interconnection strategy in interconnected networks, i.e., finding the optimal level of interconnection that maximizes network resilience with respect to malware propagation and cascade failure, while satisfying required safety and traffic demand constraints. An optimal interconnection design problem can have important implications in several applications, such as transportation and communication networks, where traffic flow among nodes has inherent possibilities of propagating infections/malware. Therefore, it is important to design an interconnection in such a way that not only satisfies traffic demands, but also minimizes chances of malware propagation. Our results in Chapter 4 can provide essential tools to formulate this problem.

Our results for competitive spreading over multilayer networks in Chapter 5 leaves the door open for several important research directions. Not only is the final status of competitors important, but so is the time evolution of the competition. Transient dynamics study of the competitive processes provides informative data regarding the competition. However, the study of transient dynamics is technically challenging, as it is not even well-understood for single-virus propagation on a single virus. Transient dynamics is more tractable when the competition is very aggressive, i.e., both viruses have high infection rates. Two dynamics are involved in an aggressive competitive spreading process: 1) a fast dynamics where a susceptible node becomes infected, and 2) a slow dynamics where an infected node recovers and then gets infected again, but this time with the other virus. Therefore, application of nonlinear dynamic systems tools to separate these two dynamics reduces the complexity of the problem, allowing for analytical tractability. Interestingly, the assumption of very

aggressive viruses is realistic in many practical applications of competition. For example, in viral marketing, competitive companies put their maximum effort into spreading their products. Similar characteristics can be observed in an active defense against malicious attacks in computer networks.

Another critical problem regarding competitive spreading processes over multilayer networks is scalability to a higher number of viruses. One great analytical challenge is that for a system of m competitive viruses, the phase space has 2^m states; as each virus can either survive or succumb. This exponential explosion of phase space imposes technical difficulties on the problem analysis. One possibility might be to tackle the multivirus problem by induction method, i.e., analyzing an m-virus problem from an $(m-1)$-virus problem. This line of research contributes importantly to the current understanding of the competitive spreading process, with a potentially broader impact on other dynamics on multilayer networks with more than two layers.

In conclusion, studying dynamic processes over multilayer and interconnected networks is a promising research direction, with numerous challenges and opportunities both in theory and application.

Bibliography

[1] F. Sahneh, C. Scoglio, and P. Van Mieghem, "Generalized epidemic mean-field model for spreading processes over multilayer complex networks," *Networking, IEEE/ACM Transactions on*, vol. 21, no. 5, pp. 1609–1620, 2013.

[2] F. Sahneh and C. Scoglio, "Competitive epidemic spreading over arbitrary multilayer networks," *Physical Review E*, vol. 89, no. 6, p. 062817, 2014.

[3] F. Sahneh, F. N. Chowdhury, and C. M. Scoglio, "On the existence of a threshold for preventive behavioral responses to suppress epidemic spreading," *Scientific reports*, vol. 2, 2012.

[4] F. Sahneh, F. Chowdhury, G. Brase, and C. Scoglio, "Individual-based information dissemination in multilayer epidemic modeling," *Mathematical Modelling of Natural Phenomena*, vol. 9, no. 02, pp. 136–152, 2014.

[5] F. Sahneh and C. Scoglio, "Epidemic spread in human networks," in *Proceedings of 50th IEEE Conference on Decision and Control and European Control Conference (CDC-ECC)*, 2011, pp. 3008–3013.

[6] ——, "Optimal information dissemination in epidemic networks," in *Proceedings of IEEE 51st Annual Conference on Decision and Control (CDC)*, Dec 2012, pp. 1657–1662.

[7] F. Sahneh, C. Scoglio, and F. Chowdhury, "Effect of coupling on the epidemic threshold in interconnected complex networks: A spectral analysis," in *American Control Conference (ACC)*, 2013, pp. 2307–2312.

[8] J. Kephart and S. White, "Directed-graph epidemiological models of computer viruses," in *Society Symposium on Research in Security and Privacy*, may 1991, pp. 343–359.

[9] J. Kleinberg, "Computing: The wireless epidemic," *Nature*, vol. 449, no. 7160, pp. 287–288, 2007.

[10] M. Meisel, V. Pappas, and L. Zhang, "A taxonomy of biologically inspired research in computer networking," *Computer Networks*, vol. 54, no. 6, pp. 901–916, 2010.

[11] S. Staniford, V. Paxson, N. Weaver *et al.*, "How to own the internet in your spare time." in *USENIX Security Symposium*, 2002, pp. 149–167.

[12] C. C. Zou, W. Gong, and D. Towsley, "Code red worm propagation modeling and analysis," in *Proceedings of the 9th ACM conference on Computer and communications security*. ACM, 2002, pp. 138–147.

[13] M. Garetto, W. Gong, and D. Towsley, "Modeling malware spreading dynamics," in *INFOCOM 2003. Twenty-Second Annual Joint Conference of the IEEE Computer and Communications. IEEE Societies*, vol. 3. IEEE, 2003, pp. 1869–1879.

[14] C. C. Zou, W. Gong, D. Towsley, and L. Gao, "The monitoring and early detection of internet worms," *IEEE-ACM Transactions on Networking*, vol. 13, no. 5, pp. 961–974, 2005.

[15] B. K. Mishra and D. K. Saini, "Seirs epidemic model with delay for transmission of malicious objects in computer network," *Applied Mathematics and Computation*, vol. 188, no. 2, pp. 1476–1482, 2007.

[16] N. Bailey, *The mathematical theory of infectious diseases and its applications*. London, 1975.

[17] Y. Moreno, R. Pastor-Satorras, and A. Vespignani, "Epidemic outbreaks in complex heterogeneous networks," *The European Physical Journal B - Condensed Matter and Complex Systems*, vol. 26, pp. 521–529, 2002.

[18] R. Pastor-Satorras and A. Vespignani, "Epidemic dynamics and endemic states in complex networks," *Phys. Rev. E*, vol. 63, no. 6, p. 066117, May 2001.

[19] Y. Wang, D. Chakrabarti, C. Wang, and C. Faloutsos, "Epidemic spreading in real networks: An eigenvalue viewpoint," *Proc. 22nd Int. Symp. Reliable Distributed Systems*, pp. 25–34, 2003.

[20] M. Keeling and K. Eames, "Networks and epidemic models," *Journal of the Royal Society Interface*, vol. 2, no. 4, pp. 295–307, 2005.

[21] P. Van Mieghem, J. Omic, and R. Kooij, "Virus spread in networks," *IEEE/ACM Transactions on Networking*, vol. 17, no. 1, pp. 1–14, 2009.

[22] A. Ganesh, L. Massoulie, and D. Towsley, "The effect of network topology on the spread of epidemics," in *Proceedings IEEE INFOCOM*, vol. 2, 2005, pp. 1455–1466.

[23] V. Nicosia, G. Bianconi, V. Latora, and M. Barthelemy, "Growing multiplex networks," *Physical review letters*, vol. 111, no. 5, p. 058701, 2013.

[24] A. Cardillo, J. Gómez-Gardeñes, M. Zanin, M. Romance, D. Papo, F. del Pozo, and S. Boccaletti, "Emergence of network features from multiplexity," *Scientific reports*, vol. 3, 2013.

[25] S. V. Buldyrev, R. Parshani, G. Paul, H. E. Stanley, and S. Havlin, "Catastrophic cascade of failures in interdependent networks," *Nature*, vol. 464, no. 7291, pp. 1025–1028, 2010.

[26] J. Gao, S. V. Buldyrev, H. E. Stanley, and S. Havlin, "Networks formed from interdependent networks," *Nature Physics*, vol. 8, no. 1, pp. 40–48, 2011.

[27] J. Shao, S. Buldyrev, S. Havlin, and H. Stanley, "Cascade of failures in coupled network systems with multiple support-dependence relations," *Physical Review E*, vol. 83, no. 3, p. 036116, 2011.

[28] C. D. Brummitt, R. M. D'Souza, and E. A. Leicht, "Suppressing cascades of load in interdependent networks," *Proceedings of the National Academy of Sciences*, 2012.

[29] F. Radicchi and A. Arenas, "Abrupt transition in the structural formation of interconnected networks," *Nature Physics*, 2013.

[30] S. Gómez, A. Díaz-Guilera, J. Gómez-Gardeñes, C. J. Perez-Vicente, Y. Moreno, and A. Arenas, "Diffusion dynamics on multiplex networks," *Physical review letters*, vol. 110, no. 2, p. 028701, 2013.

[31] J. Um, P. Minnhagen, and B. J. Kim, "Synchronization in interdependent networks," *Chaos*, vol. 21, p. 025106, 2011.

[32] J. Gómez-Gardeñes, C. Gracia-Lázaro, L. M. Floría, and Y. Moreno, "Evolutionary dynamics on interdependent populations," *Physical Review E*, vol. 86, no. 5, p. 056113, 2012.

[33] Z. Wang, A. Szolnoki, and M. Perc, "Evolution of public cooperation on interdependent networks: The impact of biased utility functions," *EPL (Europhysics Letters)*, vol. 97, no. 4, p. 48001, 2012.

[34] S. Funk and V. A. Jansen, "Interacting epidemics on overlay networks," *Physical Review E*, vol. 81, no. 3, p. 036118, 2010.

[35] M. Dickison, S. Havlin, and H. E. Stanley, "Epidemics on interconnected networks," *Physical Review E*, vol. 85, no. 6, p. 066109, 2012.

[36] A. Saumell-Mendiola, M. A. Serrano, and M. Boguñá, "Epidemic spreading on interconnected networks," *Phys. Rev. E*, vol. 86, p. 026106, Aug 2012.

[37] Y. Wang and G. Xiao, "Effects of interconnections on epidemics in network of networks," in *Wireless Communications, Networking and Mobile Computing (WiCOM), 2011 7th International Conference on*, sept. 2011, pp. 1–4.

[38] X. Wei, N. Valler, B. A. Prakash, I. Neamtiu, M. Faloutsos, and C. Faloutsos, "Competing memes propagation on networks: a case study of composite networks," *ACM SIGCOMM Computer Communication Review*, vol. 42, no. 5, pp. 5–12, 2012.

[39] X. Wei, N. C. Valler, B. A. Prakash, I. Neamtiu, M. Faloutsos, and C. Faloutsos, "Competing memes propagation on networks: A network science perspective," *Selected Areas in Communications, IEEE Journal on*, vol. 31, no. 6, pp. 1049–1060, 2013.

[40] C. Granell, S. Gómez, and A. Arenas, "Dynamical interplay between awareness and epidemic spreading in multiplex networks," *Physical review letters*, vol. 111, no. 12, p. 128701, 2013.

[41] A. V. Goltsev, S. N. Dorogovtsev, J. G. Oliveira, and J. F. F. Mendes, "Localization and spreading of diseases in complex networks," *Phys. Rev. Lett.*, vol. 109, p. 128702, Sep 2012.

[42] P. Van Mieghem, "Epidemic phase transition of the sis type in networks," *EPL (Europhysics Letters)*, vol. 97, no. 4, p. 48004, 2012.

[43] A. Barabási and Z. Oltvai, "Network biology: understanding the cell's functional organization," *Nature Reviews Genetics*, vol. 5, no. 2, pp. 101–113, 2004.

[44] C. Lindemann and A. Thümmler, "Performance analysis of the general packet radio service," *Computer Networks*, vol. 41, no. 1, pp. 1–17, 2003.

[45] C. Riddalls, S. Bennett, and N. Tipi, "Modelling the dynamics of supply chains," *International Journal of Systems Science*, vol. 31, no. 8, pp. 969–976, 2000.

[46] S. Karlin and H. Taylor, *A second course in stochastic processes*. Academic Pr, 1981.

[47] P. Van Mieghem, *Performance analysis of communications networks and systems*. Cambridge Univ Press, 2006.

[48] P. Erdős and A. Rényi, *On the evolution of random graphs*. Akad. Kiadó, 1960.

[49] A. Barabási and R. Albert, "Emergence of scaling in random networks," *science*, vol. 286, no. 5439, pp. 509–512, 1999.

[50] J. Doyle, D. Alderson, L. Li, S. Low, M. Roughan, S. Shalunov, R. Tanaka, and W. Willinger, "The robust yet fragile nature of the internet," *Proceedings of the National Academy of Sciences*, vol. 102, no. 41, p. 14497, 2005.

[51] M. Youssef and C. Scoglio, "An individual-based approach to SIR epidemics in contact networks," *Journal of Theoretical Biology*, vol. 283, no. 1, pp. 136–144, 2011.

[52] R. Diestel, "Graph theory, volume 173 of graduate texts in mathematics," *Springer, Heidelberg*, vol. 91, p. 92, 2005.

[53] P. Van Mieghem, *Graph Spectra for Complex Networks*. Cambridge Univ Pr, 2011.

[54] M. De Domenico, A. Solé-Ribalta, E. Cozzo, M. Kivelä, Y. Moreno, M. A. Porter, S. Gómez, and A. Arenas, "Mathematical formulation of multilayer networks," *Physical Review X*, vol. 3, no. 4, p. 041022, 2013.

[55] M. Kivela, A. Arenas, M. Barthelemy, J. P. Gleeson, Y. Moreno, and M. A. Porter, "Multilayer networks," *arXiv:1309.7233*, 2014.

[56] O. Yağan, D. Qian, J. Zhang, and D. Cochran, "Optimal allocation of interconnecting links in cyber-physical systems: Interdependence, cascading failures, and robustness," *Parallel and Distributed Systems, IEEE Transactions on*, vol. 23, no. 9, pp. 1708–1720, 2012.

[57] O. Yağan and V. Gligor, "Analysis of complex contagions in random multiplex networks," *Physical Review E*, vol. 86, no. 3, p. 036103, 2012.

[58] W. Richoux and G. Verghese, "A generalized influence model for networked stochastic automata," *IEEE Trans. on Systems, Man and Cybernetics, Part A: Systems and Humans*, vol. 41, no. 1, pp. 10–23, 2011.

[59] S. Ross, *Stochastic processes*. John Wiley & Sons New York, 1983, vol. 23.

[60] C. Gardiner, *Handbook of stochastic methods: For physics, chemistry and the natural sciences*. Berlin: Springer, 2004.

[61] M. Taylor, P. Simon, D. Green, T. House, and I. Kiss, "From markovian to pairwise epidemic models and the performance of moment closure approximations," *Journal of Mathematical Biology*, pp. 1–22, 2011.

[62] E. Cator and P. Van Mieghem, "Second-order mean-field susceptible-infected-susceptible epidemic threshold," *Physical Review E*, vol. 85, no. 5, p. 056111, 2012.

[63] S. C. Ferreira, C. Castellano, and R. Pastor-Satorras, "Epidemic thresholds of the susceptible-infected-susceptible model on networks: A comparison of numerical and theoretical results," *Physical Review E*, vol. 86, no. 4, p. 041125, 2012.

[64] C. Li, R. van de Bovenkamp, and P. V. Mieghem, "The sis mean-feld n-intertwined and pastor-satorras & vespignani approximation: a comparison," *Physical Review E*, vol. 86, no. 2, p. 026116, 2012.

[65] P. Van Mieghem, "The N-intertwined SIS epidemic network model," *Computing*, pp. 1–23, 2011.

[66] Z. Chen and C. Ji, "Spatial-temporal modeling of malware propagation in networks," *Neural Networks, IEEE Transactions on*, vol. 16, no. 5, pp. 1291–1303, sept. 2005.

[67] M. E. Newman, "Threshold effects for two pathogens spreading on a network," *Physical review letters*, vol. 95, no. 10, p. 108701, 2005.

[68] M. Lipsitch, C. Colijn, T. Cohen, W. Hanage, and C. Fraser, "No coexistence for free: neutral null models for multistrain pathogens," *Epidemics*, vol. 1, no. 1, p. 2, 2009.

[69] A. Beutel, B. A. Prakash, R. Rosenfeld, and C. Faloutsos, "Interacting viruses in networks: can both survive?" in *Proceedings of the 18th ACM SIGKDD international conference on Knowledge discovery and data mining*. ACM, 2012, pp. 426–434.

[70] V. Marceau, P. Noël, L. Hébert-Dufresne, A. Allard, and L. Dubé, "Modeling the dynamical interaction between epidemics on overlay networks," *Physical Review E*, vol. 84, no. 2, p. 026105, 2011.

[71] M. Newman, D. Watts, and S. Strogatz, "Random graph models of social networks," *Proceedings of the National Academy of Sciences of the United States of America*, vol. 99, no. Suppl 1, pp. 2566–2572, 2002.

[72] B. Karrer and M. Newman, "Competing epidemics on complex networks," *Physical Review E*, vol. 84, no. 3, p. 036106, 2011.

[73] Y.-Y. Ahn, H. Jeong, N. Masuda, and J. D. Noh, "Epidemic dynamics of two species of interacting particles on scale-free networks," *Physical Review E*, vol. 74, no. 6, p. 066113, 2006.

[74] S. Aral and D. Walker, "Creating social contagion through viral product design: A randomized trial of peer influence in networks," *Management Science*, vol. 57, no. 9, pp. 1623–1639, 2011.

[75] L. Weng, A. Flammini, A. Vespignani, and F. Menczer, "Competition among memes in a world with limited attention," *Scientific Reports*, vol. 2, 2012.

[76] S. Myers and J. Leskovec, "Clash of the contagions: Cooperation and competition in information diffusion," in *Data Mining (ICDM), 2012 IEEE 12th International Conference on*, 2012, pp. 539–548.

[77] S. Shrestha, A. A. King, and P. Rohani, "Statistical inference for multi-pathogen systems," *PLoS computational biology*, vol. 7, no. 8, p. e1002135, 2011.

[78] C. Poletto, S. Meloni, V. Colizza, Y. Moreno, and A. Vespignani, "Host mobility drives pathogen competition in spatially structured populations," *PLoS computational biology*, vol. 9, no. 8, p. e1003169, 2013.

[79] M. Newman and C. R. Ferrario, "Interacting epidemics and coinfection on contact networks," *PloS one*, vol. 8, no. 8, p. e71321, 2013.

[80] Q. Wu, M. Small, and H. Liu, "Superinfection behaviors on scale-free networks with competing strains," *Journal of Nonlinear Science*, vol. 23, no. 1, pp. 113–127, 2013.

[81] Y. Wang, G. Xiao, and J. Liu, "Dynamics of competing ideas in complex social systems," *New Journal of Physics*, vol. 14, no. 1, p. 013015, 2012.

[82] B. A. Prakash, A. Beutel, R. Rosenfeld, and C. Faloutsos, "Winner takes all: competing viruses or ideas on fair-play networks," in *Proceedings of the 21st international conference on World Wide Web*. ACM, 2012, pp. 1037–1046.

[83] E. Cozzo, R. A. Banos, S. Meloni, and Y. Moreno, "Contact-based social contagion in multiplex networks," *Physical Review E*, vol. 88, no. 5, p. 050801, 2013.

[84] H. Wang, Q. Li, G. DAgostino, S. Havlin, H. E. Stanley, and P. Van Mieghem, "Effect of the interconnected network structure on the epidemic threshold," *Phys. Rev. E*, vol. 88, p. 022801, 2013.

[85] E. Cator, R. van de Bovenkamp, and P. Van Mieghem, "Susceptible-Infected-Susceptible epidemics on networks with general infection and cure times," *Phys. Rev. E*, vol. 87, p. 062816, 2013.

[86] G. Hardin *et al.*, "The competitive exclusion principle," *Science*, vol. 131, no. 3409, pp. 1292–1297, 1960.

[87] R. H. Bartels, J. C. Beatty, and B. A. Barsky, *An introduction to splines for use in computer graphics and geometric modeling.* Morgan Kaufmann, 1987.

[88] T. Antunović, E. Mossel, and M. Z. Rácz, "Coexistence in preferential attachment networks," *arXiv preprint arXiv:1307.2893*, 2013.

[89] Z. Cvetkovski, *Inequalities: Theorems, Techniques and Selected Problems.* Springer, 2012.

[90] A. Graham, *Kronecker products and matrix calculus: with applications.* Horwood Chichester, 1981.

[91] N. Ferguson, "Capturing human behaviour," *Nature*, vol. 446, no. 7137, p. 733, 2007.

[92] S. Funk, M. Salath, and V. A. A. Jansen, "Modelling the influence of human behaviour on the spread of infectious diseases: a review," *Journal of The Royal Society Interface*, vol. 7, pp. 1247–1256, 2010.

[93] S. Kitchovitch and P. Lio, "Risk perception and disease spread on social networks," *Procedia Computer Science*, vol. 1, no. 1, pp. 2339–2348, 2010.

[94] S. Funk, E. Gilad, C. Watkins, and V. Jansen, "The spread of awareness and its impact on epidemic outbreaks," *Proceedings of the National Academy of Sciences*, vol. 106, no. 16, pp. 6872–6877, 2009.

[95] S. Funk, E. Gilad, and V. Jansen, "Endemic disease, awareness, and local behavioural response," *Journal of Theoretical Biology*, vol. 264, no. 2, pp. 501–509, 2010.

[96] I. Kiss, J. Cassell, M. Recker, and P. Simon, "The impact of information transmission on epidemic outbreaks," *Mathematical biosciences*, vol. 225, no. 1, pp. 1–10, 2010.

[97] S. Tracht, S. Del Valle, J. Hyman, and D. Carter, "Mathematical modeling of the effectiveness of facemasks in reducing the spread of novel influenza a (h1n1)," *PloS ONE*, vol. 5, no. 2, p. e9018, 2010.

[98] G. Theodorakopoulos, J.-Y. L. Boudec, and J. S. Baras, "Selfish response to epidemic propagation," in *American Control Conference*, 2011, to apear.

[99] P. Poletti, B. Caprile, M. Ajelli, A. Pugliese, and S. Merler, "Spontaneous behavioural changes in response to epidemics," *Journal of Theoretical Biology*, vol. 260, no. 1, pp. 31–40, 2009.

[100] N. Perra, D. Balcan, B. Gonasalves, and A. Vespignani, "Towards a characterization of behavior-disease models," *PLoS ONE*, vol. 6, no. 8, p. e23084, 08 2011.

[101] H. Khalil and J. Grizzle, *Nonlinear systems*. Prentice hall Englewood Cliffs, NJ, 2002, vol. 3.

[102] B. Buonomo, A. dOnofrio, and D. Lacitignola, "Global stability of an sir epidemic model with information dependent vaccination," *Mathematical biosciences*, vol. 216, no. 1, pp. 9–16, 2008.

[103] P. Manfredi and A. d'Onofrio, *Modeling the interplay between human behavior and the spread of infectious diseases*. Springer, 2013.

[104] F. Chen, "A susceptible-infected epidemic model with voluntary vaccinations," *Journal of mathematical biology*, vol. 53, no. 2, pp. 253–272, 2006.

[105] T. C. Reluga, "Game theory of social distancing in response to an epidemic," *PLoS computational biology*, vol. 6, no. 5, p. e1000793, 2010.

[106] T. Gross and B. Blasius, "Adaptive coevolutionary networks: a review," *Journal of The Royal Society Interface*, vol. 5, no. 20, pp. 259–271, Mar. 2008.

[107] T. Gross, C. DLima, and B. Blasius, "Epidemic dynamics on an adaptive network," *Physical review letters*, vol. 96, no. 20, p. 208701, 2006.

[108] V. Marceau, P. Noël, L. Hébert-Dufresne, A. Allard, and L. Dubé, "Adaptive networks: Coevolution of disease and topology," *Physical Review E*, vol. 82, no. 3, p. 036116, 2010.

[109] S. Risau-Gusmán and D. Zanette, "Contact switching as a control strategy for epidemic outbreaks," *Journal of theoretical biology*, vol. 257, no. 1, pp. 52–60, 2009.

[110] G. Demirel and T. Gross, "Absence of epidemic thresholds in a growing adaptive network," *arXiv preprint arXiv:1209.2541*, 2012.

[111] S. Van Segbroeck, F. C. Santos, and J. M. Pacheco, "Adaptive contact networks change effective disease infectiousness and dynamics," *PLoS Comput Biol*, vol. 6, no. 8, p. e1000895, Aug. 2010.

[112] S. Meloni, N. Perra, A. Arenas, S. Gomez, Y. Moreno, and A. Vespignani, "Modeling human mobility responses to the large-scale spreading of infectious diseases," *Scientific Reports*, vol. 1, no. 62, 2011.

[113] V. Preciado, F. Sahneh, and C. Scoglio, "A convex framework for optimal investment on disease awareness in social networks," in *Global Conference on Signal and Information Processing (GlobalSIP), 2013 IEEE*, Dec 2013, pp. 851–854.

[114] D. Guo, S. Trajanovski, R. van de Bovenkamp, H. Wang, and P. Van Mieghem, "Epidemic threshold and topological structure of susceptible-infectious-susceptible epidemics in adaptive networks," *Phys. Rev. E*, vol. 88, p. 042802, Oct 2013.

[115] B. Lemmens and R. Nussbaum, *Nonlinear Perron-Frobenius Theory*. Cambridge University Press, 2012, no. 189.